1991

Diffusion effects in eddy current nondestructive evaluation

Paul Andrew Stucky
Iowa State University

Diffusion Effects in
Eddy Current Nondestructive Evaluation

by

Paul A. Stucky

A Dissertation Submitted to the

Graduate Faculty in Partial Fulfillment of the

Requirements for the Degree of

MASTER OF SCIENCE

Department: Electrical and Computer Engineering
Major: Electrical Engineering (Electromagnetics)

Iowa State University
Ames, Iowa
1991

The issue is Socialism versus Capitalism. I am for Socialism because I am for humanity. We have been cursed with the reign of gold long enough. Money constitutes no proper basis of civilization. The time has come to regenerate society—we are on the eve of a universal change.

Eugene V. Debs

Union organizer

TABLE OF CONTENTS

LIST OF TABLES

LIST OF FIGURES

ACKNOWLEDGEMENTS

Experience is an elusive "animal." While the inexperienced may eventually achieve similar ends through different means, the experienced pick a path which cuts through the waste and strikes at the fundamental. Such is my observation of Dr. William Lord, my thesis adivisor. It has been my distinct pleasure to be his student.

I extend my gratitude to the members of my committee: Dr. Anand Garikepati, Dr. David Jiles, and Dr. Robert Weber, all of whom have been my teachers in and out of the classroom. Their interest in and tolerance of all my questions created a productive learning environment in which I began to answer my own questions.

The use of John Moulder's eddy current laboratory and the facilities at the Center for NDE, Iowa State Universtiy, were crucial to the timely completion of this thesis. John's enthusiasm and helpful comments directed aspects of the experiments and gave this thesis a completeness. My work at the Center reinforces my belief that experiments are the sobering element. If you look at the computer long enough you begin to believe it! Also, I express my gratitude to Dr. Donald Thompson and the Center for the financial support provided via an Institute for Physical Research and Technology (IPRT) fellowship.

I wish to thank Gaylord Scandrett, mechanical engineering department technician, for all of his help preparing the experimental samples and teaching me just enough about a metal lathe to be dangerous!

ABSTRACT

Transducer response in nondestructive evaluation (NDE) requires fundamental knowledge of the field interaction with the material under test. Specifically, in eddy current NDE the transducer is an inductive coil or some combination of coils with an electromagnetic induction field surrounding the coil. The coil is used predominantly for surface or near-surface inspection of electrical conductors (metals). The change of impedance of the coil at its terminals is used as the criterion for defect detection. The impedance change due to a defect depends upon the relative disruption of the steady state field configuration in a given testing situation. A spatially smaller defect relative to the coil dimensions usually causes a smaller impedance change, therefore, it is more difficult to detect. The eddy currents induced in the metal by the exciting coil decay with distance into the metal due to energy loss in the form of Ohmic heating. Consequently, a defect easily detected at the surface with a given coil becomes undetectable at some distance beneath the metal surface. The distance at which a given defect becomes "invisible" is directly related to the rate of decay of the induced currents and their spatial distribution. The classical skin depth, $\delta_s = \sqrt{2/\omega\mu\sigma}$, is the usual measure of the decay rate of currents in metals, but it is derived assuming a source field of infinite spatial extent and no inhomogeneity. In contrast, coils are often very small relative to the metal object under test and their useful fields are

confined to a finite region surrounding the coil; therefore, assuming the classical skin depth in place of the actual skin depth may lead to erroneous conclusions about a coil's ability to detect and size the defect.

This thesis compares the actual decay of induced time-harmonic, steady-state current densities in conductors to the classical skin depth for an air-core coil over a conductor of both infinite (half-space) and finite thickness and for a pair of differential coils inside a conducting tube of infinite and finite thickness. In each case the finite element method (FEM) in its axisymmetric form is used to solve for the magnetic vector potential, $\vec{A}$, from which all relevant quantities such as coil impedance and eddy current density are computed. For the coil over a half-space, the FEM is compared to an exact integral solution to confirm the validity of the FEM, while the FEM alone is used to compute quantities for coils in a tube. Actual current densities are computed and their rate of decay versus depth in the conductor, distance from exciting coil, and variations in coil and material parameters are investigated. The normalized coil impedance is computed versus coil proximity to the conductor (lift-off) and changing dimensionless parameter R_S/δ_S ($R_S \equiv$ coil mean radius). For the coil over a half-space, experimental measurements of coil impedance were performed and compared with the computed analytical solution and the FEM. In general, the experimental measurements show the range of validity of the analytical and FEM solutions.

The experiments and computer simulations show the actual eddy current density distribution and decay is significantly different from the classical exponential decay in regions of operation where the coil is most useful for NDE but does approach the classical solution in the extreme region $R_S/\delta_S \gg 1$. Caution should therefore be

used when applying the classical skin depth approximation when $R_S/\delta_S \sim 1$. This study also shows the validity and usefulness of the axisymmetric FEM for modelling field/material interaction in spite of inherent simplifying assumptions. The analytical solution, while elegant and important in its own right, cannot model complex defects or material inhomogeneities in general, yet the FEM handles these situations with relative ease.

CHAPTER 1. INTRODUCTION

From the industrial revolution onward humans have increasingly entrusted life and limb to machines whose complexity has grown exponentially, for example, compare the first steam engine and a modern automoble or the space shuttle. As the complexity grows so does the danger of system or subsystem failure due to component fatigue. These failures can be catastrophic (the space shuttle Challenger, for example) so that early detection of stress and fatigue becomes critical for machine function and human safety. To reduce the cost and time of inspection, machines must be designed with periodic fatigue testing as a foundation. Regions of high stress must be made easily accessible for inspection. Machine design for testing must be in concert with the methods and techniques by which testing is accomplished. The methods and techniques embody the vast subject of nondestructive evaluation (NDE). NDE research seeks to refine well known techniques and to develop new methods for machine inspection which do not require machine disassembly. Libby [24] defines electromagnetic NDE as

> any test or measurement method for inspecting or evaluating materials or products which does not adversely affect their serviceability and which uses the effect of electromagnetic induction, electromagnetic fields, or varying currents for probing, measuring, or inspecting. (p. 1)

Accurate and reliable NDE methods are being utilized in such critical situations as inspection of nuclear power plant steam generator tubing and oil and gas pipelines, just to name a few.

Nondestructive evaluation relies on the interaction of an energy source with the material under test. Various forms of energy such as acoustic waves, alternating electric current, and electromagnetic waves are conveyed to the material from the energy source via a transducer specific to the form of energy. The energy/material interaction is detected with a transducer—often the same transducer which was the energy's source. From the material/energy interaction the existence of defects or material inhomogeneities can be determined. In all cases noted above there are limitations on defect detection such as instrument sensitivity and improper calibration (human error), attenuation, and so forth.

Scope of the Thesis

This thesis compares the classical skin effect current density distributions governed by exponenetial decay and linear phase to the actual current distributions induced by finite size coils. A coil over a conducting half-space and a pair of differential coils inside a conducting tube with an infinitely thick wall provide practical models for investigation. The axisymmetric finite element method is used as the general computer simulation tool. Comparisons of normalized coil impedance from the FEM and experiment are given for varying physical situations.

Chapter 2 reviews the finite element method starting with the underlying partial differential equation (PDE) and the energy functional. The axisymmetric form of the FEM is derived showing its local and global matrix representation. Finally, the post

processing calculations such as free-space inductance and coil impedance are derived from the solution for the magnetic vector potential.

Chapter 3 provides a slight digression into aspects important to diffusion and the skin effect, yet is not completely necessary to results and conclusions drawn in this thesis. Diffusion is shown as the limit of a stochastic or random process at the beginning of the chapter. Next, an analogy between thermal and electromagnetic (EM) diffusion provides insight to the meaning of certain physical constants arising in the diffusion equation for both heat and current density. The similarities and differences of EM diffusion and thermal diffusion are discussed with specfic regard to the correspondence between the thermal and EM physical constants. Charge and field relaxation in conductors is not as simple as presented in many EM texts. A more complete classical description is presented which exposes interesting physics, but which has a tangential relationship to the cases considered in thesis. As a conclusion to this chapter, assumptions necessary for the classical skin effect approximation are discussed. If these assumptions are violated the skin effect approximation may be a poor estimate of the field decay within the conductor.

The results presented in chapter 4 confirm the equivalence of the FEM and the classical Dodd and Deeds solutions [10]. Considered are the coil over a conducting half-space and a differential coil pair in a conducting tube. These represent practical eddy current NDE testing situations. The induced eddy current density in the half-space and tube are plotted for various changing parameters such as frequency and distance from the coil(s). The analytical and FEM results are compared to experimental results showing, in general, the validity of the simulations.

Chapter 5 includes conclusions drawn from this research and ideas for future

work. Specifically, more work on the *remote field effect* is suggested.

CHAPTER 2. FINITE ELEMENT MODELLING

The finite element method (FEM), long used by civil engineers in the analysis of structures consisting of beams and shells, has been firmly established as an accurate model for two-dimensional and axisymmetric quasi-static electromagnetic field problems [8] [25] [30] [31] [32]. The FEM in its axisymmetric formulation is the foundation of the current study. In this chapter a brief summary of the energy functional in both its three-dimensional form and two-dimensional axisymmetric form is given, followed by an overview of the energy functional minimization via the finite element method. A concluding section discusses the post processing calculations for coil parameters, such as eddy currents, coil impedance and inductance, from the finite element solution.

Calculus of Variations and Functional Minimization

The numerical code employed in this study uses a functional minimization technique to solve for the magnetic vector potential at each node point in the finite element mesh, then, via a linear approximating function, the vector potential is known throughout the whole mesh. The solution is achieved by requiring a certain energy functional comprised of the field variables to be minimal within the solution region, that is, the fields are determined such that the total electromagnetic energy in the

region is a minimum. The technique rests upon one's ability to derive the energy functional—not always straightforward or even possible. Following this is a presentation of the energy functional in its three-dimensional and axisymmetric forms. It is shown that the functional in the axisymmetric form satisfies the corresponding Euler equation and is therefore the correct functional.

Energy functional

The governing partial differential equation (PDE) for the quasi-static eddy current phenomenon is given by

$$\nabla \times \frac{1}{\mu} \nabla \times \vec{A} = +\vec{J}_s - j\omega\sigma\vec{A} \tag{2.1}$$

where all quantities are ac phasors ($\frac{\partial}{\partial t} \Longrightarrow j\omega$), the material properties are linear, homogeneous, and isotropic, and the Coulomb gauge, $\nabla \cdot \vec{A} = 0$, is assumed. The left-hand side (LHS) of equation 2.1 represents the spatial variation of the magnetic vector potential. The right-hand side (RHS) consists of the source current density (with sign), $+\vec{J}_s$, and the eddy current density, $-j\omega\sigma\vec{A}$, which is induced by the field in conducting structures present in the region of interest. The difference in sign between the source current density and the eddy current density is a mathematical interpretation of Newton's third law or, more specifically, Lenz's law: "the (induced) electromotive force (emf) *tries to oppose* any change in flux" or more precisely "the direction of an induced emf is always such that if a current were to flow in the direction of the emf, it would produce a flux of $\vec{B}$ that opposes the change in $\vec{B}$ that produces the emf" (see Feynman [15]). Overall, equation 2.1 is a linear vector diffusion equation. In the time domain it is parabolic or evolving in nature while in the phasor domain (steady state ac) it becomes an elliptic PDE.

The energy functional in three dimensions for a vector Helmholtz equation of the form

$$\nabla^2\vec{U} + k^2\vec{U} = \vec{V} \tag{2.2}$$

is given by Konrad and Silvester [23] and Silvester and Ferrari [37] as

$$\begin{aligned} F(\vec{U}) &= \iiint_V \left[|\nabla \times \vec{U}|^2 - \vec{U}\cdot\nabla(\nabla\cdot\vec{U}) - k^2|\vec{U}|^2 + 2\vec{V}\cdot\vec{U}\right] dV \\ &\quad - \oint_{\partial V} \vec{U}\times\nabla\times\vec{U}\cdot d\vec{S} \end{aligned} \tag{2.3}$$

where $\vec{U}$ and $\vec{V}$ are a general field and source vector, respectively, k^2 is a constant (usually in the electromagnetic wave case $k^2 = \omega^2\mu\epsilon - j\omega\mu\sigma$), and ∂V denotes the boundary surface of volume V. If the substitutions $\vec{U} \equiv \vec{A}$, $\vec{V} \equiv -\mu\vec{J}_s$, and $k^2 = -j\omega\mu\sigma$ are made[1] the resulting functional becomes

$$\begin{aligned} F(\vec{A}) &= \iiint_V \left[|\nabla \times \vec{A}|^2 - \vec{A}\cdot\nabla(\nabla\cdot\vec{A}) + j\omega\mu\sigma|\vec{A}|^2 - 2\mu\vec{J}_s\cdot\vec{A}\right] dV \\ &\quad - \oint_{\partial V} \vec{A}\times\nabla\times\vec{A}\cdot d\vec{S}. \end{aligned} \tag{2.5}$$

By dividing through by 2μ and applying the Coulomb gauge to the second term the general energy functional for the quasi-static eddy current case becomes

$$\begin{aligned} F'(\vec{A}) = \frac{F(\vec{A})}{2\mu} &= \iiint_V \left[\frac{1}{2\mu}|\nabla \times \vec{A}|^2 + \frac{j\omega\sigma}{2}|\vec{A}|^2 - \vec{J}_s\cdot\vec{A}\right] dV \\ &\quad - \frac{1}{2\mu}\oint_{\partial V} \vec{A}\times\nabla\times\vec{A}\cdot d\vec{S}. \end{aligned} \tag{2.6}$$

[1] The term $\omega^2\mu\epsilon$ is dropped since it represents displacement current density, but mathematically displacement current density is negligible in this situation since $\frac{\omega\epsilon}{\sigma} \ll 1$ in the vector potential wave equation

$$\nabla\times\frac{1}{\mu}\nabla\times\vec{A} = \vec{J}_s - j\omega\sigma(1 + j\frac{\omega\epsilon}{\sigma})\vec{A}. \tag{2.4}$$

The prime can be dropped from the $F'(\vec{A})$ since the constant ultimately has no effect on the functional.

The surface term will be identically zero if for every point on the boundary (∂V) the magnetic vector potential is zero

$$\vec{A}\Big|_{\partial V} = \vec{0}. \tag{2.7}$$

In other words, the vector potential satisfies the Dirichlet boundary condition. The surface term can also be identically zero if the integrand is zero along the boundary, or

$$\vec{A} \times \nabla \times \vec{A} \cdot \hat{n}\Big|_{\partial V} = 0, \tag{2.8}$$

which is the vector equivalent of the Neumann boundary condition encountered in scalar analysis. Of course, it is possible to have a situation where one of the two conditions is satisfied everywhere on the boundary and the surface term is again zero. In this study the Dirichlet condition is imposed everywhere on the boundary; therefore, the surface term can be neglected.

Energy functional: axisymmetric case From the general three dimensional energy functional the specific functional for the axisymmetric case can be derived. Assuming cylindrical coordinates, (ρ, ϕ, z), a single component vector potential and a single component source current density,

$$\vec{A} = A_\phi(\rho, z)\hat{\phi} \tag{2.9}$$

$$\vec{J}_s = J_\phi(\rho, z)\hat{\phi}, \tag{2.10}$$

the functional becomes

$$F(A_\phi\hat{\phi}) = \iiint_V \left[\frac{1}{2\mu}\left\{\left(\frac{1}{\rho}\frac{\partial(\rho A_\phi)}{\partial\rho}\right)^2 + \left(\frac{\partial A_\phi}{\partial z}\right)^2\right\} + \frac{j\omega\sigma}{2}(A_\phi)^2 - J_\phi A_\phi\right]\rho d\rho d\phi dz. \tag{2.11}$$

The functional can be integrated once since it is independent of the coordinate ϕ, but the integration in ϕ will be delayed until a later point for reasons of clarity. Upon expansion of the derivative terms the functional becomes

$$F(A_\phi\hat{\phi}) = \iiint_V \left[\frac{1}{2\mu}\left\{\left(\frac{\partial A_\phi}{\partial\rho}\right)^2 + \frac{2A_\phi}{\rho}\frac{\partial A_\phi}{\partial\rho} + \left(\frac{A_\phi}{\rho}\right)^2 + \left(\frac{\partial A_\phi}{\partial z}\right)^2\right\} + \frac{j\omega\sigma}{2}(A_\phi)^2 - J_\phi A_\phi\right]\rho d\rho d\phi dz. \tag{2.12}$$

The functional's validity is shown by its satisfaction of the corresponding Euler equation which in this case is

$$\frac{\partial}{\partial\rho}\left(\frac{\partial f}{\partial\left[\frac{\partial A_\phi}{\partial\rho}\right]}\right) + \frac{\partial}{\partial z}\left(\frac{\partial f}{\partial\left[\frac{\partial A_\phi}{\partial z}\right]}\right) - \frac{\partial f}{\partial A_\phi} = 0 \tag{2.13}$$

where

$$\begin{aligned} f &= f\left(\rho, z, A_\phi, \frac{\partial A_\phi}{\partial\rho}, \frac{\partial A_\phi}{\partial z}\right) \\ &= \left[\frac{1}{2\mu}\left\{\left(\frac{\partial A_\phi}{\partial\rho}\right)^2 + \frac{2A_\phi}{\rho}\frac{\partial A_\phi}{\partial\rho} + \left(\frac{A_\phi}{\rho}\right)^2 + \left(\frac{\partial A_\phi}{\partial z}\right)^2\right\} + \frac{j\omega\sigma}{2}(A_\phi)^2 - J_\phi A_\phi\right]\rho. \end{aligned} \tag{2.14}$$

The derivatives of f with respect to the terms A_ϕ, $\frac{\partial A_\phi}{\partial\rho}$, and $\frac{\partial A_\phi}{\partial z}$ are each taken while holding all other terms constant. In contrast, the derivatives of f with respect

to the coordinates ρ and z are obtained while treating only these two variables as independent since the vector potential and its derivatives are functions of the coordinates [18].

From variational calculus the magnetic vector potential which minimizes the axisymmetric energy functional, equation 2.12, is the vector potential that solves the underlying PDE, equation 2.1. The minimization is achieved by requiring the first variation of the functional, $\delta F(A_\phi\hat{\phi})$, be equal to zero. Specifically, the first variation is as follows:

$$\begin{aligned}\delta F(A_\phi\hat{\phi}) &= \delta\iiint_V \left[\frac{1}{2\mu}\left\{\left(\frac{\partial A_\phi}{\partial\rho}\right)^2+\frac{2A_\phi}{\rho}\frac{\partial A_\phi}{\partial\rho}+\left(\frac{A_\phi}{\rho}\right)^2+\left(\frac{\partial A_\phi}{\partial z}\right)^2\right\}\right.\\ &\quad \left.+\frac{j\omega\sigma}{2}(A_\phi)^2-J_\phi A_\phi\right]\rho d\rho d\phi dz\\ &= \iiint_V \left[\frac{1}{\mu}\left\{\frac{\partial A_\phi}{\partial\rho}\frac{\partial\delta A_\phi}{\partial\rho}+\frac{1}{\rho}\delta A_\phi\frac{\partial A_\phi}{\partial\rho}+\frac{1}{\rho}A_\phi\frac{\partial\delta A_\phi}{\partial\rho}+\frac{A_\phi\delta A_\phi}{\rho^2}\right.\right.\\ &\quad \left.\left.+\frac{\partial A_\phi}{\partial z}\frac{\partial\delta A_\phi}{\partial z}\right\}+j\omega\sigma A_\phi\delta A_\phi-J_\phi\delta A_\phi\right]\rho d\rho d\phi dz, \qquad (2.15)\end{aligned}$$

with the variation operation, $\delta(\cdot)$, being interchangeable with integration and differentiation. The first variation, equation 2.15, can be rewritten as

$$\begin{aligned}\delta F(A_\phi\hat{\phi}) &= \iiint_V \left[\frac{1}{\mu}\nabla\times(A_\phi\hat{\phi})\cdot\nabla\times(\delta A_\phi\hat{\phi})\right.\\ &\quad \left.+j\omega\sigma A_\phi\delta A_\phi-J_\phi\delta A_\phi\right]\rho d\rho d\phi dz. \qquad (2.16)\end{aligned}$$

This can be transformed by applying *Green's first identity* in vector form,

$$\begin{aligned}\iiint_V \nabla\times\vec{V}\cdot\nabla\times\vec{U}dV &= \iiint_V \vec{U}\cdot\nabla\times\nabla\times\vec{V}dV\\ &\quad +\iint_{\partial V}\vec{U}\times\nabla\times\vec{V}\cdot d\vec{S}, \qquad (2.17)\end{aligned}$$

with the definitions $\vec{U} \equiv \delta A_\phi \hat{\phi}$ and $\vec{V} \equiv A_\phi \hat{\phi}$. Applying Green's identity equation 2.16 becomes

$$\begin{aligned}\delta F(A_\phi\hat{\phi}) &= \iiint_V \left[\frac{1}{\mu}(\delta A_\phi\hat{\phi})\cdot\nabla\times\nabla\times(A_\phi\hat{\phi})\right. \\ &\quad \left.+j\omega\sigma A_\phi\delta A_\phi - J_\phi\delta A_\phi\right]\rho d\rho d\phi dz \\ &\quad +\frac{1}{\mu}\iint_{\partial V}(\delta A_\phi\hat{\phi})\times\nabla\times(A_\phi\hat{\phi})\cdot(\rho d\phi dz\hat{\rho}+\rho d\rho d\phi\hat{z}) \qquad (2.18)\end{aligned}$$

but the Coulomb gauge has been assumed so the first term can be transformed to $-(\delta A_\phi\hat{\phi})\cdot\nabla^2(A_\phi\hat{\phi}) = -\delta A_\phi\nabla^2 A_\phi(\hat{\phi}\cdot\hat{\phi})$. Rewriting equation 2.18 in its expanded axisymmetric form and factoring δA_ϕ out of each term in the integrand the first variation becomes

$$\begin{aligned}\delta F(A_\phi\hat{\phi}) &= \iiint_V \delta A_\phi\left[\frac{1}{\mu}\left(\frac{\partial^2 A_\phi}{\partial\rho^2}+\frac{1}{\rho}\frac{\partial A_\phi}{\partial\rho}-\frac{A_\phi}{\rho^2}+\frac{\partial^2 A_\phi}{\partial z^2}\right)\right. \\ &\quad \left.+j\omega\sigma A_\phi - J_\phi\right]\rho d\rho d\phi dz \\ &\quad +\frac{1}{\mu}\iint_{\partial V}\delta A_\phi\left[\left(\frac{\partial A_\phi}{\partial\rho}+\frac{A_\phi}{\rho}\right)\hat{\rho}+\frac{\partial A_\phi}{\partial z}\hat{z}\right]\cdot(\rho d\phi dz\hat{\rho}+\rho d\rho d\phi\hat{z}). \\ &\qquad (2.19)\end{aligned}$$

For an arbitrary variation δA_ϕ the remaining portions of the integrands must be identically zero if the overall first variation $\delta F(A_\phi\hat{\phi})$ is to be zero. For the situation in this study, the surface term will be zero since Dirichlet conditions exist everywhere on the boundary.

Finite Element Approximation

For all its beauty and elegance, the energy functional cannot be minimized analytically for all arbitrary situations. The point has been reached where the finite

element approximation must be introduced through the linear approximating function or *first order triangle* which is the simplest form of the finite element. Each element matrix equation can be assembled into an overall global matrix and the minimization proceeds with the solution of the set of linear algebraic equations.

First order triangles

The solution region is discretized and a mesh of first order triangles is defined. The axisymmetric vector potential is assumed to be a linear function over the region of each triangle; it can be defined by

$$A_{\phi p}(\rho, z) = \beta_1 + \beta_2 \rho + \beta_3 z = \begin{bmatrix} 1 & \rho & z \end{bmatrix} \begin{bmatrix} \beta_1 \\ \beta_2 \\ \beta_3 \end{bmatrix} \tag{2.20}$$

where subscript p denotes an arbitrary point within the triangle ℓmn (see Figure 2.1).

The β's are dependent on the complex vector potentials, $A_{\phi\ell}$, $A_{\phi m}$, $A_{\phi n}$, at each of the triangle's three vertices. The vector potential at each vertex written in a matrix form is

$$\begin{bmatrix} A_{\phi\ell} \\ A_{\phi m} \\ A_{\phi n} \end{bmatrix} = \begin{bmatrix} 1 & \rho_\ell & z_\ell \\ 1 & \rho_m & z_m \\ 1 & \rho_n & z_n \end{bmatrix} \begin{bmatrix} \beta_1 \\ \beta_2 \\ \beta_3 \end{bmatrix}. \tag{2.21}$$

The matrix can be inverted and the β's become

$$\begin{bmatrix} \beta_1 \\ \beta_2 \\ \beta_3 \end{bmatrix} = \frac{1}{2\Delta} \begin{bmatrix} \rho_m z_n - \rho_n z_m & \rho_n z_\ell - \rho_\ell z_n & \rho_\ell z_m - \rho_m z_\ell \\ z_m - z_n & z_n - z_\ell & z_\ell - z_m \\ \rho_n - \rho_m & \rho_\ell - \rho_n & \rho_m - \rho_\ell \end{bmatrix} \begin{bmatrix} A_{\phi\ell} \\ A_{\phi m} \\ A_{\phi n} \end{bmatrix} \tag{2.22}$$

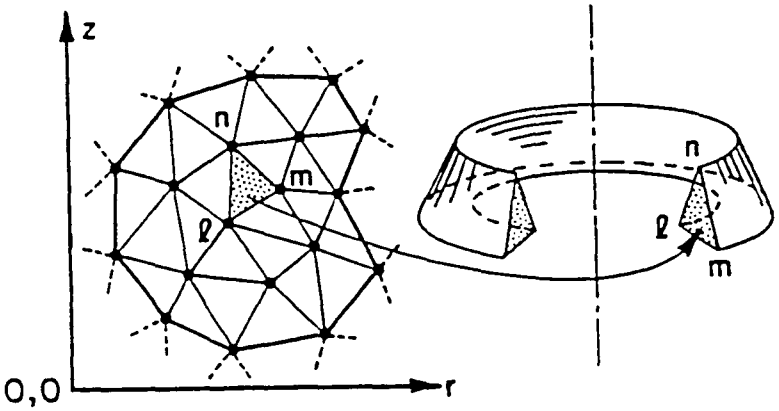

(a)

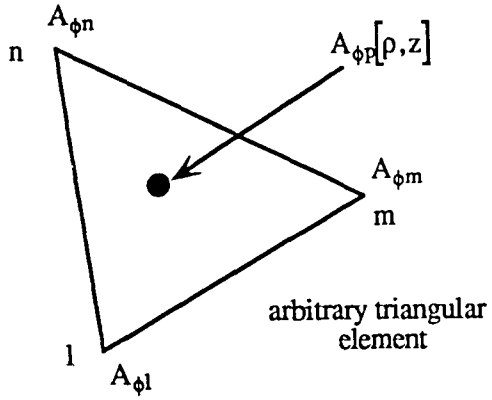

(b)

Figure 2.1: Axisymmetric finite element mesh showing arbitrary point, $A_{\phi p}(\rho, z)$, (a) element rotated about the axis after Lord, (b) a single element

with

$$2\Delta = \begin{vmatrix} 1 & \rho_\ell & z_\ell \\ 1 & \rho_m & z_m \\ 1 & \rho_n & z_n \end{vmatrix} \tag{2.23}$$

where Δ is the area of the triangle and $|\cdot|$ denotes the determinant. In equation 2.20 $A_{\phi p}(\rho, z)$ can be rewritten solely in terms of the vertex coordinates, (ρ_ℓ, z), (ρ_m, z_m), (ρ_n, z_n), and the vector potential at these vertices, $A_{\phi\ell}$, $A_{\phi m}$, $A_{\phi n}$:

$$A_{\phi p}(\rho, z) = \frac{1}{2\Delta}[\ 1 \quad \rho \quad z\ ] \begin{bmatrix} \rho_m z_n - \rho_n z_m & \rho_n z_\ell - \rho_\ell z_n & \rho_\ell z_m - \rho_m z_\ell \\ z_m - z_n & z_n - z_\ell & z_\ell - z_m \\ \rho_n - \rho_m & \rho_\ell - \rho_n & \rho_m - \rho_\ell \end{bmatrix} \times \begin{bmatrix} A_{\phi\ell} \\ A_{\phi m} \\ A_{\phi n} \end{bmatrix} \tag{2.24}$$

with the unknowns being the coefficients $A_{\phi\ell}$, $A_{\phi m}$, and $A_{\phi n}$.

As shown by Chari [8] for the two-dimensional case and by Brauer [4] for the axisymmetric case the vector potential for each triangle, equation 2.24, is substituted into the energy functional, equation 2.12, and the functional is differentiated with respect to the unknown coefficients $A_{\phi\ell}$, $A_{\phi m}$, and $A_{\phi n}$, respectively. The sum is then set equal to zero:

$$\sum_{i=\ell,m,n} \frac{\partial F(A_{\phi p})}{\partial A_{\phi i}} = \iiint_V \left[\frac{1}{\mu} \left\{ \frac{\partial A_{\phi p}}{\partial \rho} \frac{\partial}{\partial A_{\phi i}} \left(\frac{\partial A_{\phi p}}{\partial \rho} \right) + \frac{1}{\rho} \frac{\partial}{\partial A_{\phi i}} \left(A_{\phi p} \frac{\partial A_{\phi p}}{\partial \rho} \right) + \frac{1}{\rho^2} A_{\phi p} \frac{\partial A_{\phi p}}{\partial A_{\phi i}} + \frac{\partial A_{\phi p}}{\partial z} \frac{\partial}{\partial A_{\phi i}} \left(\frac{\partial A_{\phi p}}{\partial z} \right) \right\} + j\omega\sigma A_{\phi p} \frac{\partial A_{\phi p}}{\partial A_{\phi i}} - J_{\phi p} \frac{\partial A_{\phi p}}{\partial A_{\phi i}} \right] \rho d\rho d\phi dz$$

$$= 0. \tag{2.25}$$

An element matrix equation results with the form

$$\{[S]_e + j[R]_e\}[A]_e = [Q]_e \tag{2.26}$$

where $[S]_e$ is a 3×3 matrix called the *element matrix*, $[R]_e$ the 3×3 *constant element matrix*, and $[Q]_e$ the 3×1 *source element matrix* [25] [8] [4]. The matrix $[A]_e$ is a 3×1 matrix of the coefficients $A_{\phi\ell}$, $A_{\phi m}$, and $A_{\phi n}$. This matrix equation is the foundation of the axisymmetric finite element formulation of the energy functional for one triangular element in the solution region. The method is extended to all elements in the region and the individual element matrices combined to form a *global matrix equation*,

$$[G][A] = [Q]. \tag{2.27}$$

The matrix $[G]$ is an $N \times N$ banded symmetric complex matrix and $[A]$ and $[Q]$ are $N \times 1$ are complex matrices. A direct Gaussian elimination technique is used to invert $[G]$ and obtain the vector potentials at each triangle vertex, or node point, in the solution region. The vector potential determined is the potential which minimizes the original energy functional, equation 2.12, at least approximately due to the discretization. It will be seen later that the approximation becomes almost indistinguishable from the analytic solution if the discretization is made very fine.

Post Processing

With the magnetic vector potential certain other quantities can be determined. Primarily of interest in this study are the eddy current density, coil impedance, and

the free-space inductance of the coil. These parameters are computed and compared with the well-known analytic solutions by Dodd, Deeds, and Luquire [11].

The eddy current density in the conducting media is given by the relation

$$J_{\phi e} = -j\omega\sigma A_{\phi}. \tag{2.28}$$

In general the eddy currents decay with depth into the conductor and have an increasing phase lag with respect to the eddy currents on the surface. It is their detailed behavior which is of interest in this study.

The coil impedance tends to be of prime importance in eddy current NDT since it can easily be measured and provides a simple and compact observable quantity which can indicate variations of material properties in the region near the coil. The phasor impedance of an i^{th} filamentary current loop in the coil, as given in Palanisamy [29], is equal to the ratio of electromotive force (emf) in the loop to the total current in the loop and can be represented by the relation

$$Z_i = \frac{-\int_0^{2\pi} E_{\phi i}\hat{\phi}\cdot\hat{\phi}\rho_i d\phi}{I_s} = \frac{j\omega 2\pi\rho_i A_{\phi i}}{I_s} \tag{2.29}$$

with I_s the impressed *rms* source current. The summation (integration) of equation 2.29 over all loops gives the total coil impedance. In the case of finite elements, the centroidal values of vector potential, A_{cj}, and radius, ρ_{cj}, for j^{th} triangular element can be substituted for all the values A_i and ρ_i occurring in each element without serious loss of accuracy (see Figure 2.2); for completeness they are given:

$$A_{cj} = \sqrt{\frac{1}{12}\left[A_{\phi\ell}^2 + A_{\phi m}^2 + A_{\phi n}^2 + (A_{\phi\ell} + A_{\phi m} + A_{\phi n})^2\right]} \tag{2.30}$$

$$\rho_{cj} = \sqrt{\frac{1}{12}\left[\rho_{\ell}^2 + \rho_m^2 + \rho_n^2 + (\rho_{\ell} + \rho_m + \rho_n)^2\right]}. \tag{2.31}$$

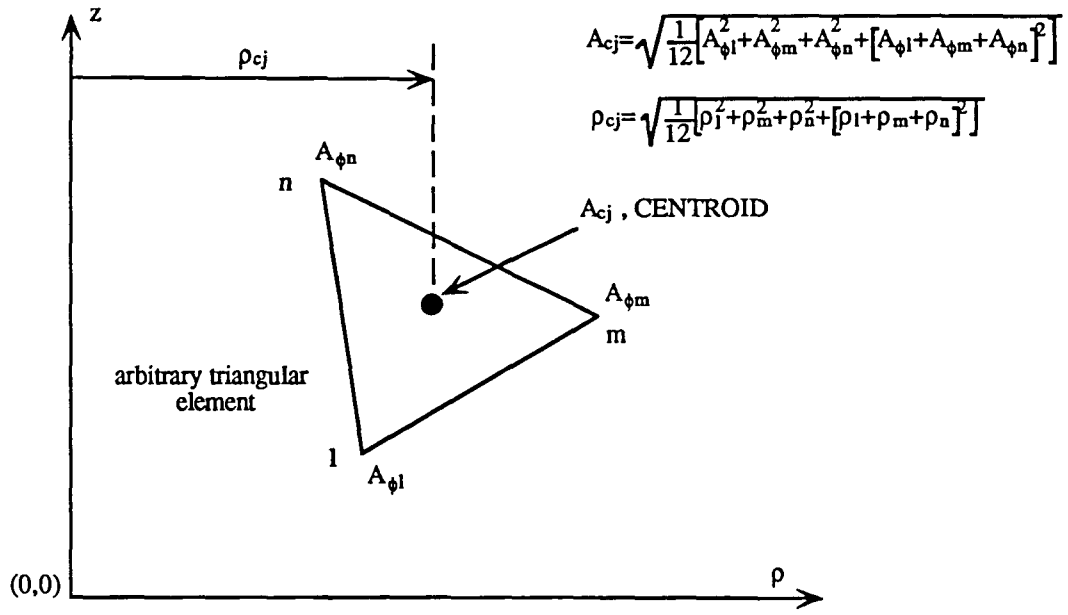

Figure 2.2: Definition of centroidal vector potential, A_{cj}, and centroidal radius, ρ_{cj}

For a constant turn density, N_s (turns/m^2), the total number of turns in a given triangular element with an area Δ_j is $N_s\Delta_j$, therefore, the total impedance of all turns in element j is from [29]

$$Z_j = \frac{j\omega 2\pi r_{cj} A_{cj}(N_s\Delta_j)}{I_s} \tag{2.32}$$

and the total impedance of the coil with N elements is

$$Z_{coil} = \frac{j\omega 2\pi N_s}{I_s} \sum_{j=1}^{N} (\rho_{cj}\Delta_j)A_{cj} \tag{2.33}$$

or with the relationship $J_{\phi s} = N_s I_s$ this can be rewritten as

$$Z_{coil} = \frac{j\omega 2\pi J_{\phi s}}{I_s^2} \sum_{j=1}^{N} (\rho_{cj}\Delta_j)A_{cj}. \tag{2.34}$$

This final expression for the coil impedance, equation 2.34, becomes more accurate as a larger number of smaller elements are used to model the coil cross-section.

Usually, the coil impedance is normalized to the magnitude of the coil impedance in air. In terms of computation, the coil is modelled with no conductors in the solution region and the air inductance, L_o, is then given by

$$L_o = \left|\frac{Z_{coil}}{j\omega}\right|_{air} = \frac{2\pi|J_{\phi s}|}{|I_s^2|} \sum_{j=1}^{N} (\rho_{cj}\Delta_j)|A_{cj}| \tag{2.35}$$

and the magnitude of the normalizing impedance is then

$$|Z_n| = \omega L_o. \tag{2.36}$$

The above quantities are computed for various situations and are compared with the computed analytical expressions and to some actual experimental results. Verification by these methods is necessary to give confidence in the finite element code when situations not easily determined analytically are investigated.

CHAPTER 3. THE SKIN EFFECT

The distribution of electromagnetic fields and electric currents in conductors has been a subject of research from at least the time of Maxwell [26]. The existence of analytic solutions to eddy current distributions in structures of practical interest, such as solid wires, tubes, and flat bus bars, has made the subject unique. These solutions, at least those for cylindrical wires and tubes, have been confirmed by extensive experiments such as those performed by Kennelly et. al. [21] [22] (see these references for an extensive bibliography on early work in the area).

Electromagnetic and Thermal Diffusion

The subtleties of electromagnetic (EM) and thermal diffusion on the scale of the ions and electrons in metals is beyond the immediate scope of this study, but some discussion is necessary for completeness and to suggest further investigation. Specifically, a comparison of the underlying PDE's for both EM and thermal diffusion is given as well as the assumptions involved. Next, an overview of simple, linear theories of electric charge relaxation in conductors is given in order to clarify a common mistake found in many EM texts. Finally, a discussion of the skin effect and the assumptions made in deriving the classical skin effect equation are presented.

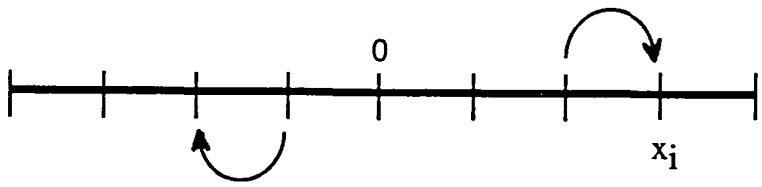

Figure 3.1: A random walk in one-dimension

Partial differential equations of diffusion

It is interesting to begin this section with a development given briefly by Prigogine [33] and with greater detail by Chandrasekhar [7] of the well-known *random walk* problem in one dimension. This problem is the simplest of a general class of stochastic processes called *random flights.*

Consider a particle constrained to move in one dimension (see Figure 3.1).

The particle moves in unit steps at regular time intervals in either direction with an equal probability of one-half ($\frac{1}{2}$), that is, either direction is equally likely and each movement is completely independent of the preceding movements. After N steps the particle could be at any of the positions from $-N \leq x_i \leq N$. The question becomes [7]: What is the probability $W(m,N)$ that the particle arrives at the point m after undergoing N displacements? For details of the derivation one is referred to the references [7] [33], where it is shown that

$$W(m,N) = \frac{N!}{[\frac{1}{2}(N+m)]![\frac{1}{2}(N-m)]!}\left(\frac{1}{2}\right)^N \tag{3.1}$$

where the probability of any given sequence of N steps is $(\frac{1}{2})^N$ and there are $\frac{1}{2}(N+m)$ steps to the right (positive) and $\frac{1}{2}(N-m)$ to the left (negative). The sum of the

steps to the left and right is N, as required, and their difference is m, the point to be achieved. In the case where N is large and $m \ll N$ the asymptotic value is

$$W(m,N) = \sqrt{\frac{2}{\pi N}} e^{-m^2/2N}. \tag{3.2}$$

Substituting $D = \frac{1}{2}nl^2$ and $x = ml$ into equation 3.2, where n is the number of displacements per unit time, l the length of each displacement, and x the resultant displacement, gives

$$W(x,t) = \frac{1}{2\sqrt{\pi Dt}} e^{-x^2/4Dt} \tag{3.3}$$

which is exactly the solution of the one dimensional diffusion equation

$$\frac{\partial W(x,t)}{\partial t} = D\frac{\partial^2 W(x,t)}{\partial x^2}. \tag{3.4}$$

In general the solution is written

$$W(x,t) = \frac{A}{\sqrt{t}} e^{-x^2/4Dt} \tag{3.5}$$

where A is an arbitrary constant. The constant, A, can be determined by solving for

> the total amount of substance M diffusing in a cylinder (infinite half-space) of infinite length and unit cross-section, (Crank [9])

$$M = \int_{-\infty}^{\infty} W(x,t)dx = 2A\sqrt{\pi D}; \tag{3.6}$$

in this case $M = 1$ in equation 3.3. The diffusion equation can therefore be derived as the limit of probability arguments and can be used to quantify how irreversible processes evolve with time. The implication is if the displacement current is neglected then the EM fields are not governed by wave-like phenomena, but by physical processes akin to the random walk.

Similarities Some of the similarities between thermal and EM diffusion can be enumerated by comparing diffusion of heat and electric current density in a conducting half-space where diffusion proceeds in the postive $\hat{z}$-direction. The fundamental equations for one-dimensional linear diffusion of heat and current density are, respectively,

$$\frac{\partial q}{\partial t} = \frac{\mathcal{K}}{\mathcal{C}}\frac{\partial^2 q}{\partial z^2} \tag{3.7}$$

$$\frac{\partial J_x}{\partial t} = \frac{1}{\mu\sigma}\frac{\partial^2 J_x}{\partial z^2}. \tag{3.8}$$

These equations describe *transient* phenomena not necessarily periodic with respect to time. The q in equation 3.7 represents heat energy density (J/m^3) and J_x in equation 3.8 represents current density or the current passing through a unit area in the $\hat{x}$-direction (A/m^2). It is important to consider the multiplying constants and their possible meanings. First, the constants $\mathcal{K}$ and $\mathcal{C}$ in equation 3.7 are the thermal conductivity and the heat capacity per unit volume, respectively. They are mathematically defined by the relationships

$$J_Q = \mathcal{K}(-\nabla T) \tag{3.9}$$

$$\begin{aligned} T &\equiv \text{temperature distribution, } K \\ J_Q &\equiv \text{heat flux, } \frac{J}{m^2 s} \\ \mathcal{K} &\equiv \text{thermal conductivity, } \frac{J}{msK} \end{aligned}$$

$$\mathcal{C} = \frac{dq}{dt} \tag{3.10}$$

$$\begin{aligned} q &\equiv \text{heat energy density, } \frac{J}{m^3} \\ \mathcal{C} &\equiv \text{heat capacity, } \frac{J}{Km^3}. \end{aligned}$$

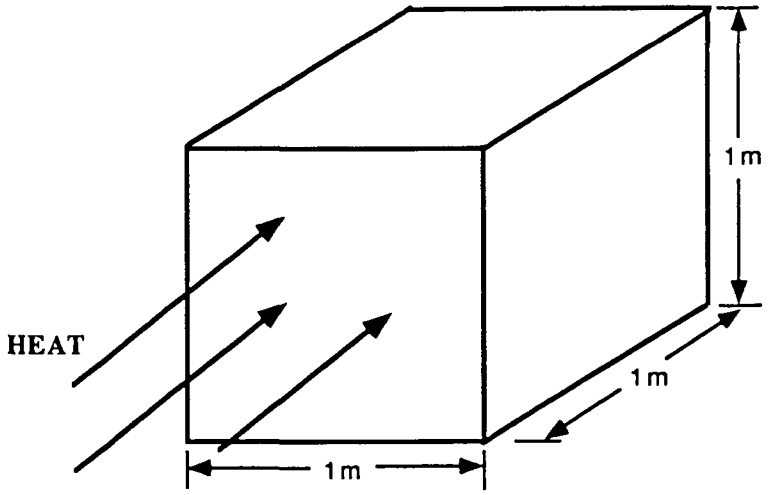

Figure 3.2: A unit volume into which heat flows

In words, the thermal conductivity is the amount of heat energy per unit time (*Watts*) crossing a unit area perpendicularly due to a unit difference in temperature between the two opposite faces one unit of distance apart, that is, due to a unit temperature gradient between the faces (see Figure 3.2).

It is assumed there is no heat lost through the other faces. The heat capacity is the amount of heat energy which must be transferred to a unit volume of substance to raise its temperature by a unit degree (1 K).

Similarly, the defining relations for conductivity and permeability are

$$J_x = \sigma E_x \tag{3.11}$$

$$E_x \equiv \text{electric field intensity, } \frac{V}{m}$$

$$J_x \equiv \text{electric current density, } \frac{C}{m^2 s}$$

$$\sigma \equiv \text{electrical conductivity, } \frac{C}{msV}$$

$$B_y = \mu H_y \tag{3.12}$$

$$
\begin{aligned}
H_y &\equiv \text{magnetic field intensity, } \frac{A}{m} \\
B_y &\equiv \text{magnetic flux density, } T, \left(\frac{Wb}{m^2}\right) \\
\mu &\equiv \text{permeability, } \frac{Wb}{mA}.
\end{aligned}
$$

In words the electrical conductivity is the amount of charge per unit time (*Ampere*) crossing a unit area perpendicularly due to a unit difference in electromotive force (*voltage*) between the two opposite faces one unit distance apart (see Figure 3.2). It is with purpose that the term potential gradient is not used in the electrical case since in general the electric field intensity is not only the gradient of a scalar potential, i.e. $\vec{E} = -\nabla\phi - \partial\vec{A}/\partial t$. The permeability has a less clear interpretation, but one could say it is the amount of magnetic flux or magnetic induction, B_y, produced per unit area due to a unit magnetic field intensity, H_y.

In the two diffusion equations, equations 3.7 and 3.8, the constants appear in pairs, specifically $\mathcal{K}/\mathcal{C}$ and $1/\mu\sigma$. The ratio $\mathcal{K}/\mathcal{C}$ does have meaning and can be interpreted by considering each constant in turn:

$\frac{1}{\mathcal{C}}$ $\equiv$ the reciprocal of heat capacity per unit volume, $\frac{m^3K}{J}$, is the number of cubic meters whose temperature is raised one Kelvin by the addition of one Joule of heat *or* the number of degrees Kelvin by which the temperature of one cubic meter would rise due to the addition of one Joule of heat.

$\mathcal{K}$ $\equiv$ the thermal conductivity, $\frac{J}{sm^2\frac{K}{m}}$, is the amount of heat in Joules that flows in one second through a face of a cube

one meter square in area and one meter
thick due to a temperature difference
of one degree Kelvin between the opposing
faces. It is assumed no heat flows out the
other four faces.

With these definitions the ratio $\mathcal{K}/\mathcal{C}$ has the following meaning:

$$\frac{\mathcal{K}}{\mathcal{C}} \equiv \text{the thermal diffusivity or thermometric conductivity, } \frac{m^3 K}{sm^2 \frac{K}{m}}, \text{ is the number of degrees Kelvin that one cubic meter of substance would rise due to the quantity of heat that flows in one second across a face of the cube one meter square in area and one meter thick due to a temperature difference of one degree Kelvin between the opposing faces. It is assumed no heat flows out the other four faces.}$$

The ratio $\mathcal{K}/\mathcal{C}$ in equation 3.7 is a measure of the rate at which the heat energy density, q, will change in time in the medium ($\partial q/\partial t$) due to a *given* spatial variation of the gradient of heat energy density in the medium ($\nabla \cdot \nabla q \Rightarrow \partial^2 q/\partial z^2$). The term heat energy density can be replaced by the term temperature and the interpretation is the same. In other words, assume one could sit inside a substance with a thermometer and the substance (a cube) has a temperature of T_o K throughout its whole volume (thermal equilibrium) then a heat source with temperature T, where $T > T_o$, must have been applied to one of the faces. If the ratio $\mathcal{K}/\mathcal{C}$ is relatively large, that is, large compared to some standard, then for a given spatial variation of the temperature gradient the rate at which the temperature changes with respect to time will be

Table 3.1: Comparison of thermal diffusivity

substance	Thermal conductivity, K (J/scmK)	Heat capacity, C (J/cm^3K)	Thermal diffusivity, K/C (cm^2/s)
Silver, Ag	4.10	2.48	1.65
Iron, Fe	0.670	3.62	0.185
Air	$2.30(10^{-6})$	.00121	0.00190

relatively large. If the heat source is constant in time then $\mathcal{K}/\mathcal{C}$ is also a measure of how fast the medium will approach steady state, i.e. $\partial T/\partial t = 0$ or $\nabla T = constant$.

For comparison the thermometric conductivities of the following substances are tabulated: silver (Ag), iron (Fe), air (see Table 3.1 with data taken from Hummel [19]).

In the electromagnetic case the constant $1/\mu\sigma$ is somewhat more difficult to interpret. The conductivity, σ, is analogous to thermal conductivity, $\mathcal{K}$, but inversely as explained by Maxwell [26] Art. 803:

> We have to remark in the first place, that in this problem the thermal conductivity of Fourier's medium is to be taken inversely proportional to the electric conductivity of our medium, so that the time required in order to reach an assigned stage in the process of diffusion is greater the higher the electric conductivity. This statement will not appear paradoxical if we remember the result of Art. 655, that a medium of infinite conductivity forms a complete barrier to the process of diffusion of magnetic force.

The analogy between permeability, μ, and heat capacity, $\mathcal{C}$, is not clear and probably cannot be made, but since it appears reciprocally like conductivity the implication is that a conductor with increased permeability relative to free space also requires a greater time "to reach an assigned stage in the process of diffusion." The following is an attempt to extract a meaning for the constant $1/\mu\sigma$;

$\frac{1}{\mu} \equiv \frac{A}{m\frac{Wb}{m^2}}$, is the amount of magnetic field intensity necessary to induce one unit of flux per square meter in a given medium ($Tesla = Wb/m^2$).

$\frac{1}{\sigma} \equiv$ the reciprocal conductivity or resisitivity, ρ, with units $\frac{V}{m\frac{A}{m^2}}$, is the amount of emf developed between opposing faces of one cubic meter of substance due to one Ampere flowing through the cube between opposing faces one square meter in area. No current is assumed to flow out of the other four faces.

A possible meaning for $1/\mu\sigma$ could be:

$\frac{1}{\mu\sigma} \equiv \frac{\frac{W}{m^2}}{\frac{Wb}{m^2}\frac{A}{m^2}}$, the number of Joules of energy flowing in unit time through one square meter due to one Weber of magnetic flux per square meter and one Ampere per square meter. The energy is being stored in the fields and dissipated by Ohmic effects within a unit volume of the conductor.

If there is any analogy with heat then this constant ought to be a measure of a conductor's ability to reach steady state within a given time. This interpretation is in agreement with Heaviside [17] Vol. 1 pg. 346:

> The time-constant of retardation of a conductor varies as the conductivity, as the inductivity [μ], and as the square of the linear dimensions.

> This refers to the intervals of time required to establish a definite proportion of the steady state under the action of steady forces—in bodies of different size, conductivity, and inductivity, but geometrically similar. Here the two properties, conductivity and inductivity, act conjointly, so that, for example, iron is far more obstructive than copper, although its conductivity is much inferior ...

He then continues in the same paragraph to explain some differences between increased conductivity relative to increased "inductivity." It follows:

> It is different with the heat-generation. There the inductivity and conductivity act in opposite senses, for, with the same electric force, the waste [loss] varies as the conductivity, or, with the same current-density, as the resistivity. It results that in cases of skin-conduction of rapidly alternating currents, the resistance per unit area of surface varies directly as the square root of the product of the resistivity (not conductivity), inductivity, and frequency. Thus, whilst we may increase the resistance by increasing the frequency, with a given material, and also by increasing the inductivity, we decrease it by increasing the conductivity, in spite of the fact that the internal obstruction varies as the conductivity and inductivity conjointly. The point to be attended to here is that mere internal obstruction is no necessary bar to effective skin conduction, although, of course, in a given case the resistance is greater than if the conduction were more widespread. It depends on how it is brought about, whether by conductivity or inductivity. This is how it comes about that with the complete internal obstruction of a perfect conductor, with the effective skin reduced to nothing, there is still no resistance, and the slip of electromagnetic waves along them is perfect. But it is different when we obtain the internal obstruction by increasing the inductivity, preserving the conductivity constant. Perfect internal obstruction then means infinite resistance, and no proper slipping of waves at all. If the obstruction be not complete, it will be accompanied by very rapid attenuation of waves running along the surface when the obstruction arises from high inductivity, and by relatively very slight attenuation when it arises from conductivity. (p. 346)

Poynting's theorem is another powerful tool one can utilize in situations involving the flow of EM energy via waves or diffusion. The Maxwell equations describing

quasi-static EM phenomena are

$$\nabla \times \vec{E} = -\frac{\partial \vec{B}}{\partial t} \tag{3.13}$$

$$\nabla \times \vec{H} = \vec{J}_c, \tag{3.14}$$

where displacement current, $\partial \vec{D}/\partial t$, is negligible compared to conduction current, $\vec{J}_c$. The corresponding relationship for energy flow rate is

$$-\oint_S (\vec{E} \times \vec{H}) \cdot d\vec{S} = \iiint_V \frac{\partial}{\partial t}\left[\frac{1}{2}\vec{H} \cdot \vec{B}\right] dV + \iiint_V \vec{E} \cdot \vec{J} dV. \tag{3.15}$$

The term on the left-hand side is the rate of EM energy flow into some volume V through its bounding surface S. The first term on the right is the rate of increase of energy in the magnetic fields, $\vec{H}$ and $\vec{B}$, in the region and the last term is the rate of energy dissipation in the form of Ohmic heating. One may wonder what happened to the term $\frac{\partial}{\partial t}(\frac{1}{2}\vec{E} \cdot \vec{D})$ which is the rate of increase of energy in the electric fields, $\vec{E}$ and $\vec{D}$, but displacement current was originally neglected since it was found to be negligible relative to the conduction current. It therefore appears that energy storage in a given volume element occurs mainly in the magnetic fields, but there is obviously some amount of energy being stored in the electric fields although it is negligibly small in comparison. The units of $1/\mu\sigma$ and its interpretation make sense in the light of the rate of energy flow described by Poynting's relationship, yet it is not as intuitively clear as in the case of heat.

Finally, an infinite speed of propagation is a characteristic of the linear parabolic diffusion equation. Mathematically any process modelled by the linear diffusion equation at a time $t > 0$ is dependent on all the initial data, that is, any point $\vec{r}$ in the solution region has some value which is mathematically nonzero (Duchateau and Zachmann [13]). This fact is in contrast to phenomena modelled by hyperbolic or

wave differential equations where a definite velocity of interaction is observed. The difference was noted by Maxwell [26] Art. 803,

> There is no determinate velocity which can be defined as the velocity of diffusion. If we attempt to measure this velocity by ascertaining the time requisite for the production of a given amount of disturbance at a given distance from the origin of disturbance, we find that the smaller the selected value of the disturbance the greater the velocity will appear to be, for however great the distance, and however small the time, the value of the disturbance will differ mathematically from zero.
>
> This peculiarity of diffusion distinguishes it from wave-propagation, which takes place with a definite velocity. No disturbance takes place at a given point till the wave reaches that point, and when the wave has passed, the disturbance ceases forever.

In the strictest sense linear diffusion is only an approximation to reality due to its infinite propagation velocity, but a very good approximation in many instances.

The word linear is key to the inifinite speed because if the diffusion coefficient, D, in equation 3.4 is a function of the field variable, $D(W(x,t))$, then finite interaction velocities can arise leading to new and interesting phenomena (Vasiliev et. al. [39]). A similar situation occurs when the diffusion coefficient is not a function of the field variable but the media has nonlinear *active* properties. In this case there seems to be an interaction of diffusion and wave processes such that *diffusive pulses* or *travelling fronts* can propagate with definite velocities whereas strictly wavelike disturbances damp out far too quickly to be useful (Vasiliev et. al. [39], Sachdev [34]). A classic example of a system modelled with a nonlinear diffusion equation is the nerve fiber (Scott [36]).

Differences The most obvious difference between thermal and EM diffusion phenomena is seen when the excitation source is periodic in time and therefore can

be represented with time dependence $e^{j\omega t}$. In electrical engineering such quantities are called *phasors*. The relationship between the time domain and the phasor domain is given by

$$J_x(z,t) = Re(J_x(z)e^{j\omega t}) \tag{3.16}$$

where Re represents the real part of the quantity in parentheses or

$$Re(J_x(z)e^{j\omega t}) = J_x(z)\cos(\omega t + \phi(z)). \tag{3.17}$$

The $\phi(z)$ represents any phase due to the function $J_x(z)$. The time derivative is effectively transformed to

$$\frac{\partial}{\partial t} \Longrightarrow j\omega \tag{3.18}$$

and the one-dimensional diffusion equation for current density becomes

$$j\omega J_x = \frac{1}{\mu\sigma}\frac{\partial^2 J_x}{\partial z^2}. \tag{3.19}$$

The dependence in z is assumed. At this point the equation ceases to be parabolic and becomes elliptic, that is, in the phasor domain the solutions do not evolve in time in the sense that field quantities are attempting to penetrate the conductor for the first time (initial transient). The distributions of current have assumed their final steady-state rms values. The fields are still fundamentally oscillatory in time but the general field distribution in space is stationary versus time.

Periodic heat sources are not unprecedented, in fact, for a fixed observation point on earth the sun is such a source, but in comparison, time periodic electrical phenomena hold a far more important position than do transient phenomena. Solutions based on the time periodic assumption are considered almost to the exclusion of transient phenomena in much of electrical engineering.

On a qualitative level there is a distinct difference between heat and electricity. This difference was elucidated by Maxwell in his treatise (see Maxwell [26] Art. 243). To summarize the situation, a conducting body is suspended inside a closed conducting vessel by a silk thread. The outer body is charged relative to some ground thereby giving it some relative potential. The potential of the whole vessel is then raised, including the interior, but the body on the inside shows no signs of this electrification whether it does or does not contact the vessel while inside and it continues to show no effect even if it is removed. On the other hand, if the vessel is heated to some temperature from without, eventually the body inside will also increase in temperature after a given time has elapsed. If the body is taken out it will then cool to the ambient temperature. The difference is given by Maxwell:

> The difference between the phenomena consists in the fact that bodies are capable of absorbing and emitting heat, whereas they have no corresponding property with respect to electricity. A body cannot be made hot without a certain amount heat being supplied to it, depending on the mass and specific heat of the body, but the electric potential of a body may be raised to any extent in the way already described without communicating any electricity to the body ...

He then describes the difference when the body is heated then placed inside the vessel. The vessel will heat until such time as all the initial heat energy has escaped, then it will cool down. He describes this difference with electricity:

> It is impossible to perform a corresponding electrical experiment. It is impossible so to electrify a body, and so to place it in a hollow vessel, that the outside of the vessel shall at first show no signs of electrification but shall afterwards become electrified. It was for some phenomena of this kind that Faraday sought in vain under the name of an absolute charge of electricity.

> Heat may be hidden in the interior of a body so as to have no external action, but it is impossible to isolate a quantity of electricity so as to prevent it from being constantly in inductive relation with an equal quantity of electricity of the opposite kind.
>
> There is nothing therefore among electric phenomena which corresponds to the capacity of a body for heat. This follows at once from the doctrine which is asserted in this treatise, that electricity obeys the same condition of continuity as an incompressible fluid. It is therefore impossible to give a bodily charge of electricity to any substance by forcing an additional quantity of electricity into it. (See Arts. 61, 111, 329, 334.)

As was suspected a corresponding quantity for heat capacity in electromagnetic phenomena is apparently nonexistant.

Skin Effect Approximation

This section highlights aspects of the skin effect phenomena not often considered in low frequency NDT situations. First, charge and field relaxation in conductors are considered on a more fundamental level. Second, assuming that Ohm's law is valid, as is the case in this study, there are other assumptions that must be be valid in order for the classical exponential decay of the fields to exist. These assumptions are enumerated and applied to a single loop coil over an infinite conducting half-space.

Charge and field relaxation in conductors

Fundamentally, any discussion of electromagnetic field interaction with conductors must consider the free electrons of the metal. These electrons are excited by the field and are able to absorb energy from the field. How these electrons interact with the field is the subject of charge relaxation. The following is an overview of simple theories of charge relaxation giving insight to the range of validity of certain standard

assumptions.

Upon application of an electric field to a conductor the free charges rearrange to exactly cancel the applied field, assuming electrostatics. One might ask: How long does it take for the electrons to rearrange and by what process? This question is often answered via a short derivation which utilizes the continuity equation, Ohm's law, and Gauss's law. The charge continuity equation, Gauss's law, and Ohm's law are, respectively,

$$\nabla \cdot \vec{J} = -\frac{\partial \rho_v}{\partial t} \tag{3.20}$$

$$\nabla \cdot \vec{E} = \frac{\rho_v}{\epsilon} \tag{3.21}$$

$$\vec{J} = \sigma \vec{E}. \tag{3.22}$$

Using Ohm's law and Gauss's law the continuity equation can be rewritten

$$\begin{aligned} \nabla \cdot \sigma \vec{E} &= -\frac{\partial \rho_v}{\partial t} \\ \nabla \cdot \vec{E} &= -\frac{1}{\sigma}\frac{\partial \rho_v}{\partial t} \\ \frac{\rho_v}{\epsilon} &= -\frac{1}{\sigma}\frac{\partial \rho_v}{\partial t}. \end{aligned} \tag{3.23}$$

This has a solution

$$\rho_v = \rho_{vo} e^{-\frac{\sigma}{\epsilon}t} \tag{3.24}$$

with a characteristic time

$$\tau_R = \frac{\epsilon}{\sigma}. \tag{3.25}$$

The characteristic time for copper with $\sigma = 58(10^6)\ S/m$ and $\epsilon = \epsilon_o$ is $\tau_R \approx 1.5(10^{-19})s$ which is an extremely short relaxation time, in fact, too short. To compute the average time between consecutive collisions, τ_c, for an electron in copper

use the classical formula [19]:

$$\begin{aligned} \tau_c &= \frac{m\sigma}{N_f e^2}\, s \qquad (3.26) \\ m &= 9.11(10^{-31})\ kg, \text{ free electron mass} \\ \sigma &= 5.8(10^7)\ \frac{S}{m}, \text{ conductivity} \\ N_f &= 6.3(10^{28})\ \frac{1}{m^3}, \text{ free electron density} \\ e &= -1.602(10^{-19})\ C, \text{ electron charge.} \end{aligned}$$

The result is $\tau_c \approx 3.3(10^{-14})\ s$ which is roughly a factor of 10^5 greater than the relaxation time computed via the derivation above. A moment of thought will convince one that it is unreasonable to expect the relaxation of charge to occur in a time faster than the mean time between collisions.

A more complete examination of charge and field relaxation has been given in a number of articles [2] [3] [28] [35]. The detail of their methods is not repeated here, but the conclusions are summarized so a more realistic understanding can be achieved. Their basic assumption is the electrons behave as a free electron gas according to the classic Drude model [19]. Starting with this assumption, there are roughly three stages in the charge and field relaxation process:

1. firstly, the initial electron charge density is relaxed,

2. the electromagnetic fields are expelled from the conductor and any currents are forced to the conductor's surface,

3. finally, the surface currents and exterior oscillatory fields are damped by Ohmic and radiative processes.

Another necessary assumption required for the first stage is total charge neutrality within the volume of the conductor.

In deriving the results for the first stage Ashby [2] and Bochove [3] assume that an electron inside the metal under the influence of an electric field obeys the classical equation of motion with viscous damping due to collisions:

$$\frac{\partial \vec{v}(\vec{r},t)}{\partial t} + \frac{\vec{v}(\vec{r},t)}{\tau_c} = \frac{e\vec{E}(\vec{r},t)}{m}. \tag{3.27}$$

Multiplying this equation by eN_f, the average electron density, gives an equation for the current density, $\vec{J}(\vec{r},t) = eN_f\vec{v}(\vec{r},t)$. After taking the divergence of the resulting equation for the current density and applying the continuity equation and Gauss's law, a second order differential equation for the charge density results,

$$\frac{\partial^2\rho(\vec{r},t)}{\partial t^2} + \frac{1}{\tau_c}\frac{\partial\rho(\vec{r},t)}{\partial t} + \omega_p^2\rho(\vec{r},t) = 0, \tag{3.28}$$

where ω_p is the *plasma frequency*,

$$\omega_p^2 = \frac{N_f e^2}{m\epsilon}. \tag{3.29}$$

The solution to this damped harmonic oscillator equation is

$$\rho(\vec{r},t) = \rho(\vec{r},0)e^{-st} \tag{3.30}$$

$$s = \frac{1}{2\tau_c} \pm j\sqrt{\omega_p^2 - \frac{1}{2\tau_c}} \tag{3.31}$$

$$= \frac{1}{2\tau_c} \pm i\nu \tag{3.32}$$

which shows for $\omega_p\tau_c > \frac{1}{2}$ the charge density has a characteristic relaxation time of $2\tau_c$ with oscillation frequency ν. Using the values for copper given previously

$\omega_p\tau_c \approx 470 \gg \frac{1}{2}$, $2\tau_c \approx 6.6(10^{-14}s)$, and $\nu \approx \omega_p = 1.4(10^{16})Hz$. When $\omega_p\tau_c \ll \frac{1}{2}$, or an extremely poor conductor, the solution gives two characteristic decay times:

$$s^{-1} = \tau_c, \ \frac{\epsilon}{\sigma}. \tag{3.33}$$

There are no oscillations and the greater of the two characteristic times governs the overall relaxation. In most metals $\tau_c \gg \frac{\epsilon}{\sigma}$ so relaxation is governed by the average time between collisions for the electrons.

On discussion of the second stage of the charge and field relaxation Ohanian [28] states that for low dissipative forces, corresponding to high conductivity, the charges on the conductor surface ought to "surge back and forth", due to underdamping in the equation of motion, before settling to their equilibrium positions which implies relaxation time for the second stage ought to be directly proportional to conductivity. Also, for a conductor with the same conductivity the relaxation time of the second stage should increase with the linear dimensions of the conductor.

The argument begins with the three-dimensional diffusion equation for magnetic flux density,

$$\frac{\partial \vec{B}}{\partial t} = \frac{1}{\mu\sigma}\nabla^2\vec{B}. \tag{3.34}$$

Assuming a characteristic time and length (metal thickness) one writes

$$\frac{\partial \vec{B}}{\partial t} \sim \frac{\vec{B}}{\tau_D} \tag{3.35}$$

$$\nabla^2\vec{B} \sim \frac{\vec{B}}{\ell^2} \tag{3.36}$$

$$\tau_D \sim \mu\sigma\ell^2. \tag{3.37}$$

The characteristic *diffusion time* is the quantity $\tau_D \sim \mu\sigma\ell^2$ and this has the given dependence on conductivity and conductor size. For a copper sheet with thickness

of $1mm$, this relationship gives $\tau_D \sim 100\mu s$. The diffusion time is a characteristic measure of how quickly diffusion will proceed to the steady state.

The third stage is concerned with the damping of the surface currents and oscillations in the external fields. According to Ohanian the calculation of τ_S, as he denotes it, is difficult and depends on the conductor geometry as well as its electrical parameters. In this case the conductor is considered a resonant cavity which has some Ohmic losses. If the conductor is of a standard shape, say a cuboid or circular cylinder, then the external fields can be expanded in terms of characteristic normal modes or eigenfunctions. One can then write the time constant as

$$\tau_S \sim \frac{Q\ell'}{c}, \tag{3.38}$$

where Q is a function of geometry and conductivity and is related to the common circuit "Q" (see Jackson [20] pg. 356), ℓ' is a characteristic length related to the physical size of the conductor and c is the speed of light in a vacuum. Ohanian gives a calculation for a copper "beer can" and finds $\tau_S \approx 1\mu s$.

In each case above, the characteristic times, while dependent on conductor dimensions, are vanishingly small relative to any given measurement time found in NDT. The relaxation process is therefore inconsequential to the problems of NDT, but it is not outside the scope of the basic physics of the skin effect and field diffusion in conductors. These types of consideration become more important as the frequency is increased or the conductor becomes superconducting (see Casimir and Ubbink [6] parts 2, 3).

Assumptions for the classical skin effect

The classical skin effect solution for the diffusion of current density in the phasor domain,

$$\begin{aligned} j\omega J_x(z) &= \frac{1}{\mu\sigma}\frac{\partial^2 J_x(z)}{\partial z^2} \\ J_x(0) &= J_{xo}, \end{aligned} \tag{3.39}$$

is well known and can be written in terms of the skindepth

$$\begin{aligned} J_x(z) &= J_{xo}e^{-(1+j)\frac{z}{\delta}}\ \frac{A}{m^2} \\ \delta &= \sqrt{\frac{2}{\omega\mu\sigma}}\ m, \end{aligned} \tag{3.40}$$

or in the time domain the solution becomes

$$J_x(z,t) = Re(J_x(z)e^{j\omega t}) = J_{xo}e^{-\frac{z}{\delta}}\cos(\omega t - \frac{z}{\delta})\ \frac{A}{m^2}. \tag{3.41}$$

Inherent in this derivation are certain assumptions which lead to the classic exponential decay of the fields and currents.

There are at least three main assumptions which must be satisfied in order for the exponential decay to be a reasonable approximation (see Smith [38]). Firstly, assume the fields are confined to within a distance of about three classical skin-depths of the surface of the conductor, $\Delta \approx 3\delta$; the other assumptions follow (see Figure 3.3):

1. the conductor is considered a good conductor, that is, $\frac{\sigma}{\omega\epsilon} \gg 1$, therefore displacement current can be neglected,

2. the minimum radius of curvature, R_{min}, and the minimum thickness, t_{min}, of the conductor obey the relationships:

$$R_{min} \gg \Delta \tag{3.42}$$

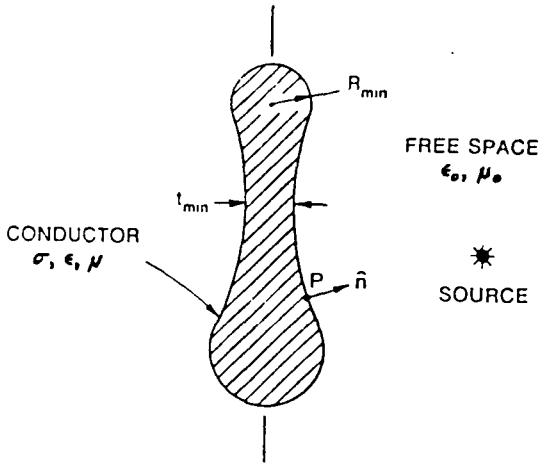

(a)

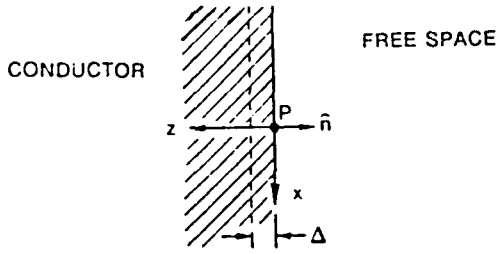

(b)

Figure 3.3: A representative conductor shape, (a) conductor, (b) conductor surface after Smith

$$t_{min} > 2\Delta, \tag{3.43}$$

3. the variations of the fields in directions other than the direction normal to the conductor, the local $\hat{z}$-direction, and within a distance Δ of the surface are small compared to the variation of the field in the direction normal to the surface, that is,

$$\left|\frac{\partial^2 F_x}{\partial x_i^2}\right| \ll \left|\frac{\partial^2 F_x}{\partial z^2}\right| \tag{3.44}$$

$$\left|\frac{\partial^2 F_y}{\partial x_i^2}\right| \ll \left|\frac{\partial^2 F_y}{\partial z^2}\right| \tag{3.45}$$

$$\left|\frac{\partial^2 F_z}{\partial x_i^2}\right| \ll \left|\frac{\partial^2 F_z}{\partial z^2}\right| \tag{3.46}$$

$F \equiv$ any field variable

$x_i = x,\ y.$

Assuming a field dependence as in equation 3.40 these relationships can be rewritten as follows [38]:

$$\frac{\delta^2}{2}\left|\frac{\partial^2 F_u/\partial x_i^2}{F_u}\right|_{w=0} \ll 1 \tag{3.47}$$

$$\frac{\delta^2}{2}\left|\frac{\partial^2 F_v/\partial x_i^2}{F_v}\right|_{w=0} \ll 1 \tag{3.48}$$

$$\frac{\delta^2}{2}\left|\frac{\partial^2 F_w/\partial x_i^2}{F_w}\right|_{w=0} \ll 1 \tag{3.49}$$

$F \equiv$ any field variable

$x_i = u,\ v$

where the "running" coordinates (u, v, w) are the local coordinates on the conductor surface $w = 0$ and have replaced (x, y, z).

The first assumption is a standard one and needs no discussion. The second assumption essentially relates frequency and material parameters embodied in $\Delta = 3\delta$ to the minimum curvature and thickness of the body. If the minimum curvature and minimum thickness are fixed in advance they can be rewritten as

$$\omega \gg \frac{18}{R_{min}^2 \mu\sigma} \tag{3.50}$$

$$\omega > \frac{72}{t_{min}^2 \mu\sigma} \tag{3.51}$$

and the frequency fixed by the larger of the two results. Qualitatively, these requirements ensure no geometry is assumed, given frequency and material parameters, which would allow significant field interaction throughout the conductor. In other words, the dimensions of the conductor are large relative to the depth of penetration of the field quantities so the field locally sees a relatively infinite conductor. The choice of $\Delta = 3\delta$ implies the field will have decayed to $e^{-3} \approx 0.05$ its value at the surface, therefore, no significant change in the overall field configuration will occur due to a perturbation below this distance. This assumption has been verified somewhat by Hagemaier [16] where conductivity measurements on a varying thickness metal with known conductivity showed as the metal thickness increased beyond approximately 2.8δ the measured conductivity equalled the known conductivity.

The final assumption is often overlooked, but is important since it imposes restrictions on the variation of the field distribution at the conductor. It more generally implies that one must consider the source of the exciting field and its proximity and dimensions realtive to the conductor. The last assumption has obvious implications for eddy current NDT inspection where finite dimension coils are used as the exciter/detector. The assumptions one and three above are closely related and may be

equivalent in some instances.

Smith [38] applies these assumptions to three common situations: a plane wave incident on a conducting half-space, an inifinitely long current-carrying wire, and a line current over a conducting half-space. For each case he shows the classical skin effect approximation to be a very good approximation to the field decay subject to these assumptions. Specifically, for the line current over a half-space he shows the exponential decay is valid for the condition $(d/\delta)^2 \gg 1$ where d is the height of the wire above the half-space. He also shows, via a pair of plots, the decay of the magnitude of the magnetic field in the half-space is faster than $e^{-z/\delta}$ when the line current is relatively close to the conductor or $(d/\delta)^2 \leq 1$ and z is taken directly under the line current in the conductor. Lord [25] solved the same problem via the two-dimensional finite element method and obtained similar field behavior (see Figure 3.4).

The solution for the magnetic vector potential of a single loop current above a two-conductor layered half-space (see Figure 3.5) is given by Dodd and et. al. [12] eqn. (3.40) as (using his notation)

$$A_\phi^{(IV)}(r,z) = \mu I r_o \int_0^\infty J_1(\alpha r_o) J_1(\alpha r) e^{-\alpha_o \ell} \times \left[\frac{2\alpha\beta_1 e^{(\alpha_1+\alpha_2)c} e^{\alpha_2 z}}{(\alpha_o-\beta_1)(\beta_1-\beta_2)+(\alpha_o+\beta_1)(\beta_1+\beta_2)e^{2\alpha_1 c}} \right] d\alpha \quad (3.52)$$

where

$$\begin{aligned} \alpha &\equiv \text{the separation constant} \\ \alpha_o &= \sqrt{\alpha^2 - \omega^2\mu_o\epsilon_o} \approx \alpha \end{aligned} \quad (3.53)$$

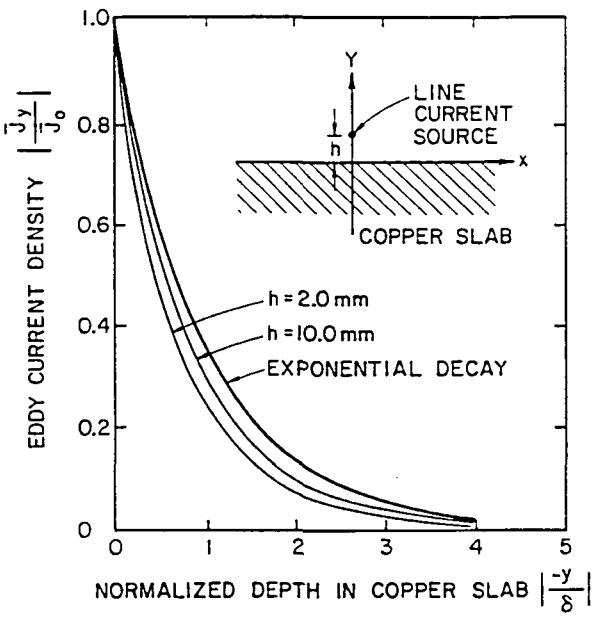

Figure 3.4: Current density decay versus proximity of conductor after Lord

$$\alpha_i = \sqrt{\alpha^2 - \omega^2\mu_i\epsilon_i + j\omega\mu_i\sigma_i} \approx \sqrt{\alpha^2 + j\omega\mu_i\sigma_i} \tag{3.54}$$

$$\beta_i = \frac{\mu_o}{\mu_i}\alpha_i \tag{3.55}$$

$$i = 1,\ 2$$

If the cladding thickness, c, is allowed to go to zero and the conductor is nonmagnetic equation 3.52 becomes

$$A_\phi^{(IV)}(r,z) = \mu_o I r_o \int_0^\infty J_1(\alpha r_o) J_1(\alpha r) e^{-\alpha\ell} \left[\frac{\alpha e^{\alpha 2 z}}{\alpha + \alpha_2}\right] d\alpha. \tag{3.56}$$

Following the method used by Smith and rewriting the parameters as

$$\alpha = k_o\xi \tag{3.57}$$

$$k_o = \frac{2\pi}{\lambda} = \omega\sqrt{\mu_o\epsilon_o} \tag{3.58}$$

$$\xi \equiv \text{dimensionless parameter} \tag{3.59}$$

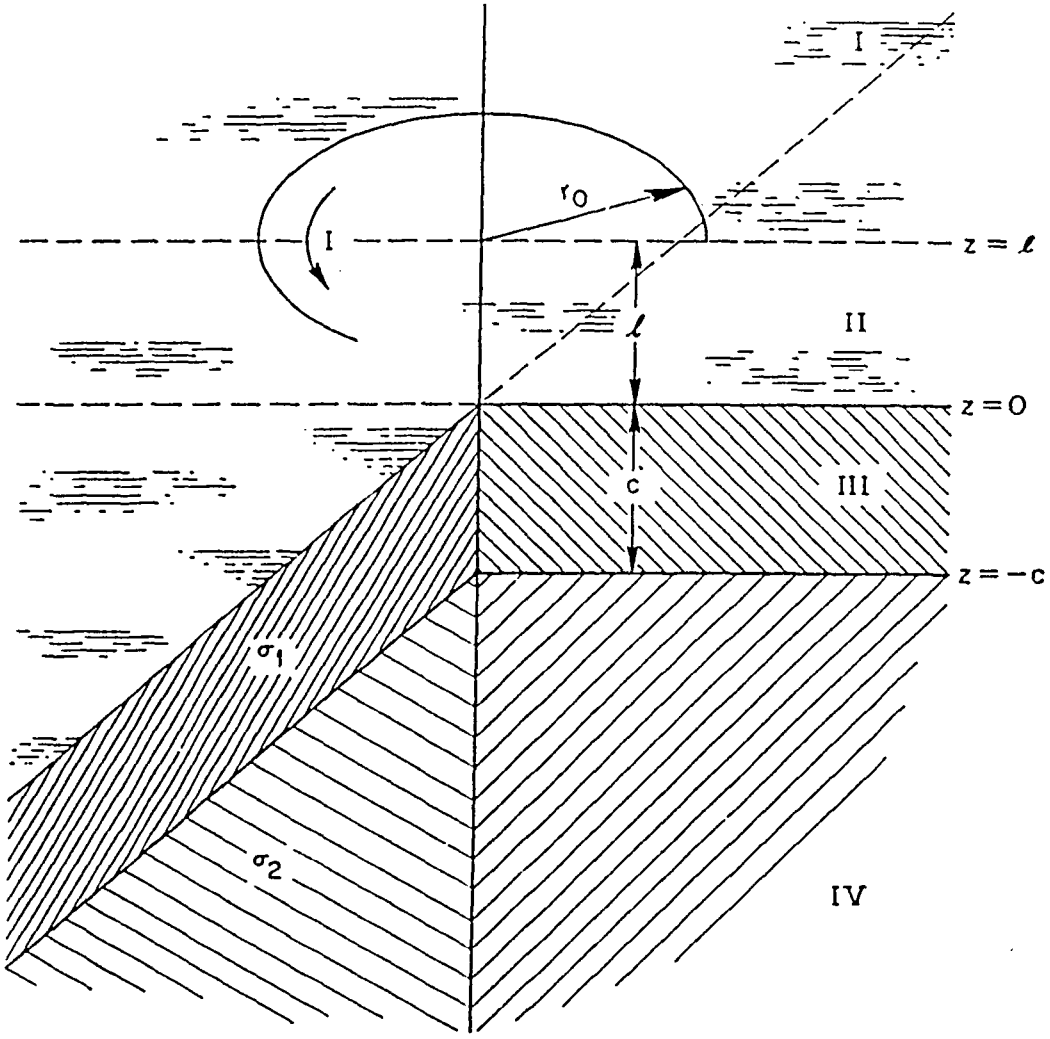

Figure 3.5: Delta function coil above a two-conductor plane after Dodd et. al.

$$\omega\mu_o\sigma_2 = \frac{2}{\delta^2} \tag{3.60}$$

$$\frac{\sigma_2}{\omega\epsilon_o} = \frac{2}{(k_o\delta)^2}, \tag{3.61}$$

gives the vector potential

$$A_\phi^{(IV)}(r,z) = \mu_o I k_o r_o \int_0^\infty J_1(k_o r_o \xi) J_1(k_o r \xi) e^{-k_o \ell \xi} \times \left[\frac{\xi e^{\sqrt{\xi^2 + j2/(k_o\delta)^2}\, k_o z}}{\xi + \sqrt{\xi^2 + j2/(k_o\delta)^2}} \right] d\xi. \tag{3.62}$$

The Bessel function of the first kind and order one, $J_1(x)$, is finite and oscillatory for all values of real x, also, the term in brackets, $[\cdot]$, is finite and bounded for all values of ξ, $0 \leq \xi < \infty$, consequently the integrand is significant for values of ξ where the condition

$$\xi \leq \frac{3}{k_o \ell} \tag{3.63}$$

is true. Defining $\xi_{max} = 3/(k_o\ell)$ then for $\xi_{max}^2 \ll 2/(k_o\delta)^2$ or approximately $(\delta/\ell)^2 \ll 1$ the square root term becomes

$$\sqrt{\xi^2 + j2/(k_o\delta)^2} \approx \sqrt{j2/(k_o\delta)^2} = \frac{(1+j)}{k_o\delta}. \tag{3.64}$$

Using this result, the vector potential in equation 3.62 can be rewritten

$$A_\phi^{(IV)}(r,z) = \mu_o I k_o r_o e^{(1+j)z/\delta} \int_0^\infty J_1(k_o r_o \xi) J_1(k_o r \xi) e^{-k_o \ell \xi} \times \left[\frac{\xi}{\xi + (1+j)/(k_o\delta)} \right] d\xi \tag{3.65}$$

which shows the classic dependence on z.

CHAPTER 4. RESULTS

The following chapter compares the finite element solution to the integral solutions of Dodd et. al. [12] for an air-core coil over a conducting half-space and for a two-coil differential probe inside a conducting tube. Measurements of air-core coils over conducting half-spaces (approximate) were performed and the results are compared with the finite element and integral solutions.

Integral Solutions

Analytical solutions are important in spite of the simplifying assumptions necessary in their derivation. They are useful for comparison and verification of more robust and flexible numerical techniques such as the finite element method (FEM). For this study a set of FORTRAN-77 routines were developed to compute the magnetic vector potential and eddy currents, $\vec{A}$ and $\vec{J}_e = -j\omega\sigma\vec{A}$, in conducting tubes and half-spaces. The routines are based on a set of integral equations derived by Dodd [10], but given in a more useful form in Dodd et. al. [12].

For a rectangular cross-section coil above a two-conductor half-space (see Figure 4.1) the vector potential for regions three and four are, respectively,

$$A_\phi^{(3)}(\rho,z) = \mu n I \int_0^\infty \frac{1}{\alpha^2\alpha_o} J(\rho_2,\rho_1) J_1(\alpha\rho)(e^{-\alpha_o \ell 1} - e^{-\alpha_o \ell 2})$$

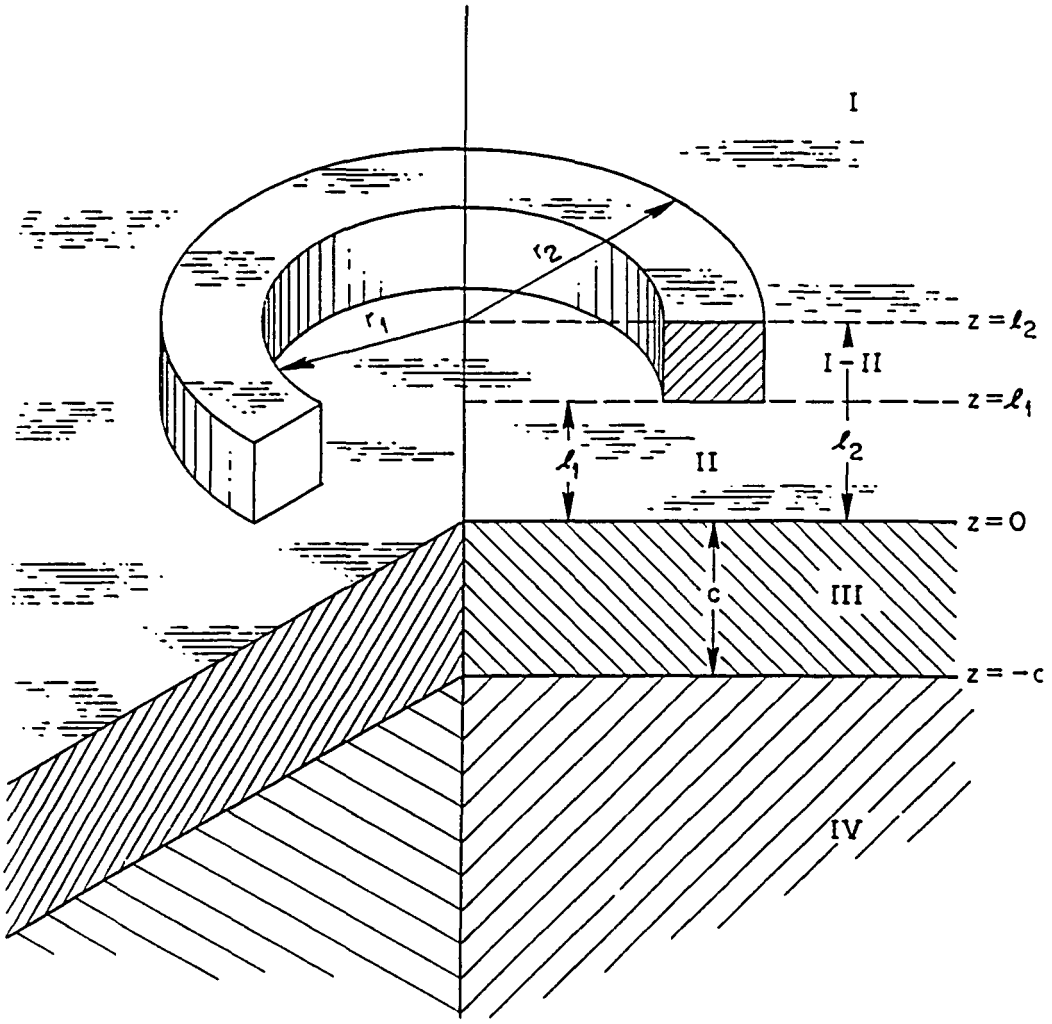

Figure 4.1: Geometry for a coil over a conducting half-space after Dodd et. al.

$$\times \left[\frac{\alpha(\beta_1+\beta_2)e^{2\alpha_1 c}e^{\alpha_1 z} + \alpha(\beta_1-\beta_2)e^{-\alpha_1 z}}{(\alpha_o-\beta_1)(\beta_1-\beta_2)+(\alpha_o+\beta_1)(\beta_1+\beta_2)e^{2\alpha_1 c}} \right] d\alpha \quad (4.1)$$

$$A_\phi^{(4)}(\rho,z) = \mu n I \int_0^\infty \frac{1}{\alpha^2\alpha_o} J(\rho_2,\rho_1) J_1(\alpha\rho)(e^{-\alpha_o \ell 1} - e^{-\alpha_o \ell 2})$$

$$\times \left[\frac{2\alpha\beta_1 e^{(\alpha_2+\alpha_1)c}e^{\alpha_2 z}}{(\alpha_o-\beta_1)(\beta_1-\beta_2)+(\alpha_o+\beta_1)(\beta_1+\beta_2)e^{2\alpha_1 c}} \right] d\alpha \quad (4.2)$$

$$J(\rho_2,\rho_1) \equiv \int_{\alpha\rho_1}^{\alpha\rho_2} x J_1(x)dx$$

$$\alpha_o \equiv \sqrt{\alpha^2 - R_s^2\omega^2\mu_o\epsilon_o} \approx \alpha$$

$$\alpha_i \equiv \sqrt{\alpha^2 - R_s^2\omega^2\mu_i\epsilon_i + jR_s^2\omega\mu_i\sigma_i} \approx \sqrt{\alpha^2 + jR_s^2\omega\mu_i\sigma_i}$$

$$\beta_i \equiv \frac{\mu_o}{\mu_i}\alpha_i$$

$$i = 1,\ 2$$

$$\rho,\ \rho_1,\ \rho_2 \equiv r,\ r_1,\ r_2.$$

$$I,\ n \equiv \text{current per turn, turn density}$$

$$In \equiv \text{coil current density, } J_\phi.$$

The α's and β's are multiplied by the coil mean radius and all coil dimensions are divided by the mean radius which, in effect, normalizes all physical dimensions. If the cladding material of region three in Figure 4.1 is the same as the material of region four and region four is nonmagnetic the above expressions simplify to

$$A_\phi^{(3,4)} = \mu_o n I \int_0^\infty \frac{1}{\alpha_o\alpha} J(\rho_2,\rho_1) J_1(\alpha\rho)(e^{-\alpha_o \ell 1} - e^{-\alpha_o \ell 2}) \left[\frac{e^{\alpha_1 z}}{\alpha_o+\alpha_1} \right] d\alpha. \quad (4.3)$$

The inductance in air and the impedance of the coil above a single conductor half-space are, respectively,

$$L_o = 2\pi\mu_o n^2 R_s \int_0^\infty \frac{1}{\alpha_o^3\alpha^3} (J(\rho_2,\rho_1))^2$$

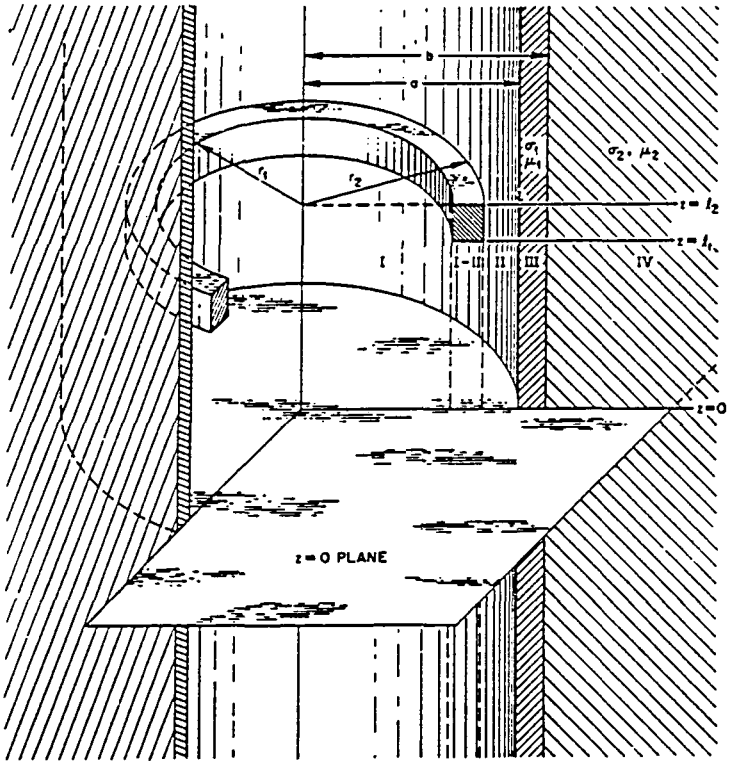

Figure 4.2: Geometry for a coil inside a two conductor tube after Dodd et. al.

$$\times \left[\alpha_o(\ell_2 - \ell_1) + e^{-\alpha_o(\ell_2-\ell_1)} - 1\right] d\alpha \tag{4.4}$$

$$Z = j\omega 2\pi\mu_o n^2 R_s \int_0^\infty \frac{1}{\alpha_o^3 \alpha^3} (J(\rho_2, \rho_1))^2 \left\{\alpha_o(\ell_2 - \ell_1) + e^{-\alpha_o(\ell_2-\ell_1)} - 1 \right.$$
$$\left. + \frac{1}{2}\left[e^{-\alpha_o \ell_2} - e^{-\alpha_o \ell_1}\right]^2 \left[\frac{\alpha_o - \alpha_1}{\alpha_o + \alpha_1}\right]\right\} d\alpha. \tag{4.5}$$

Equations 4.3, 4.4, and 4.5 were coded in FORTRAN. Analogous expressions for the vector potential and coil impedance in a two-conductor tube, as shown in Figure 4.2, exist and one is referred to the references for these expressions. For the tube case the vector potential and impedance are functions of the modified Bessel functions $I_\nu(x)$ and $K_\nu(x)$ (see Abramowitz and Stegun [1]).

When the dimensions are normalized to the coil mean radius a dimensionless

parameter, $R_s^2\omega\mu\sigma$, arises. This parameter is useful from the point of view modelling. The vector potential can be written

$$A_\phi^{(3,4)} = A_\phi^{(3,4)}(\rho, z, \rho_1, \rho_2, \ell_1, \ell_2, \mu, J_\phi, R_s^2\omega\mu\sigma) \tag{4.6}$$

with the coordinates and physical dimensions normalized to the coil mean radius. If the relative dimensions are held constant as well as the permeability and current density the vector potential is relatively unchanged as long as $R_s^2\omega\mu\sigma$ remains constant. For example, if the original half-space with conductivity σ_a and operating frequency ω_a is replaced by a half-space with conductivity σ_b and frequency ω_b such that $\sigma_b > \sigma_a$ then the solution is unchanged if $\omega_a\sigma_a = \omega_b\sigma_b$ or, in other words, if the operating frequency, ω_b, is lowered. Alternatively, if the coil mean radius is increased, but the relative dimensions are unchanged, the solution will remain unchanged if the frequency, conductivity, or some combination of the two are taken so that $R_s^2\omega\mu\sigma$ remains constant. Obviously the coil is physically larger, therefore, absolute values of parameters such as inductance and impedance will change, but it is the *relative* or *normalized* values that remain unchanged. This parameter is more conveniently written in terms of the classical skin depth, δ_s; it follows:

$$\begin{aligned} \frac{2}{\delta_s^2} &= \omega\mu\sigma \\ \Longrightarrow R_s^2\omega\mu\sigma &= 2\left(\frac{R_s}{\delta_s}\right)^2 \\ \Longrightarrow R_s\sqrt{\pi f\mu\sigma} &= \frac{R_s}{\delta_s} \end{aligned} \tag{4.7}$$

One must be careful when applying the same reasoning to the permeability since the permeability also appears in the boundary conditions. The components of the vector potential (scalar potential) are continuous across material boundaries which

Table 4.1: Coil inductance in air, impedance, and normalized impedance versus changing parameters, $R_s/\delta_s = 1$

lift-off=0 mm	Inductance, L_o (μH)	Resistance, R (Ω)	Reactance, X (Ω)	Normalized resistance, $R/\omega L_o$	Normalized reactance, $X/\omega L_o$
standard model, turns=160	87.3	1.67	13.0	0.116	0.902
$10\sigma_1$, f/10	87.3	0.167	1.30	0.116	0.902
$2R_s$, f/4, turns=640	2790	13.4	104	0.116	0.902
μ/μ_1=1, f/10	873	1.67	13.0	0.116	0.902
μ/μ_1=1/10, f/10	87.3	0.0852	2.06	0.0590	1.43

is sufficient to ensure continuity of the tangential electric field intensity and normal magnetic flux density ($\vec{E} = -\nabla\phi - \partial\vec{A}/\partial t$, $\vec{B} = \nabla \times \vec{A}$). The normal derivatives of the vector potential (scalar potential) must be discontinuous across material boundaries with discontinuous μ and ϵ in order for the normal component of the electric flux density and the tangential magnetic field intensity to be continuous in the absence of surface charges and perfect conductors ($\vec{D} = \epsilon(-\nabla\phi - \partial\vec{A}/\partial t)$, $\vec{H} = \frac{1}{\mu}\nabla \times \vec{A}$). The ratio of permeabilities is then a factor since

$$\vec{H}_a\Big|_{tangent} = \vec{H}_b\Big|_{tangent} \tag{4.8}$$

$$\Longrightarrow \frac{1}{\mu_a}\nabla \times \vec{A}_a\Big|_{tangent} = \frac{1}{\mu_b}\nabla \times \vec{A}_b\Big|_{tangent}, \tag{4.9}$$

therefore, for the solution to remain relatively unchanged not only must $R_s^2\omega\mu\sigma$ remain constant but the ratios of the permeabilities, $\mu_i/\mu_{i+1} \quad i = 1, 2, 3, \ldots, m$, must remain constant. In this study all conductors are considered nonmagnetic. As a demonstration of the above ideas refer to Figure 4.3 and Table 4.1.

The magnitude of the eddy current density on the surface of the conductor

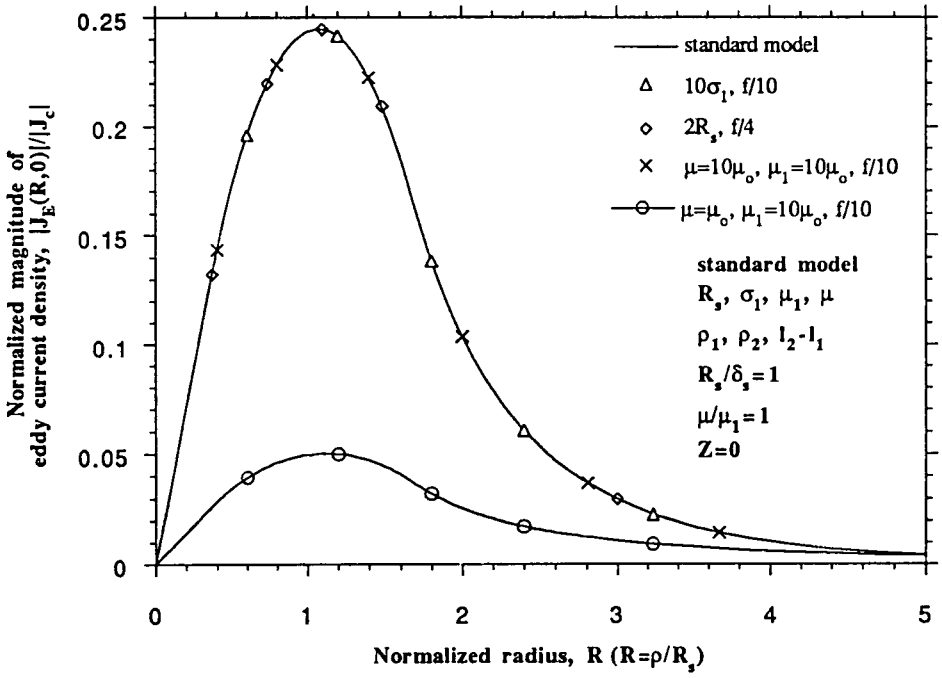

Figure 4.3: Induced eddy current density on the conductor surface, computed analytical solution

($Z = 0$) normalized to the current density of the coil, $|J_e|/|J_c|$, is plotted versus the normalized radius, $R = \rho/R_s$; the normalized radius equal to zero corresponds to the axis of the coil. Note the peak current magnitude occurs approximately under the coil mean radius and the current density goes to zero at $R = 0$ which is reasonable. The solid line corresponds to the *standard model* for this study whose physical parameters are discussed later. The graph shows how the solution remains constant with the variation of parameters such as conductivity, coil mean radius, and permeabilty, while the dimensionless parameter and the ratio of permeabilities remain constant, $R_s/\delta_s = 1$ and $\mu/\mu_1 = 1$. The permeability μ refers to the medium above the conductor. When the permeability of the conductor, μ_1, is increased by a factor of ten relative to the medium above the conductor ($\mu/\mu_1 = 1/10$) the induced current density is markedly reduced. In Table 4.1 the inductance, impedance, and normalized impedance are given which correspond to the cases of Figure 4.3. Here one notices the absolute values of inductance and impedance change for each case but the normalized impedance remains unchanged, except for the case noted above. If only the normalized impedance is considered then a model can theoretically be constructed which will behave in a similar fashion as other coils with the same relative dimensions and physical parameters. This is important from the point of view of finite element modelling because a single mesh can be used to model various situations without having to regenerate the mesh, which can often be very tedious.

Coil Above a Conductor

First, a coil over a conducting half-space (infinite thickness) is investigated. Specifically, the decay of the eddy currents induced in the half-space are compared

with the classical exponential decay for various situations. Second, the conductor is allowed to be of finite thickness and the decay and distribution of the eddy currents are again compared with exponential decay.

Eddy currents in a half-space

The coil dimensions chosen for the coil-over-half-space finite element model, or standard model, are defined by the following parameters:

$$
\begin{aligned}
R_s &= 2.667\ mm \equiv 0.105\ in \\
\rho_1 &= 0.889\ mm = \frac{1}{3}R_s \\
\rho_2 &= 4.445\ mm = \frac{5}{3}R_s \\
\ell_2 - \ell_1 &= 1.778\ mm = \frac{2}{3}R_s, \text{ (coil thickness)} \\
\sigma_1 &= 1351\ \frac{S}{mm}, \text{ (stainless steel)} \\
\mu_1 &= \mu_o \\
\mu &= \mu_o, \text{ (medium above conductor)} \\
\text{turns} &= 160
\end{aligned}
$$

These dimensions correspond to those used by Mottl [27] in a similar investigation. The following results should be considered representative of air-core coils over conductors of relatively infinite and finite thickness. No attempt is made to be exhaustive in terms of coil sensitivity to various construction parameters (see Capobianco et. al. [5]).

Eddy current density in the radial direction Figure 4.3 and Figures 4.4 to 4.7 summarize the variation of induced eddy current density in the radial direction

versus changing parameters. The similarity of solutions when R_S/δ_S is held constant is shown in Figure 4.3. Altering the ratio of permeabilities μ/μ_1 alters the solution in spite of R_S/δ_S remaining constant which is also shown in Figure 4.3. Increasing coil lift-off and reducing R_S/δ_S both reduce the induced current density as does increasing depth into the conductor (see Figures 4.4, 4.5, 4.6). The associated phase in each is case is plotted and shows the increased lag as distance from the coil increases. In general the majority of the current density is localized to a region within approximately three coil mean radii relative to the axis of the coil. The localization effect sharpens as R_S/δ_S increases as is shown in Figure 4.7. Also, the current density varies significantly with respect to normalized radius which completely violates the assumption of source uniformity for the classical skin effect solution. The localization of the field suggests detection of defects will take place only within close proximity ($R \leq 3$) of the coil. Finally, similar data computed by Mottl [27] varies from the analytical and FEM solutions computed here, especially as radius increases (see Figure 4.4).

Eddy current density in the axial direction The results in the previous section show clearly the greatest eddy current density occurs approximately at the coil mean radius. From this observation it is a reasonable assumption that a disruption in the steady state field configuration due to a defect near the mean radius would result in a relatively large impedance change for any given defect, but this study does not attempt to prove this assumption. The current density magnitude and phase have been plotted for multiples of the mean radius and depth into the conductor normalized to the classical skin depth (classical DoP), see Figures 4.8 to 4.11. The Figures 4.8, 4.9, and 4.10 show the effect of the changing parameter R_S/δ_S for the

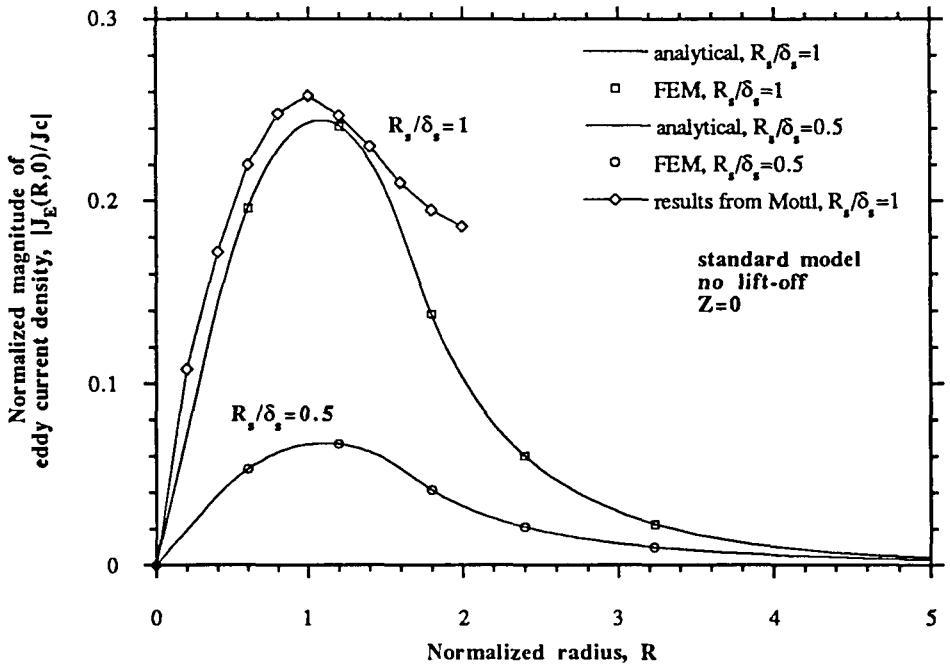

(a)

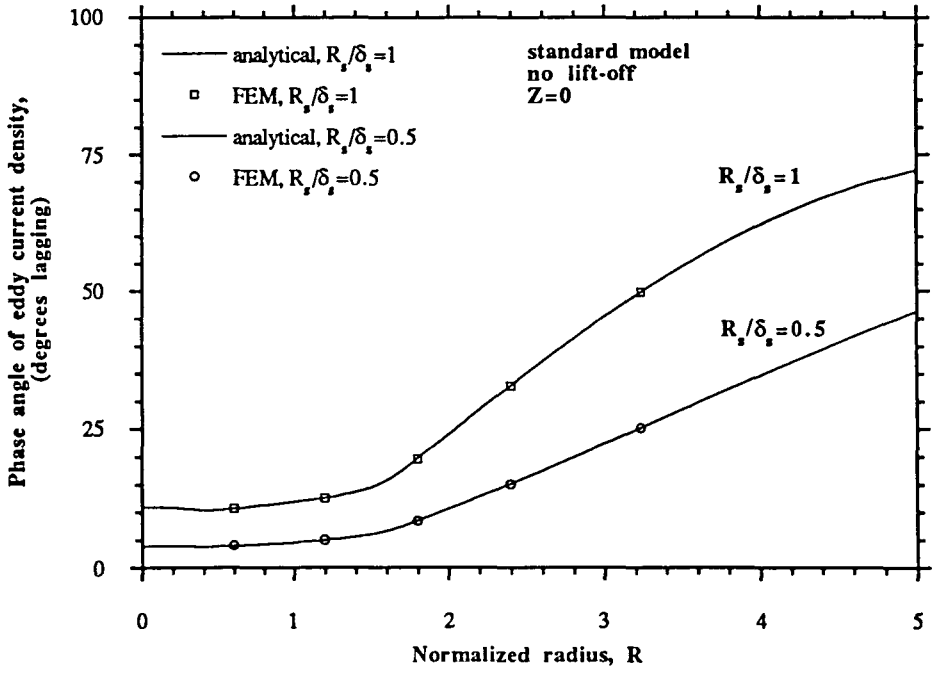

(b)

Figure 4.4: Induced eddy current density in the radial direction versus R_S/δ_S, (a) magnitude, (b) phase

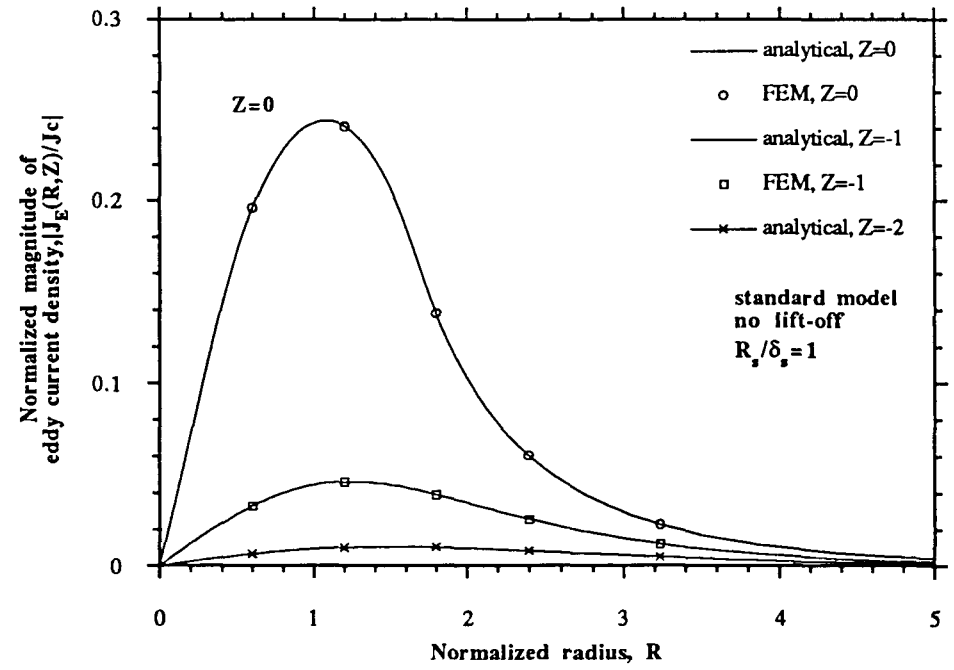

(a)

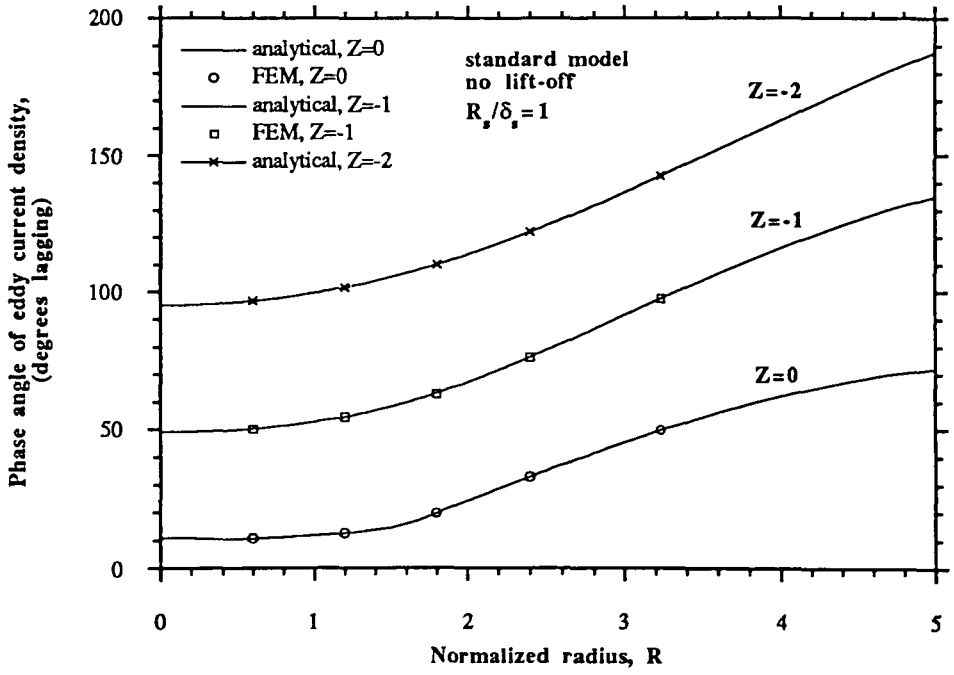

(b)

Figure 4.5: Induced eddy current density in the radial direction versus Z, (a) magnitude, (b) phase

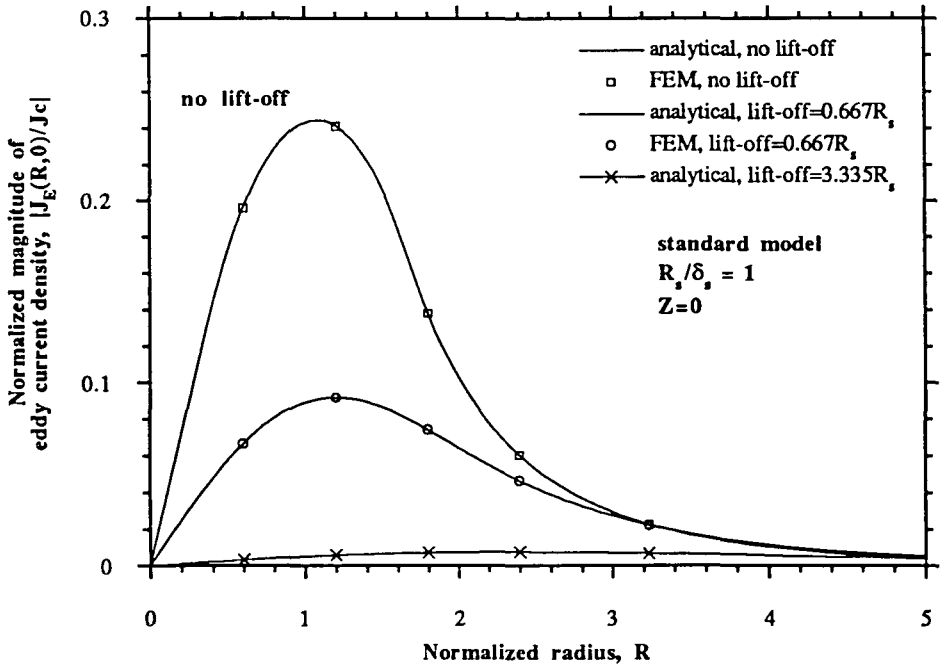

(a)

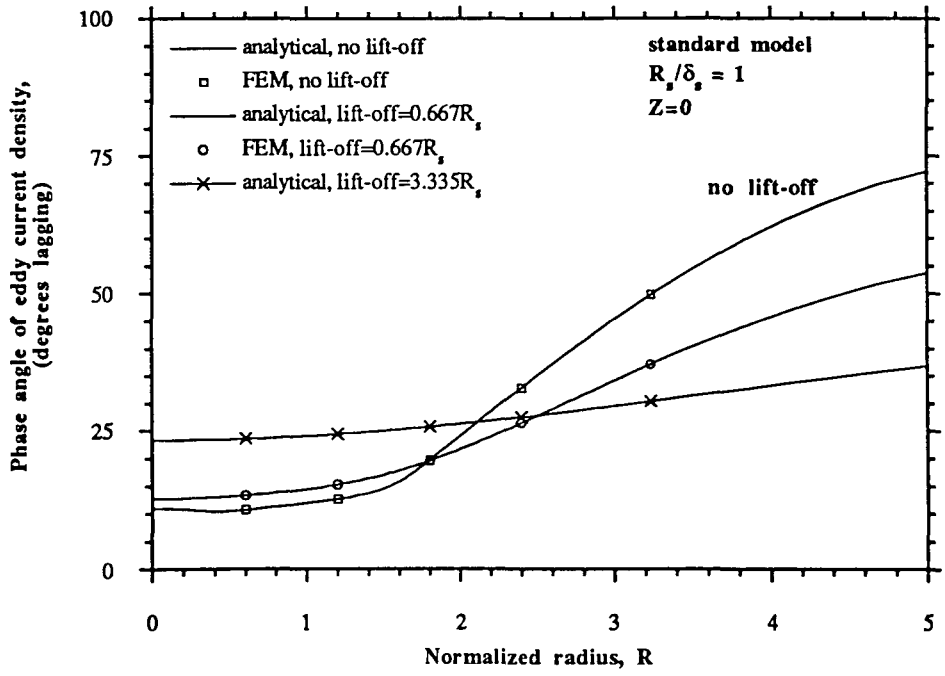

(b)

Figure 4.6: Induced eddy current density in the radial direction versus coil lift-off, (a) magnitude, (b) phase

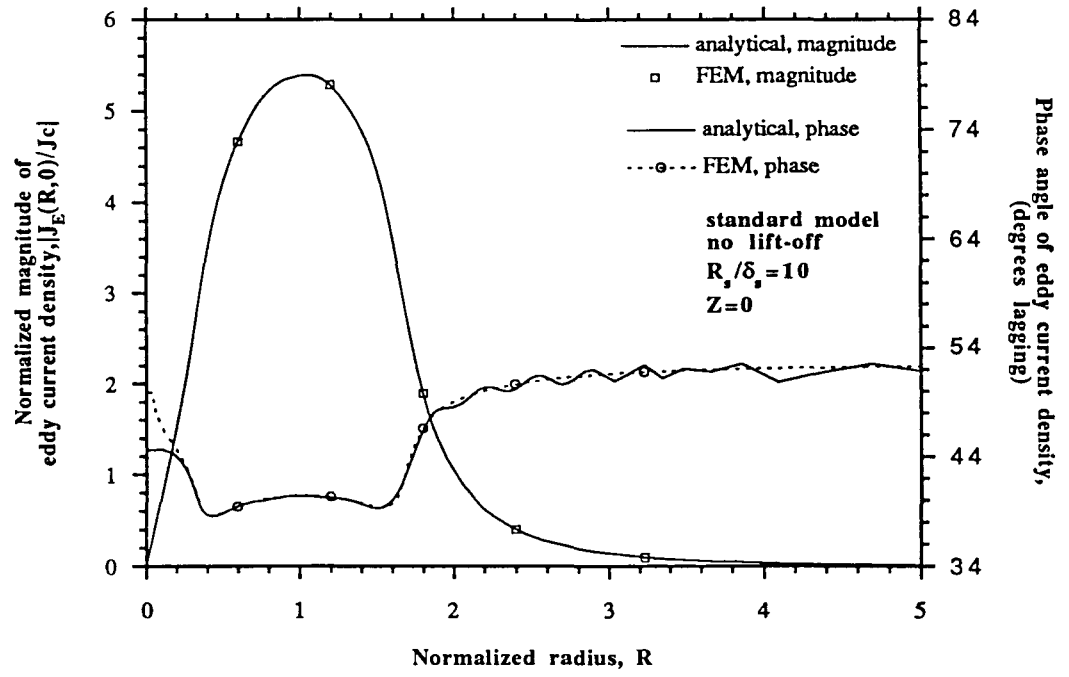

(a)

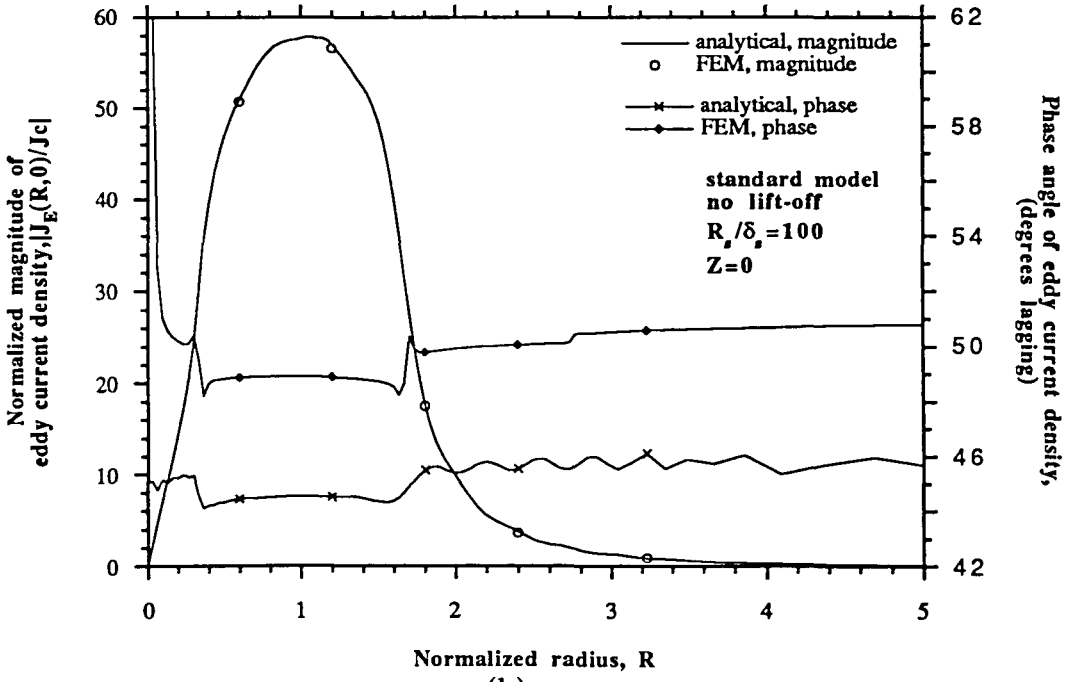

(b)

Figure 4.7: Induced eddy current density in the radial direction versus large R_s/δ_s, (a) $R_s/\delta_s = 10$, (b) $R_s/\delta_s = 100$

case $R = 1$. For small and medium values of this parameter ($R_s/\delta_s = 0.1,\ 1$) the rate of decay of the current density is significantly greater than exponential implying the classical skin depth, $\delta_s = \sqrt{2/\omega\mu\sigma}$, is a poor estimate of the decay. In these graphs the terms δ_t and δ_E appear; they are defined, respectively [27]: δ_t, the *true depth of penetration* (true DoP), is defined to be the depth at which the magnitude of the eddy current density has decayed to e^{-1} or 0.3679 of its value at the surface, and δ_E, the *effective depth of penetration* (effective DoP), is defined to be depth at which the magnitude of the eddy current density has decayed to e^{-3} or 0.0498 of its value at the surface. For example, when $R_s/\delta_s = 1$ the true DoP is approximately 40% less than the classical DoP at $R = 1$ and this difference increases with decreasing R_s/δ_s. The difference is approximately the same for the effective DoP. The phase for each situation shows the same general tendency as the magnitude, that is, it becomes more linear (classical) as the dimensionless parameter increases and increasingly lags as depth increases.

For a given R_s/δ_s the rate of decay lessens with increasing distance from the coil for a least four coil mean radii (see Figure 4.12), but the current density magnitude will decrease with radial distance in this region. In fact, as is seen in this figure, the decay actually becomes slower than exponential as the radius increases, possibly tending to what has been termed the *remote field* where the current density increases with depth. It is unknown at this time if the coil over a half-space exhibits this remote field phenomena.

It was shown earlier in Figure 4.6 that the induced eddy current density becomes more uniform in the radial direction as the coil lift-off increases; consequently, the rate of decay of the eddy current density at $R = 1$ approaches the exponential decay

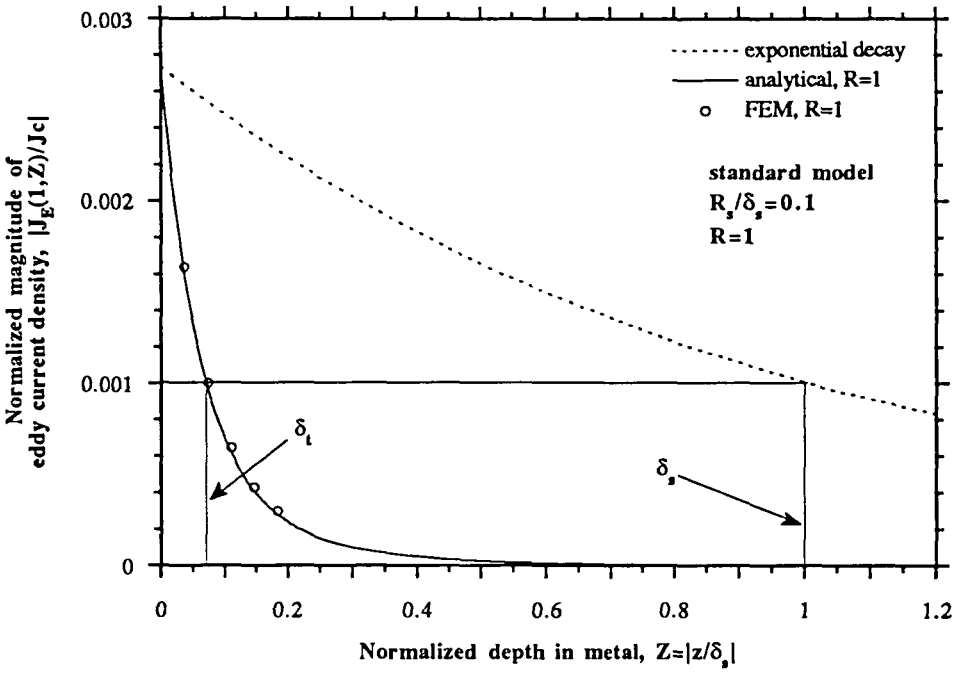

(a)

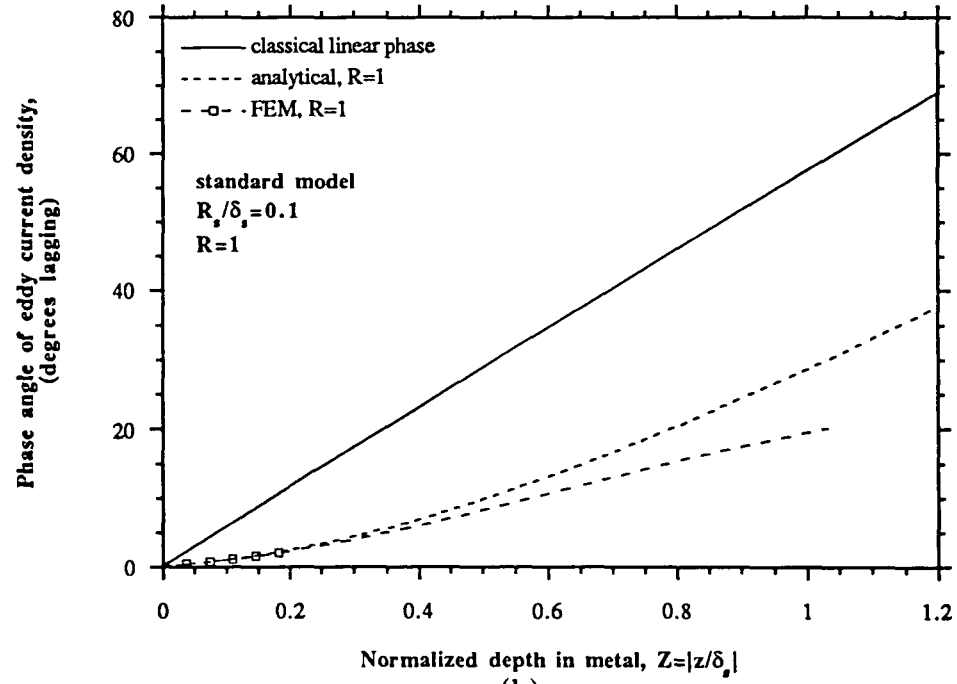

(b)

Figure 4.8: Induced eddy current density in the axial direction compared with the classical solution, $R_S/\delta_S = 0.1$, (a) magnitude, (b) phase

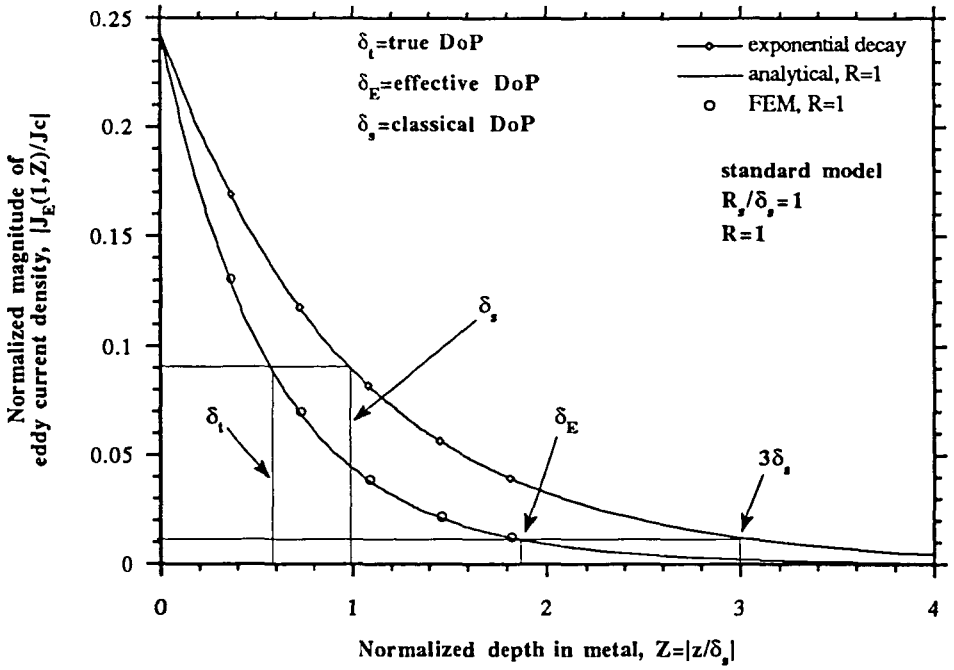

(a)

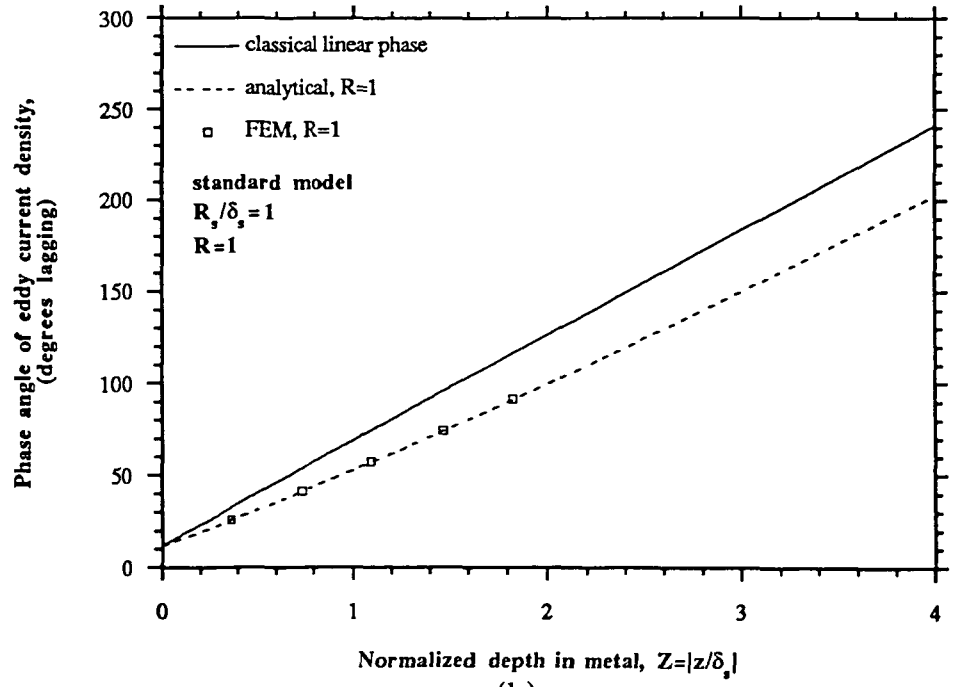

(b)

Figure 4.9: Induced eddy current density in the axial direction compared with the classical solution, $R_S/\delta_S = 1$, (a) magnitude, (b) phase

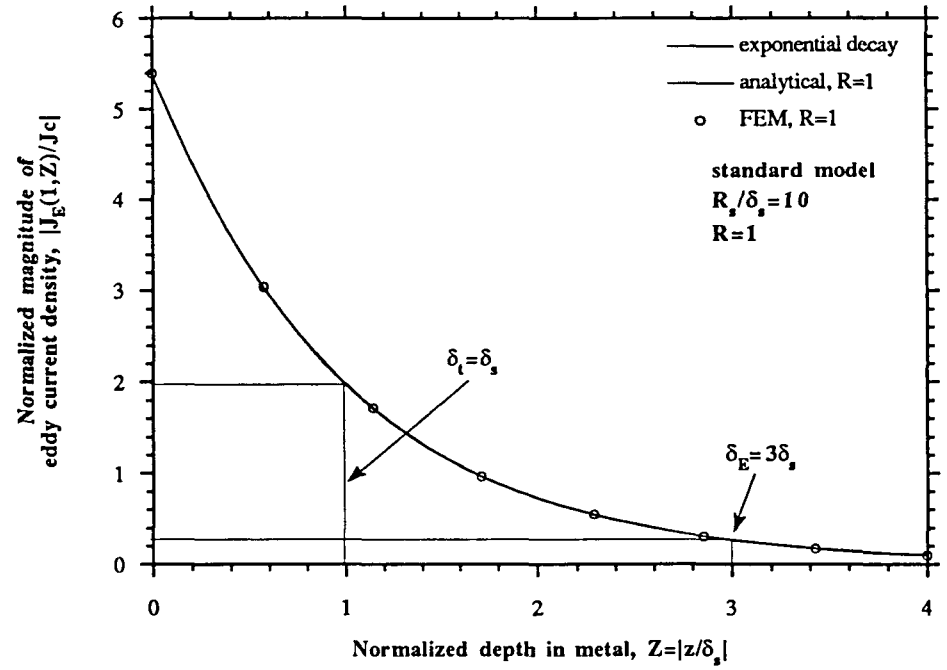

(a)

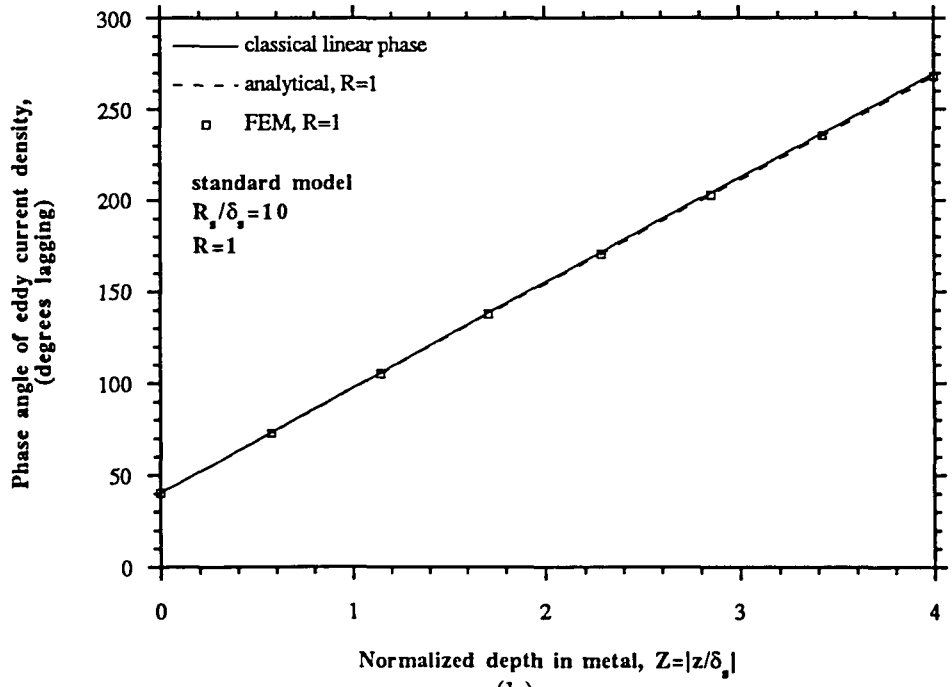

(b)

Figure 4.10: Induced eddy current density in the axial direction compared with the classical solution, $R_S/\delta_S = 10$, (a) magnitude, (b) phase

(see Figure 4.11). For this case the magnitude is normalized to one and the phase to zero at the surface since these parameters change with lift-off.

True depth of penetration and R_s/δ_s Figures 4.13 and 4.14 describe the change of the true and effective DoP as the dimensionless parameter, R_s/δ_s, varies from 0.1 to 100 [27]. The true and effective DoP are each normalized to the classical DoP and the coil mean radius and the computations are for $R = 1$. It is clear from these graphs the classical solution is only valid (for $R = 1$) when $R_s/\delta_s \geq 10$ otherwise the true DoP is less than the classical DoP. For decreasing R_s/δ_s the true DoP does not exceed approximately $0.7R_s$. Similar conclusions hold for the effective DoP. The phase angles in these figures are defined as follows: $\beta_t(\delta_t)$ is the phase angle at the true DoP, $\beta_t(\delta_s)$ is defined as the true phase angle at the classical DoP, and $\beta_s(\delta_s)$ is the classical phase angle at the classical DoP. Analogous definitions hold for the phase angles associated with the effective DoP.

In each of these figures there is excellent correspondence between the computed analytical solution and the FEM solution except when $R_s/\delta_s > 30$ because the discretization becomes too coarse relative to the rate of change of the field quantities. In this model the number of finite elements per classical skin depth at $R_s/\delta_s = 30$ is about 8 and the number of node points in the axial direction is about 4. A general rule for these computations requires roughly 5 finite elements per classical skin depth.

Experiment for a coil over a half-space A coil with physical dimensions corresponding to the standard model, but with 275 turns instead of 160, was constructed and its impedance measured over a range of R_s/δ_s for varying lift-off above effective half-spaces made of stainless steel, brass, and aluminum. The measurement

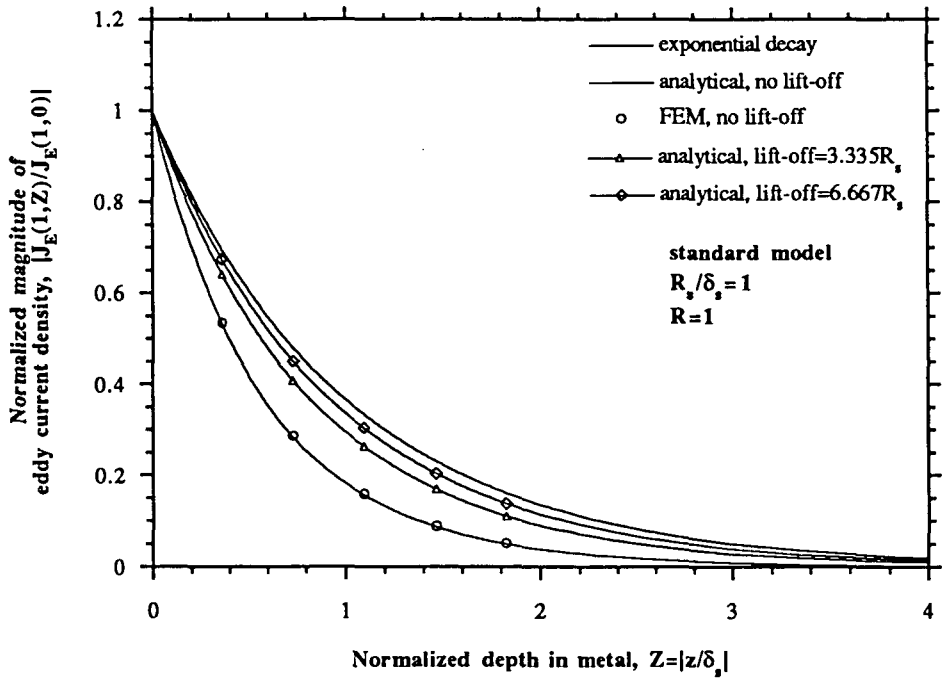

(a)

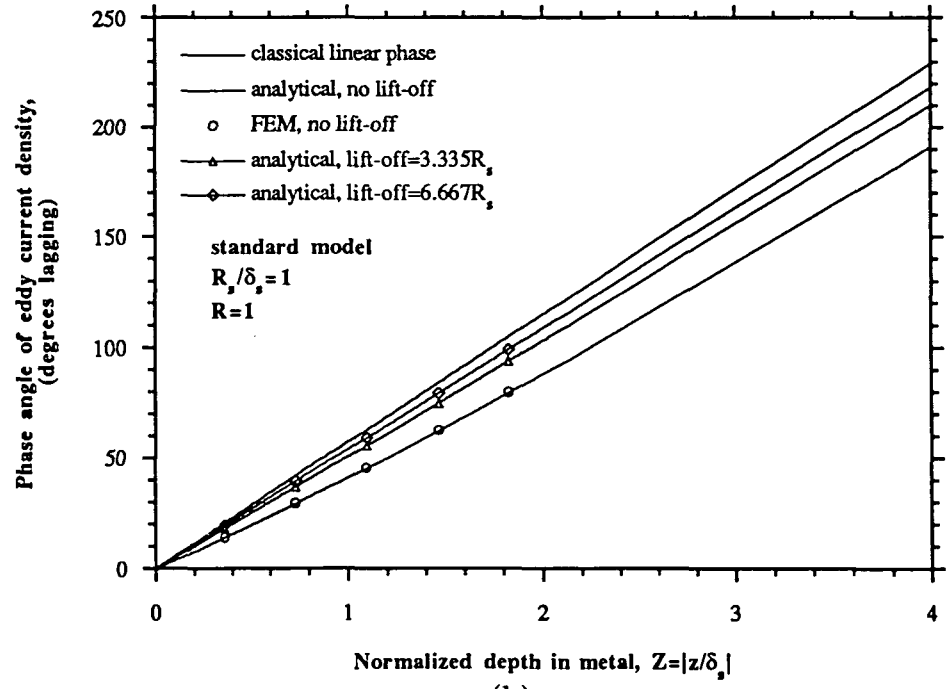

(b)

Figure 4.11: Normalized eddy current density in the axial direction versus coil lift-off compared with the classical solution, (a) magnitude, (b) phase

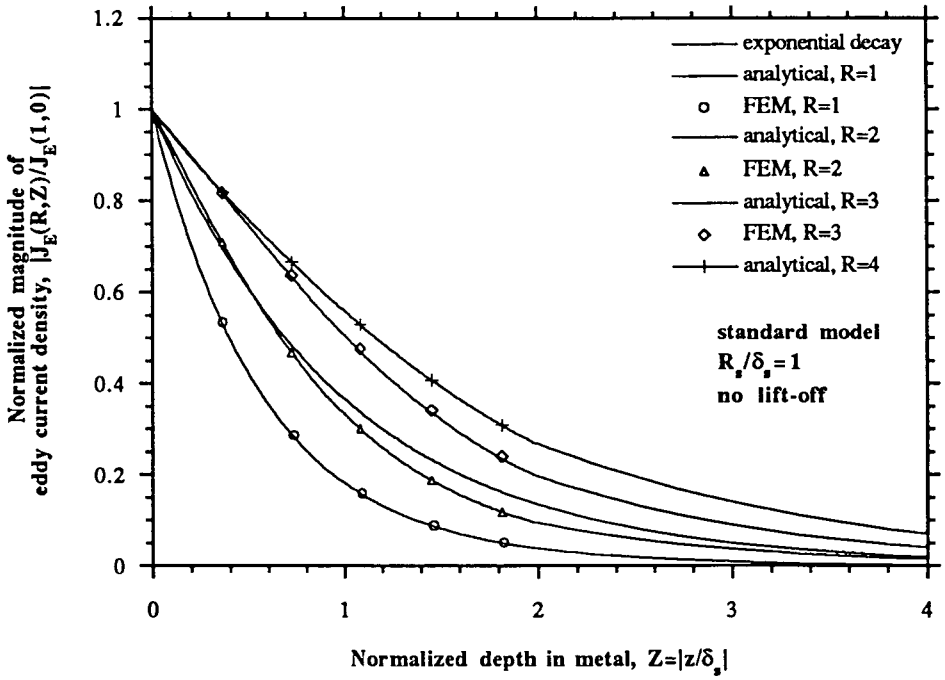

(a)

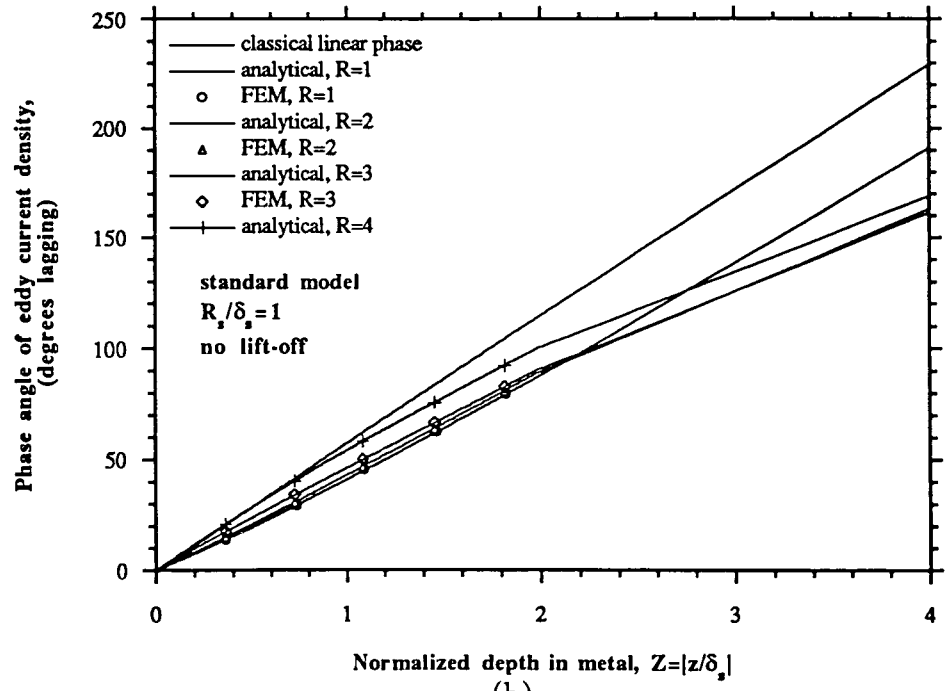

(b)

Figure 4.12: Normalized eddy current density in the axial direction versus R compared with the classical solution, (a) magnitude, (b) phase

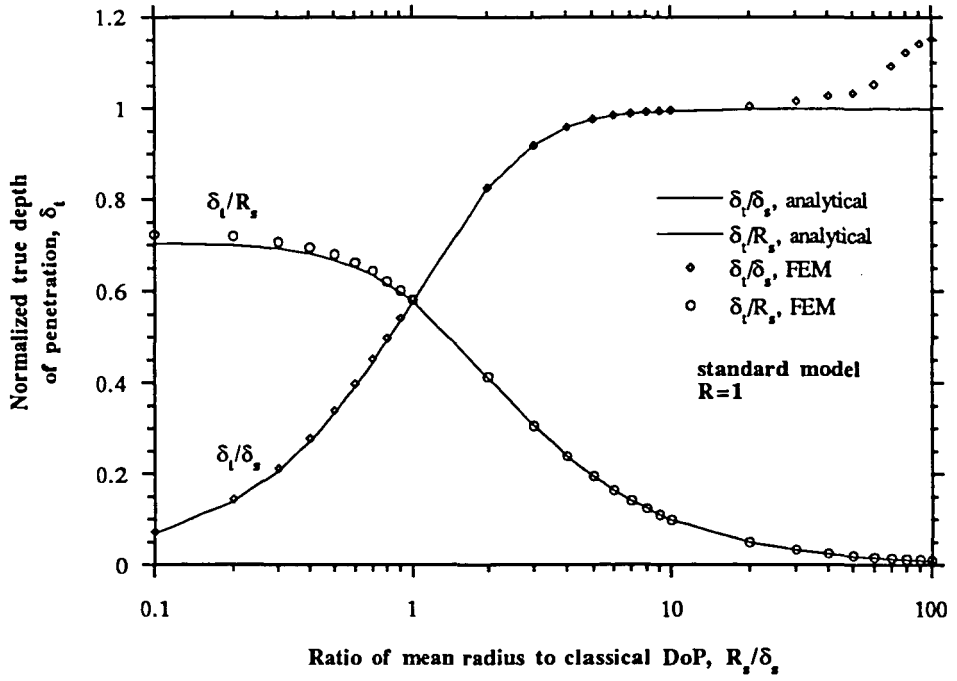

(a)

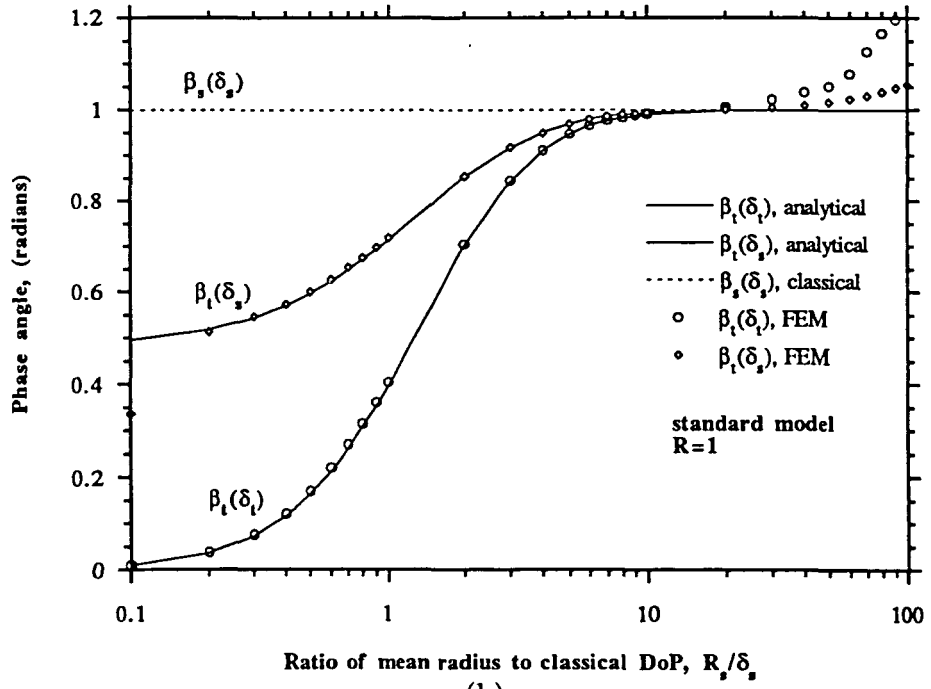

(b)

Figure 4.13: Normalized true depth of penetration versus R_S/δ_S for $R = 1$ (a) DoP, (b) phase angle

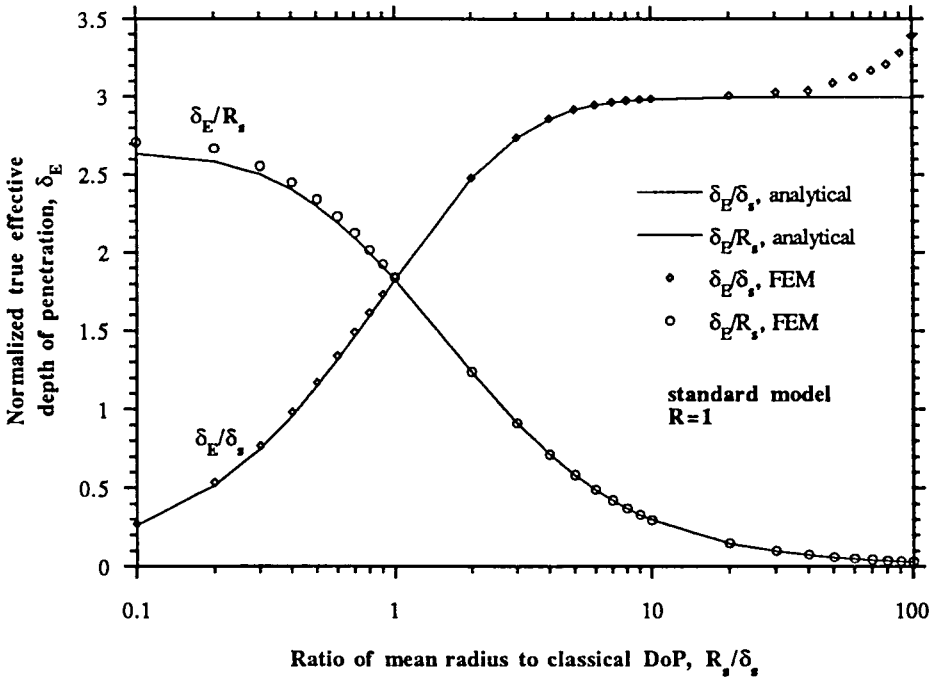

(a)

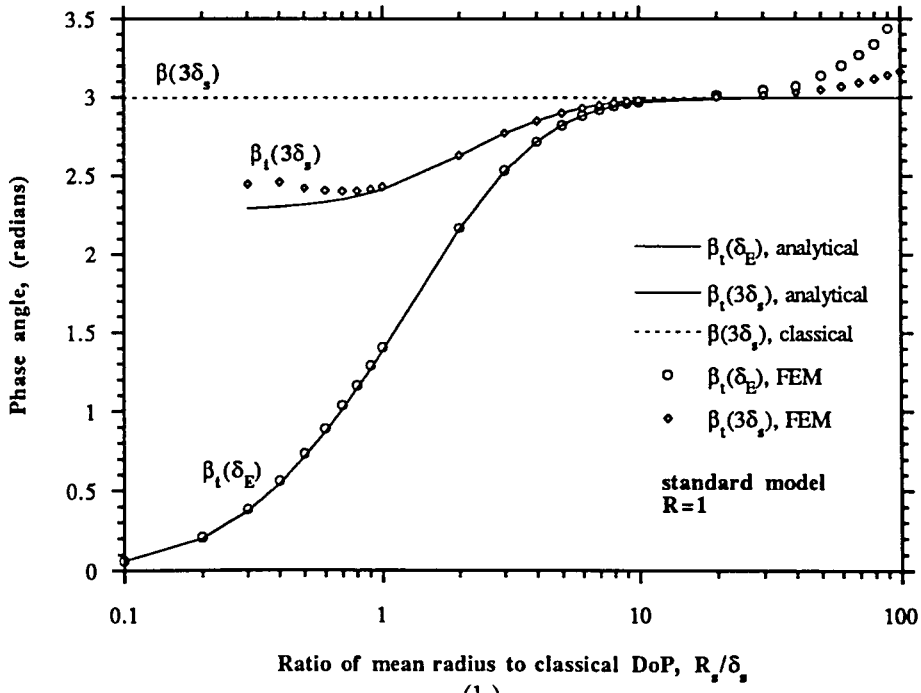

(b)

Figure 4.14: Normalized effective depth of penetration versus R_S/δ_S for $R = 1$ (a) DoP, (b) phase angle

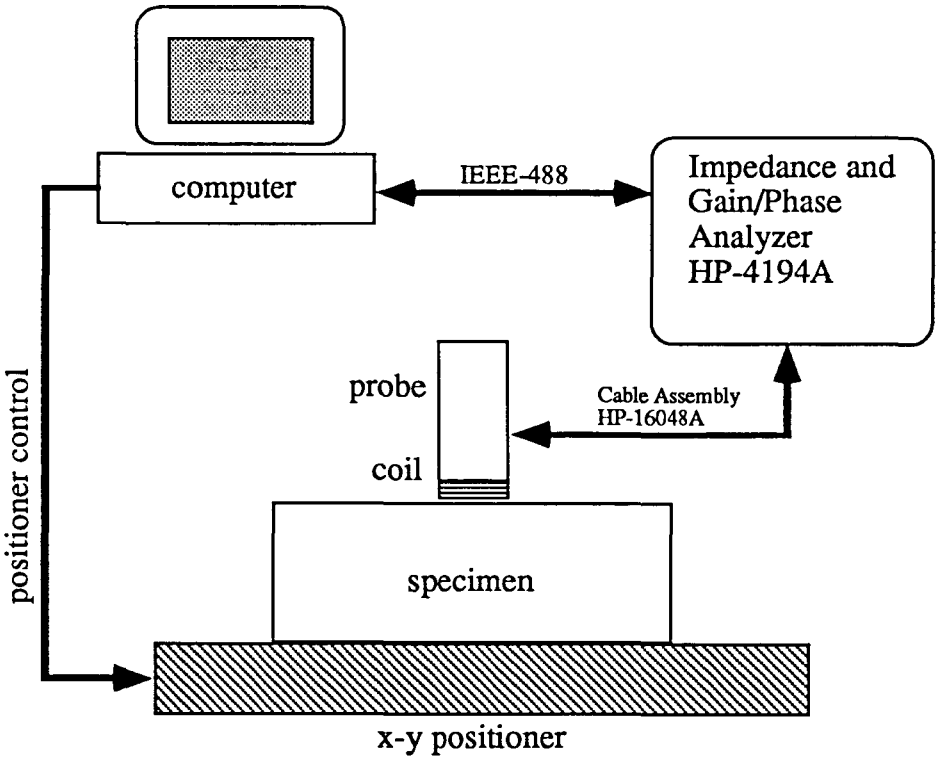

Figure 4.15: Block diagram of experimental arrangement

block diagram is given in Figure 4.15.

A comparison of the analytical solution to the FEM for varying coil lift-off is presented in Figure 4.16. In Figures 4.17 to 4.19 the results of the experiment are compared with the analytical solution. Considering the crudeness of the coil the results in general show the validity of the analytical and FEM solutions in the region where the coil is most useful, at least for the normalized reactance. At low values of R_s/δ_s, or effectively low frequency, the impedance is small which loads down the

impedance analyzer (HP4194A) and causes inaccurate measurements. At large $R_s\delta_s$ or high frequency the coil passes through a resonance caused by the parallel combination of the inductance and inter-winding capacitance of the coil. The impedance is maximum at the resonant frequency, f_o, and looks capacitive at frequencies above f_o. This aspect of the coil is not modelled by either the analytical or FEM. In each model the coil is considered to be a homogeneous region of constant current density and not discrete loops with a non-conducting medium, such as air, between the loops. The number of turns for the coil in each model is only a scaling factor in this case. The model approximation is valid if the loop cross-sectional area is relatively small compared with dimensions of the coil cross-section.

Another aspect of the actual coil not modelled is the conductivity of the loops. The finite conductivity causes a finite dc resistance. The effective resistance increases with increasing frequency due to the skin effect existing in each individual loop and a proximity effect [14] in each loop caused by current in all other loops. To obtain the graphs of normalized resistance the dc resistance was subtracted from the measured resistance data then the measured data was normalized to the reactance in air. The result as depicted in the figures shows the predicted behavior at least up to the point where resonance becomes dominant.

The normalized reactance is essentially the ratio of effective inductance to the inductance in air, L_{eff}/L_o. Qualitatively, the inductance of a coil is proportional to the ratio of the number of *flux linkages*, $N\Phi_B$ $(turn \cdot Wb)$, to the exciting current, i (A). For the present case the number of turns and exciting current remain constant; therefore, the flux, Φ_B, or the flux linkage is reduced with proximity to the conductor, that is, the flux does not link each turn as strongly near the conductor as it does

is free-space. At low R_s/δ_s (frequency) the induced eddy current density is small and does not strongly oppose the coil field. In the dc limit there is no induced eddy currents and the (non-magnetic) conductor does not affect the magnetostatic field so the inductance is the same as free-space. As R_s/δ_s (frequency) increases the induced current increases opposing the applied field. The penetration of the field into the conductor decreases until at large R_s/δ_s (high frequency) the field is practically excluded from the conductor and the reduction in flux linkage is complete and the effective inductance becomes essentially constant as seen in the figures.

Energy is lost in the conductor since it has finite conductivity. The loss is reflected in the coil as a resistance although the coil conductivity is zero. The predicted coil resistance is small at low frequencies since there is decreased current induced in the half-space. At high frequencies the current is excluded from the conductor resulting in less induced current flowing at depth in the conductor or Ohmic region. Between these two extremes there is a point where the field is sufficiently large and the depth of penetration sufficiently deep to give a maximum in the coil resistance.

Eddy current density in a finite thickness conductor

In most situations a conductor with a thickness greater than approximately three classical skin depths at the inspection frequency is equivalent to a conductor of infinite thickness (see Figure 4.14). Changes in current density and coil impedance versus thickness are investigated. An experiment employing a flat bottom hole with decreasing distance from the surface of an effective half-space was performed to investigate the effect.

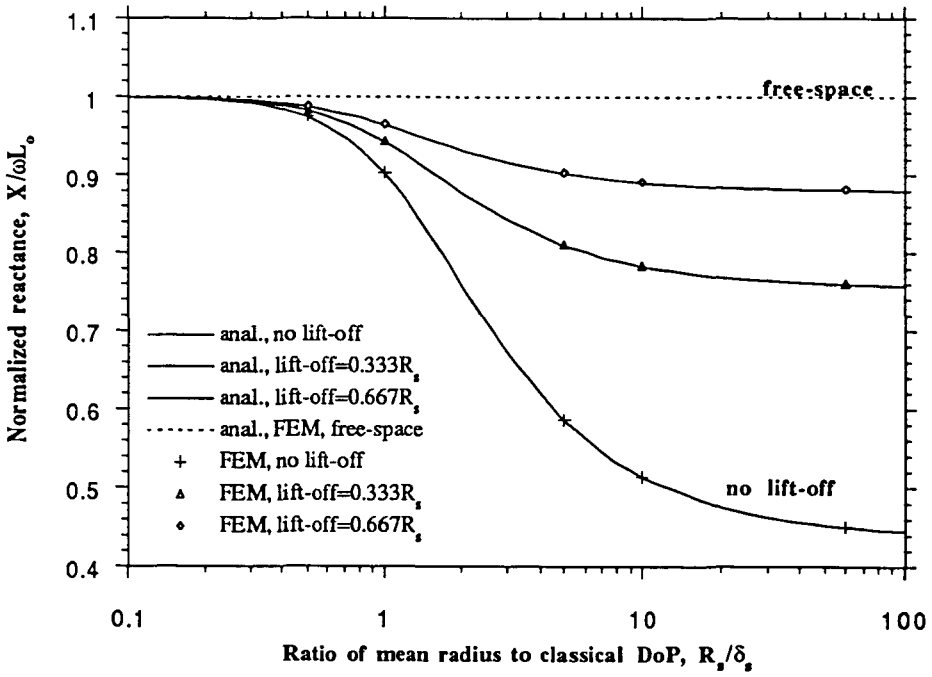

(a)

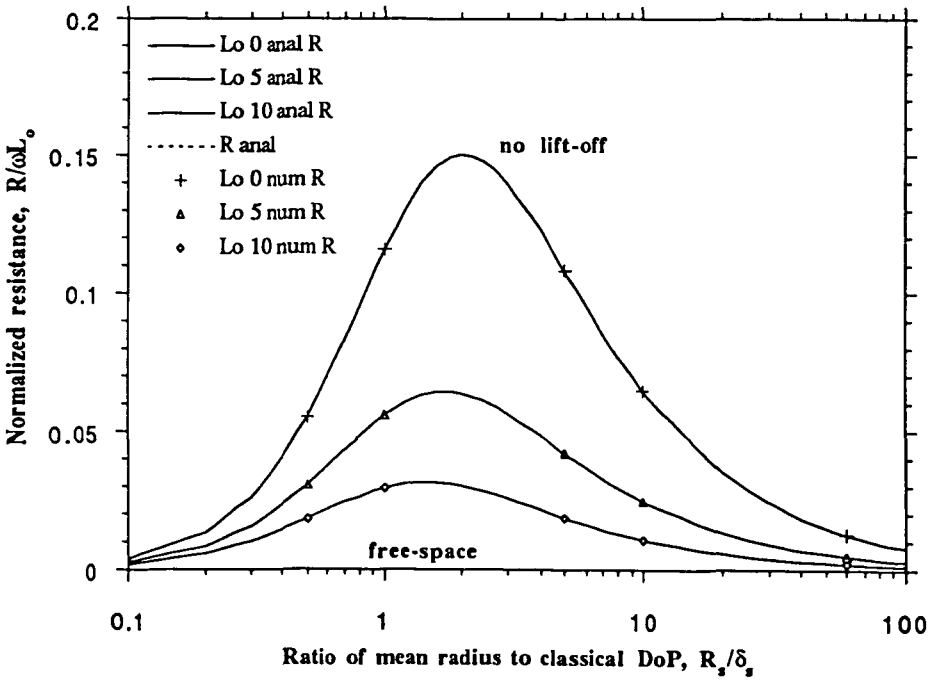

(b)

Figure 4.16: Normalized impedance, analytical and FEM, versus coil lift-off and R_S/δ_S for $R = 1$ (a) reactance, (b) resistance

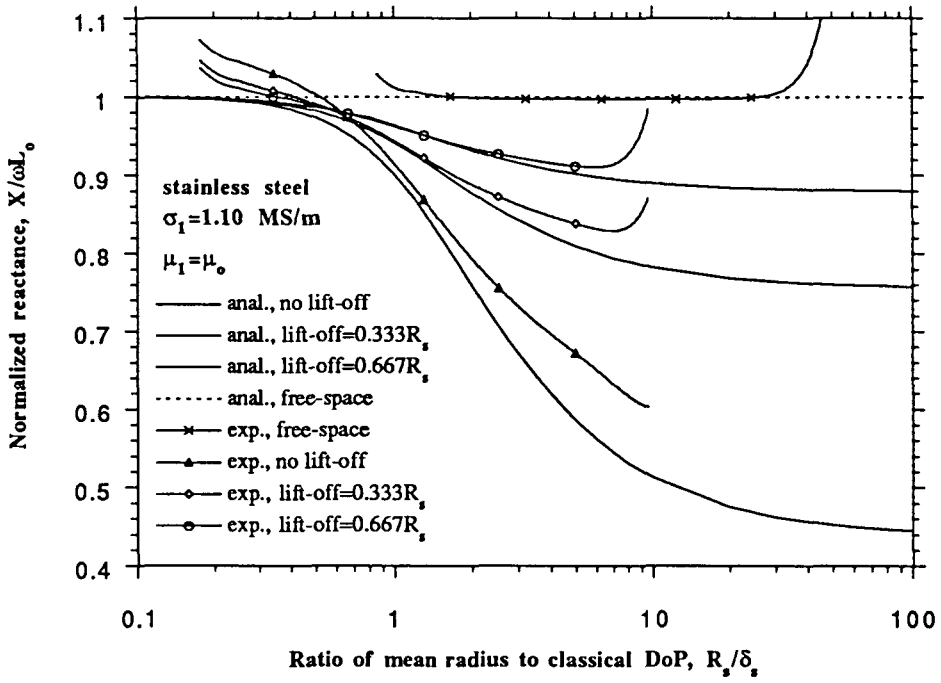

(a)

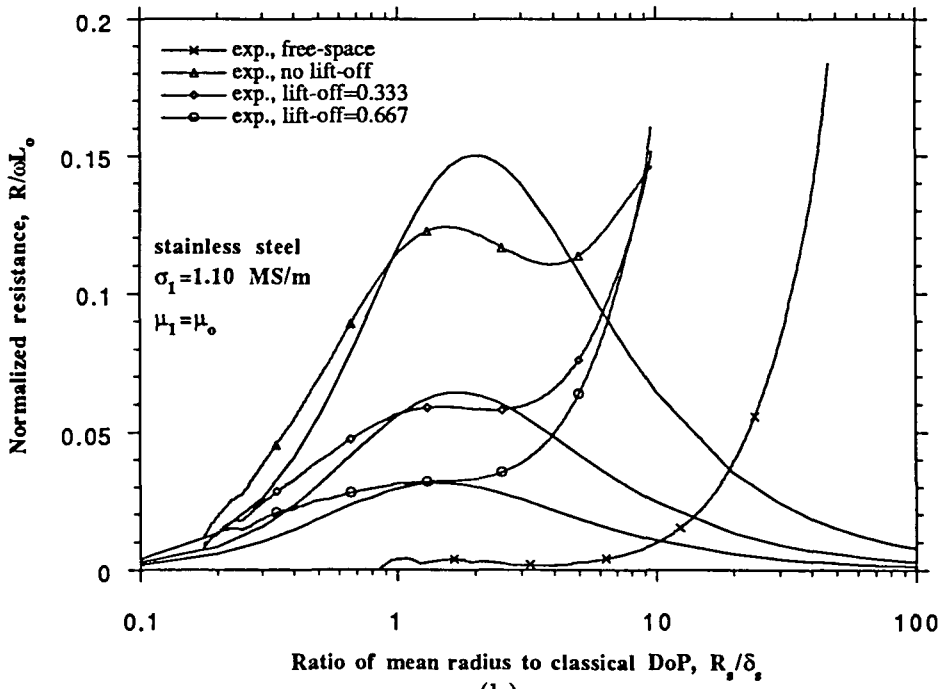

(b)

Figure 4.17: Normalized impedance for stainless steel versus coil lift-off and R_s/δ_s for $R = 1$ (a) reactance, (b) resistance

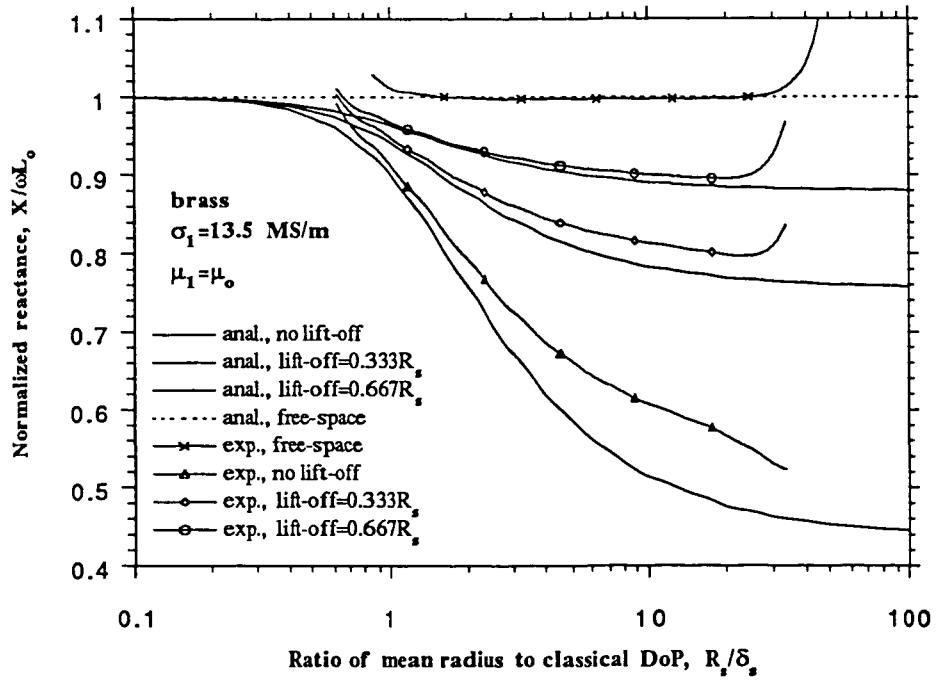

(a)

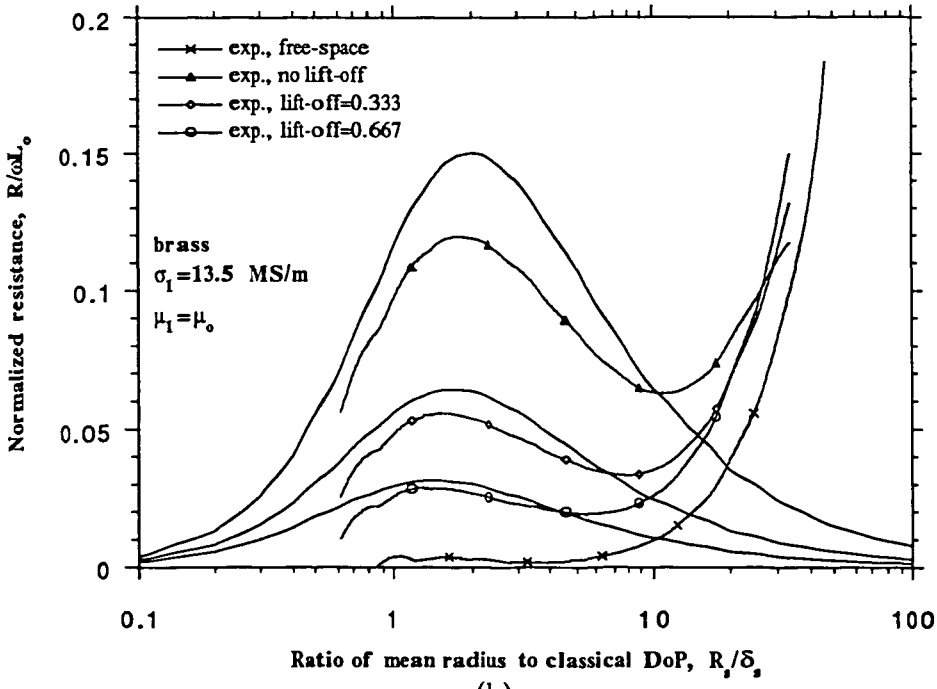

(b)

Figure 4.18: Normalized impedance for brass versus coil lift-off and R_S/δ_S for $R = 1$ (a) reactance, (b) resistance

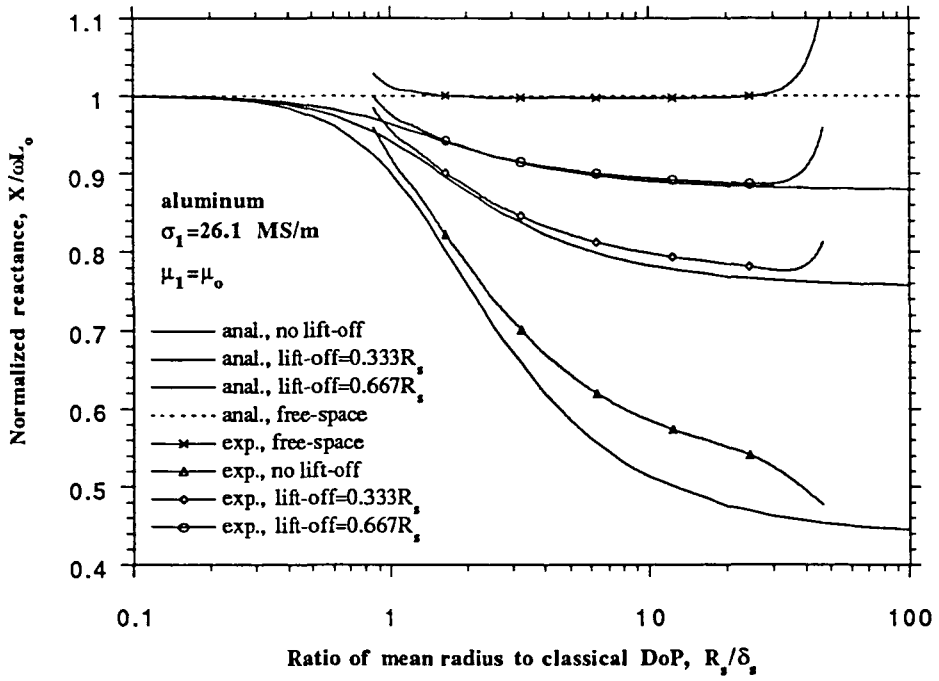

(a)

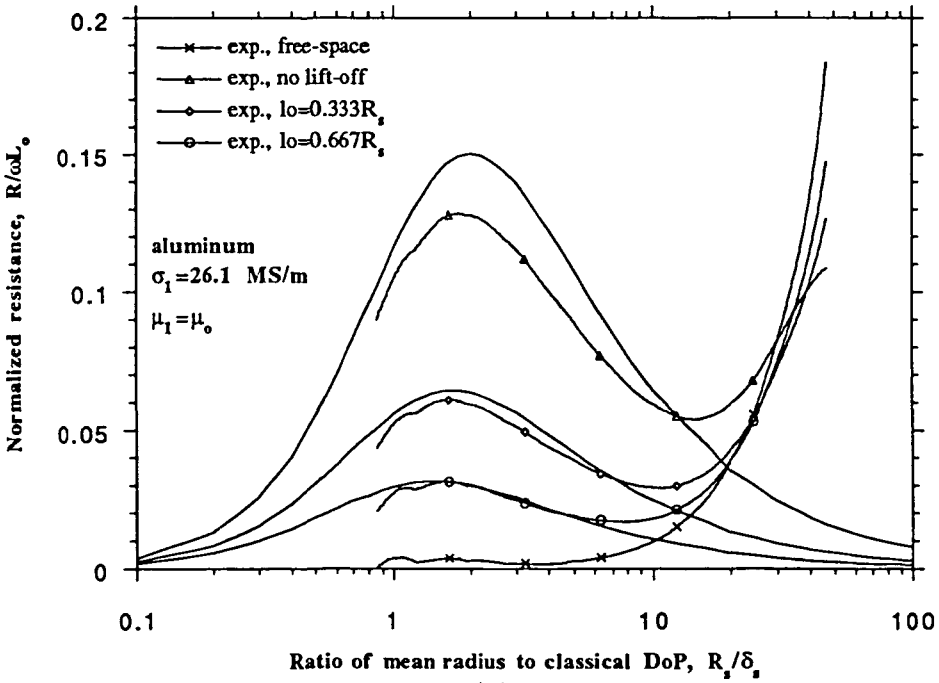

(b)

Figure 4.19: Normalized impedance for aluminum versus coil lift-off and R_S/δ_S for $R = 1$ (a) reactance, (b) resistance

Eddy current density in the axial direction Figure 4.20 shows the effect of finite conductor thickness on the eddy current density. As the thickness decreases the current density does not decay as fast as in a half-space and the lags less for decreased thickness. A more complete study of the effects of finite thickness and of a cladding material on top of a half-space could show the existence of a remote field effect and could determine ways to extract cladding thickness information from measurements, respectively.

Flat bottom hole measurements A flat bottom hole (hole diameter = 0.350in = probe diameter) was drilled in an effective half-space of aluminum (alloy 6061, $\sigma = 26.1\ MS/m$) from the bottom side. The distance between the bottom of the hole and the surface of the metal was decreased in steps and the probe was scanned across the metal surface directly above the hole. The probe impedance was measured during the scan and the results are presented in Figures 4.21 to 4.22.

Decreasing distance to the hole when the probe is centered directly above it tends to increase the normalized reactance. In this one particular instance the finite element model can be used to model the impedance change due to the hole. The finite element results and measurements are shown together in Figure 4.21. In general the FEM behaves similarly, but is less in magnitude overall. A non-zero coil lift-off could account for the difference. The normalized coil resistance versus scan position for probe one (turns=275, wire=#36 AWG) and probe two (turns=195, wire=#34 AWG) is given in Figure 4.22. Similarly, the normalized coil reactance appears in Figures 4.23 and 4.24. When the hole is completely through the half-space the greatest impedance change occurs, which is reasonable. The impedance approaches a coil

in air as the distance to the hole decreases. The first definite hole detection occurs for a surface-to-hole distance of $0.150in$ for probe one and also for probe two but it was not as strong in the second probe. This distance corresponds to $1.43\delta_s$ or about $2.38\delta_t$ for $R_s/\delta_s = 1$. This does not generally negate the assumption that three classical skin depths is the region in which defect detection can take place, but is suggests that three skin depths is a very liberal estimate. Probably a more appropriate estimate would be one or possibly two classical skin depths, but more appropriate still is to apply a general method such as the FEM to the given geometry so that many possible variations can easily be investigated.

Coils in a Conducting Tube

The FEM results for a pair of (differential) coils inside a conducting tube are presented (see Figure 4.25). The similarities to the coil over a half-space are obvious. The results are for tube with an infinitely thick wall.

Eddy currents in a tube with an infinitely thick wall

The standard model for the coils in a tube consists of the following:

$$\begin{aligned} R_s &= 1.8669\ mm \equiv 0.0735\ in \\ \rho_1 &= 1.0668\ mm = \frac{12}{21}R_s \\ \rho_2 &= 2.667\ mm = \frac{30}{21}R_s \\ \ell_2 - \ell_1 &= 1.6002\ mm \frac{18}{21}R_s, (\text{coil thickness}) \\ d &= 1.1557\ mm = \frac{13}{21}R_s \\ \sigma_1 &= 1351 \frac{S}{mm}, (\text{stainless steel}) \end{aligned}$$

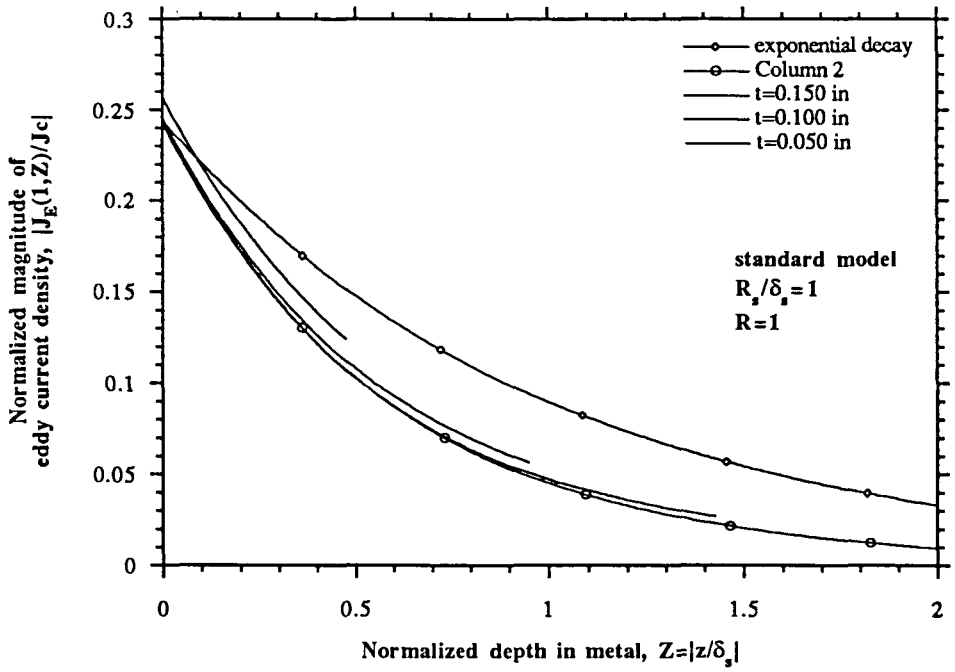

(a)

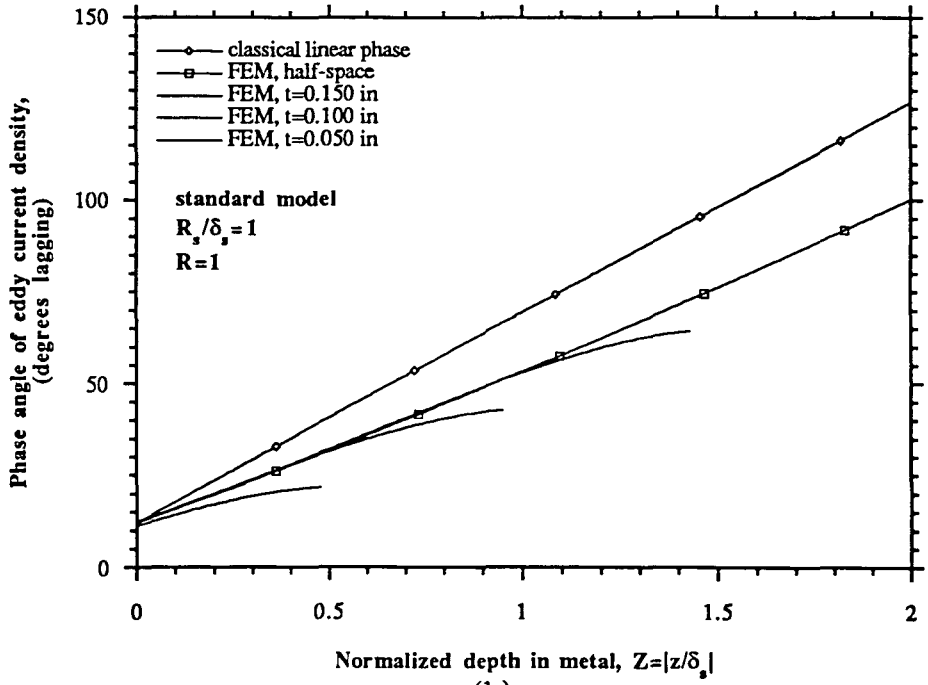

(b)

Figure 4.20: Induced eddy current density in the axial direction versus conductor thickness for $R = 1$ (a) magnitude, (b) phase

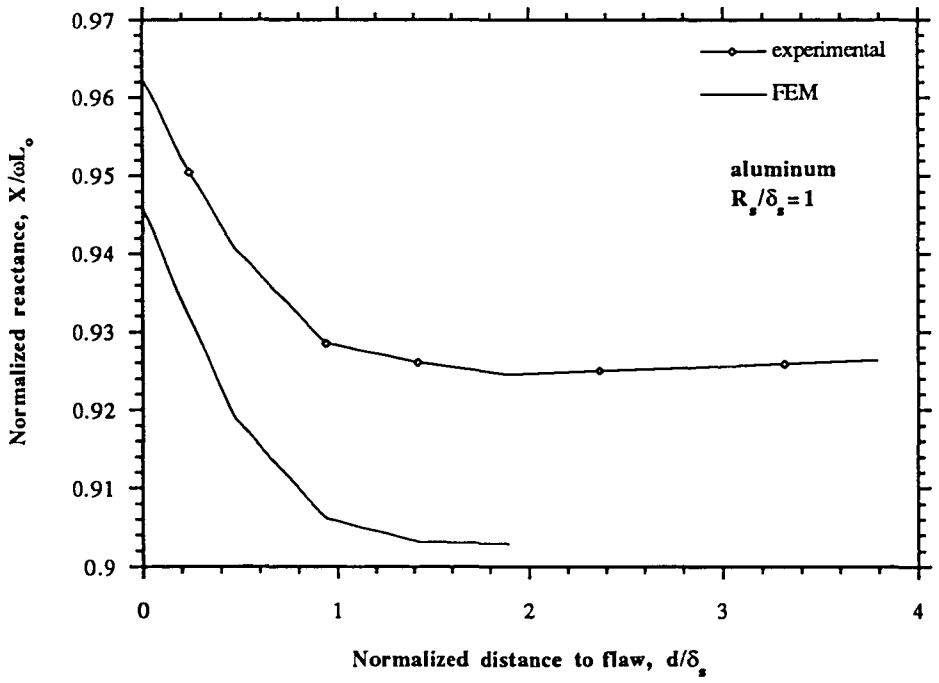

(a)

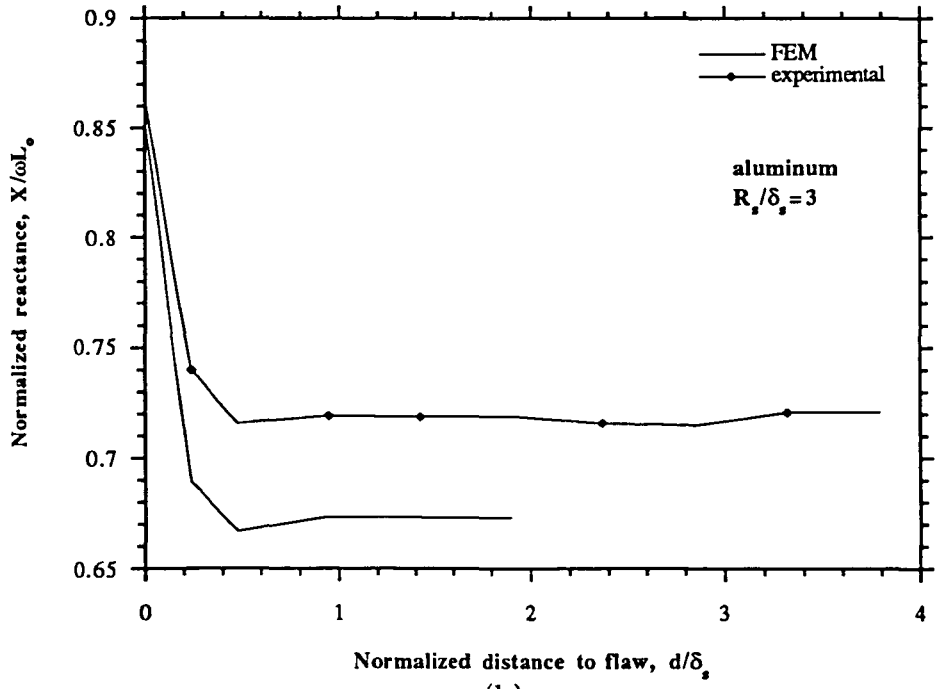

(b)

Figure 4.21: Normalized coil reactance versus distance to flaw, (a) $R_s/\delta_s = 1$, (b) $R_s/\delta_s = 3$

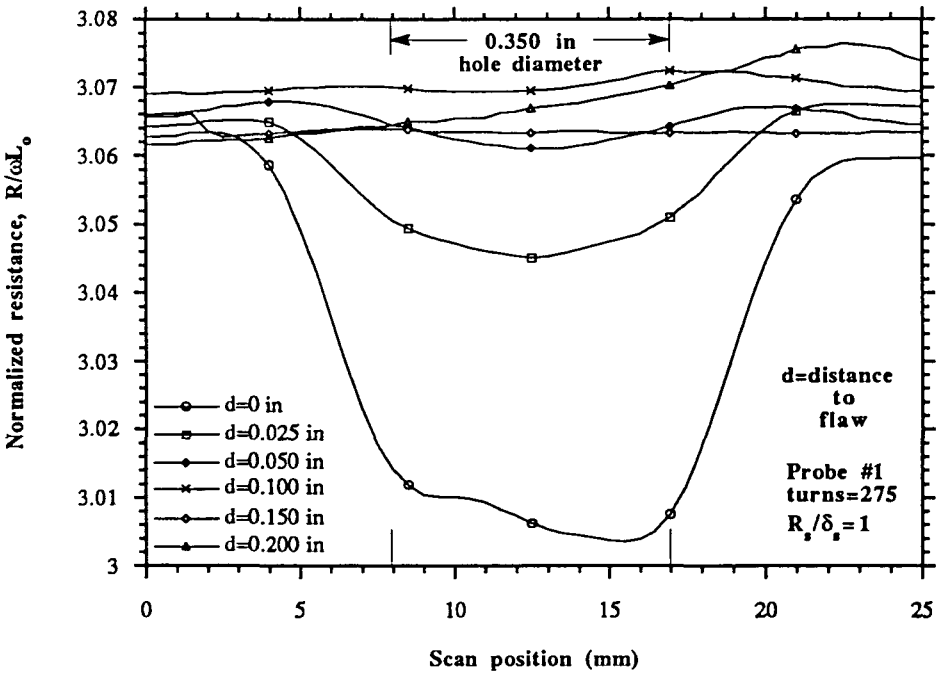

(a)

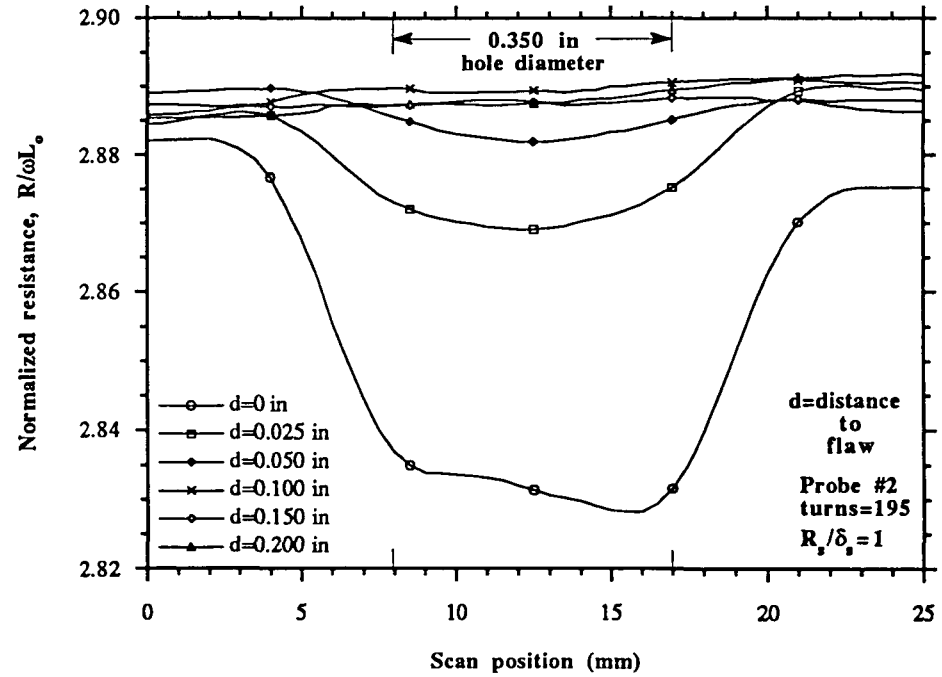

(b)

Figure 4.22: Normalized coil resistance versus scan position $R_S/\delta_S = 1$ (a) probe #1, (b) probe #2

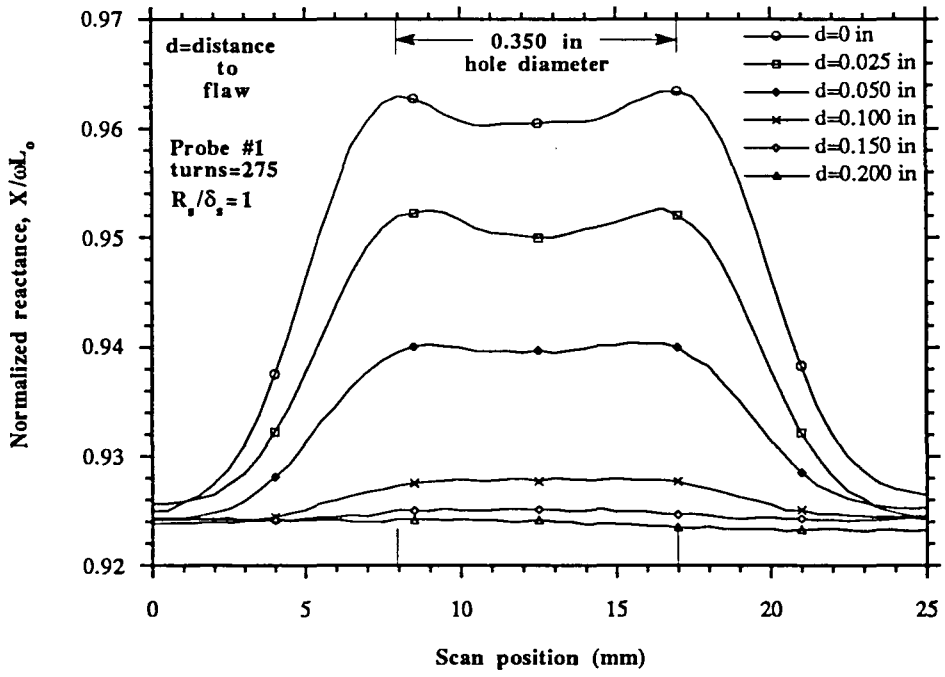

(a)

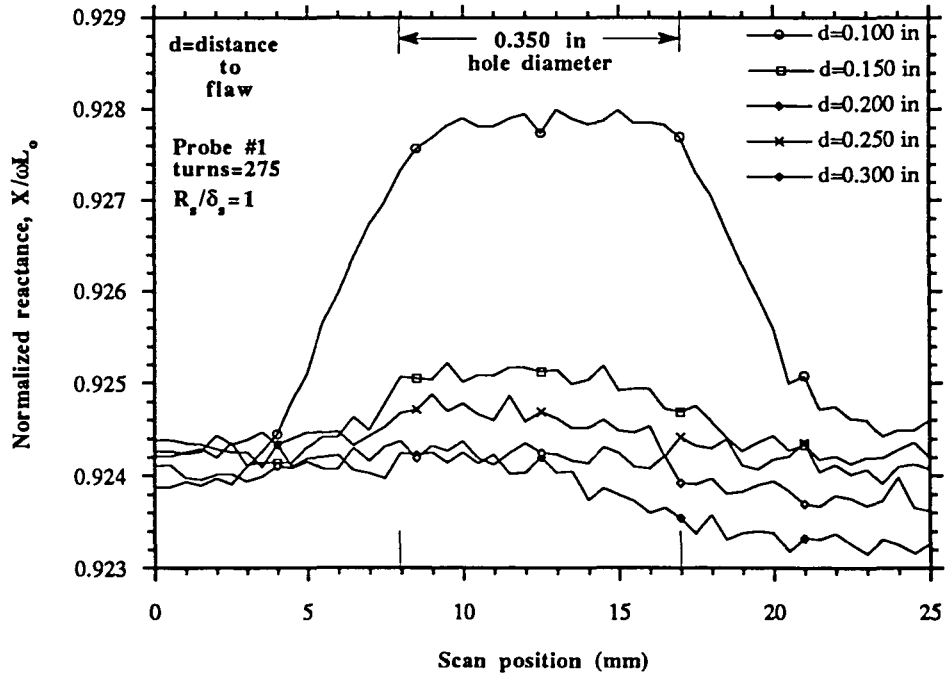

(b)

Figure 4.23: Normalized coil reactance versus scan position for probe #1, $R_S/\delta_S = 1$ (a) 0-0.200in, (b) 0.100-0.300in

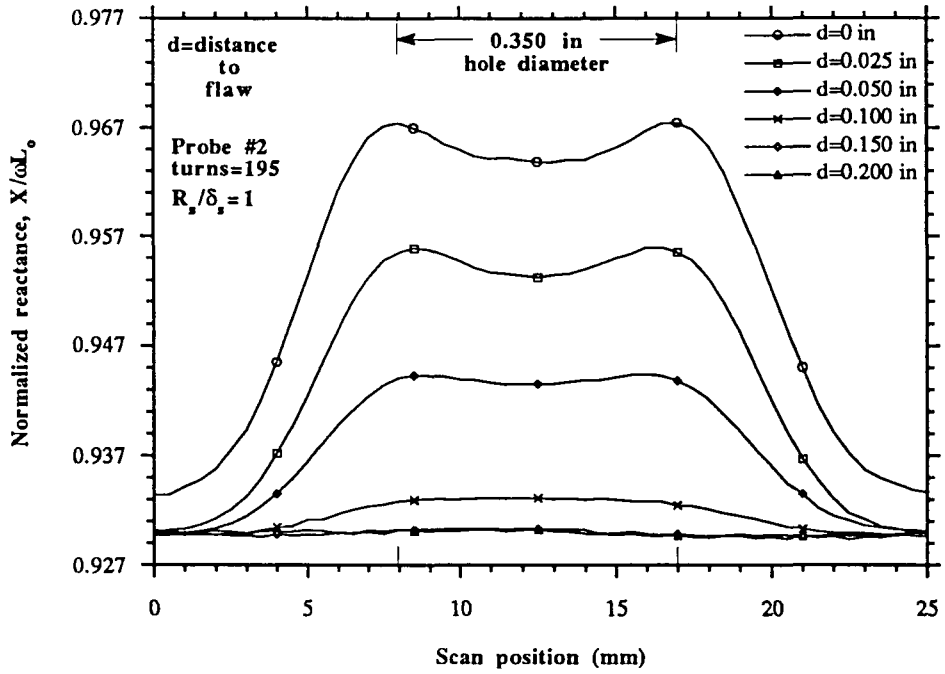

(a)

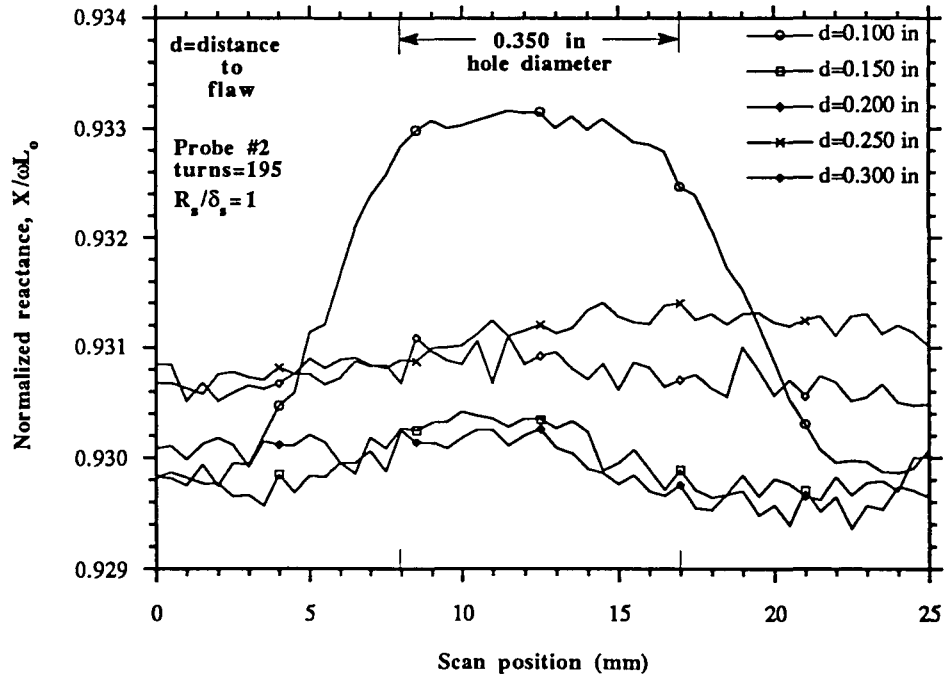

(b)

Figure 4.24: Normalized coil reactance versus scan position for probe #2, $R_s/\delta_s = 1$ (a) 0-0.200in, (b) 0.100-0.300in

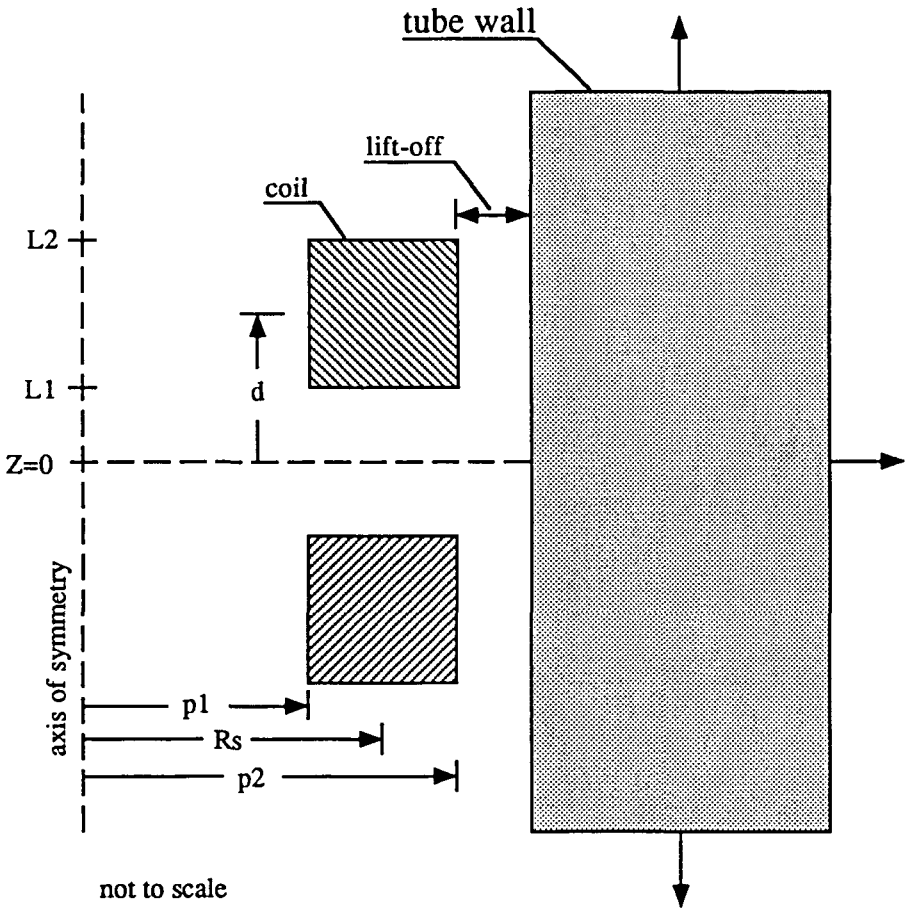

Figure 4.25: Differential coils inside a conducting tube

$$\begin{aligned} \mu_1 &= \mu_o \\ \mu &= \mu_o, \text{(medium inside tube)} \\ \text{turns (per coil)} &= 160. \end{aligned}$$

These dimensions are derived from an actual coil used for eddy current testing of stainless steel heat exchanger tubing (NASA project). In general, the coils in a tube obey the same solution dependence on R_s/δ_s as the coil over a half-space except for the depedence on the parameter d ($2d$ is the distance between the coil centers). The coils are modelled with current flowing in opposite directions which results in a zero vector potential plane at the midpoint between the coils ($Z = 0$). Length in the axial or $\hat{z}$-direction is normalized to d instead of R_s which is in a sense arbitrary but clearly shows where the induced current density peaks relative to the coil. Length in the radial direction is normalized to R_s.

Eddy current density in the axial direction The eddy current density induced on the inner surface of the tube is presented in Figures 4.26 to 4.28. In general, the results are analogous to those of the coil over a half-space. In Figure 4.26 variation in current density with respect to R_s/δ_s is given and analytical computations are also plotted. The analytical code was not refined enough at the time of writing to be utilized in all calculations, but these two comparisons shows the correspondence between analytical and FEM. In Figure 4.27 the depth in the conductor is expressed in terms of R, the normalized radial coordinate, where $R = 1.43$ corresponds to the tube inner radius.

Eddy current density in the radial direction The decay of the current density with depth into the tube wall is much faster than exponential for relatively small R_S/δ_S. It appears to be slightly faster than in the case of the coil over a half-space, but a direct comparison may not be valid. The Figures 4.29 to 4.31 describe the radial dependence. Note that in these graphs $R = 0$ corresponds to the tube radius so the depth into the conductor is measured starting at $R = 1.43$.

An interesting phenomena is observed in Figure 4.32. Here the current density in the radial direction is plotted for increasing distance from the coil. The current density at each Z value is normalized to its value at the tube radius. As distance increases the current density actually peaks inside the conductor rather than on the tube inner surface. This is probably a manifestation of the remote field effect where the current density far from the coil actually decays from the outside of the tube towards the inside, but in this case the tube is infinitely thick so the current must eventually decay with distance into the conductor. At this time a well considered qualitative explanation for this occurrence is not kwown.

True depth of penetration and R_S/δ_S The true and effective depth of penetration have the same characteristic behavior as the coil over a half-space (see Figures 4.33 and 4.34). In this particular case the true depth of penetration never becomes greater than $0.48R_S$ compared with $0.7R_S$ for the half-space. More investigation of the variation of true DoP with respect to coil mean radius could result in a useful rule for estimating the true DoP. A limiting case of the two coils in a tube would be a pair of square conductors above a half-space.

Normalized coil impedance and coil lift-off To simulate coil lift-off without changing the coil mean radius, the tube inner radius was increased. The normalized reactance and resistance for a number of coil lift-off values is plotted in Figure 4.35. The computed impedance is for one of the two coils but the impedance variation is the same for both coils. The plot symbols represent the actual points computed with the FEM and the continuous curves are the result of a cubic spline fit.

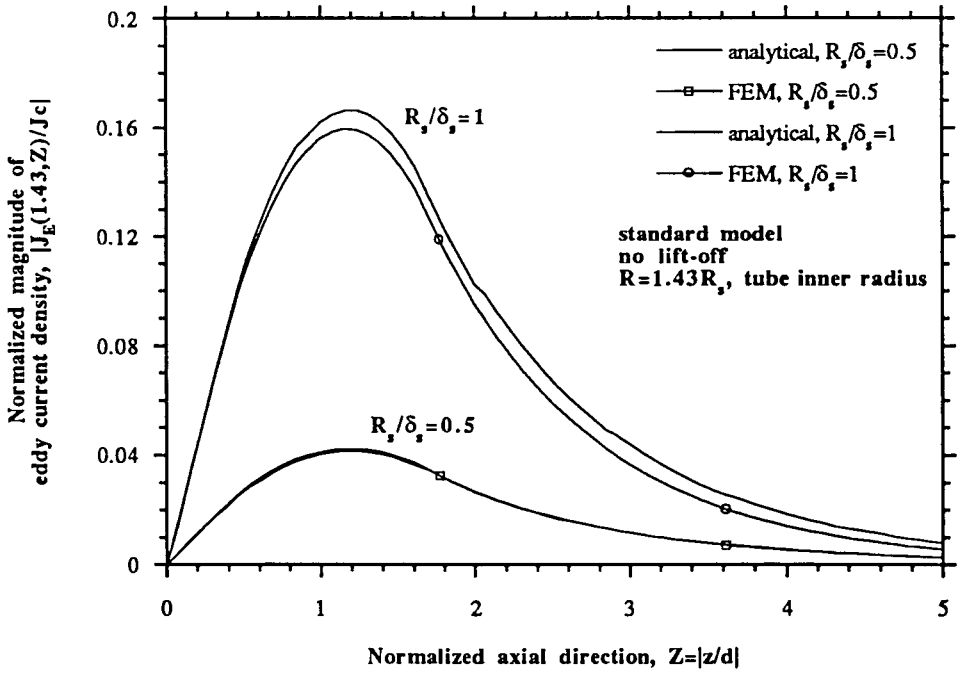

(a)

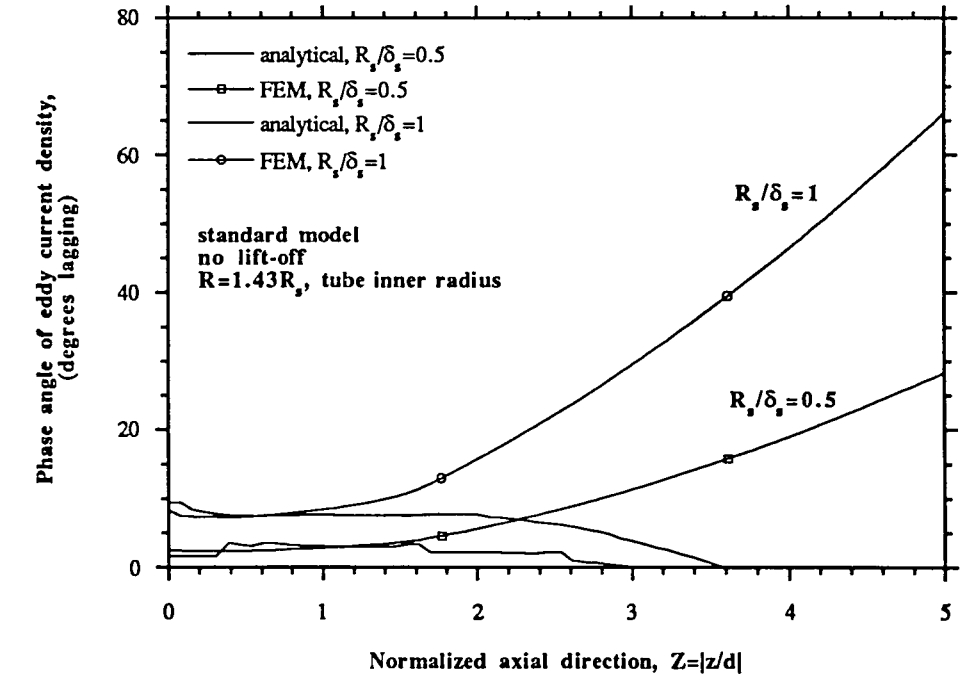

(b)

Figure 4.26: Induced eddy current density versus R_S/δ_S, (a) magnitude, (b) phase

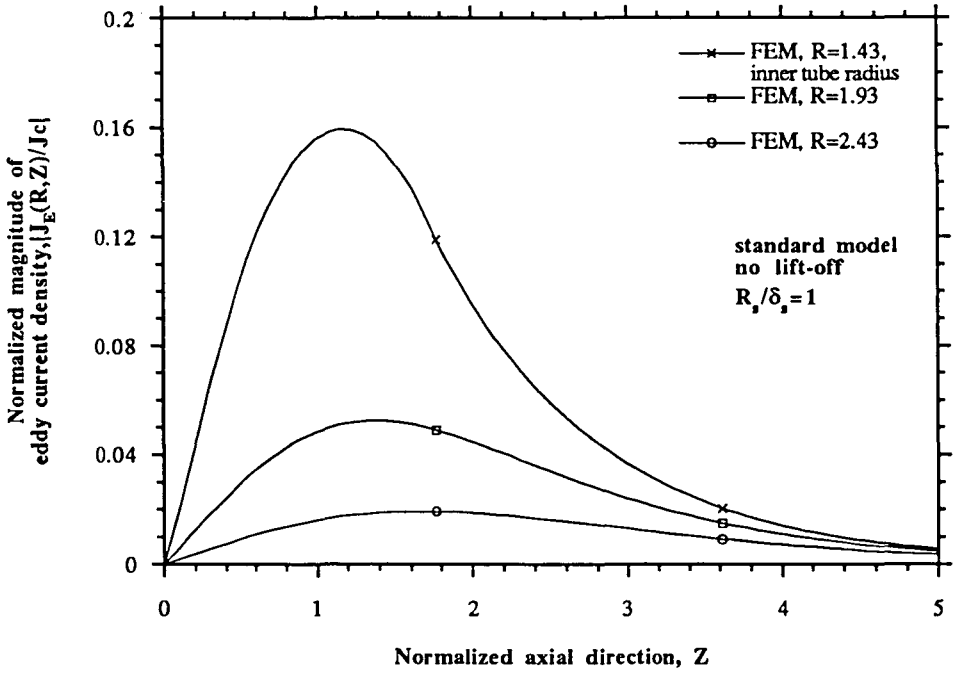

(a)

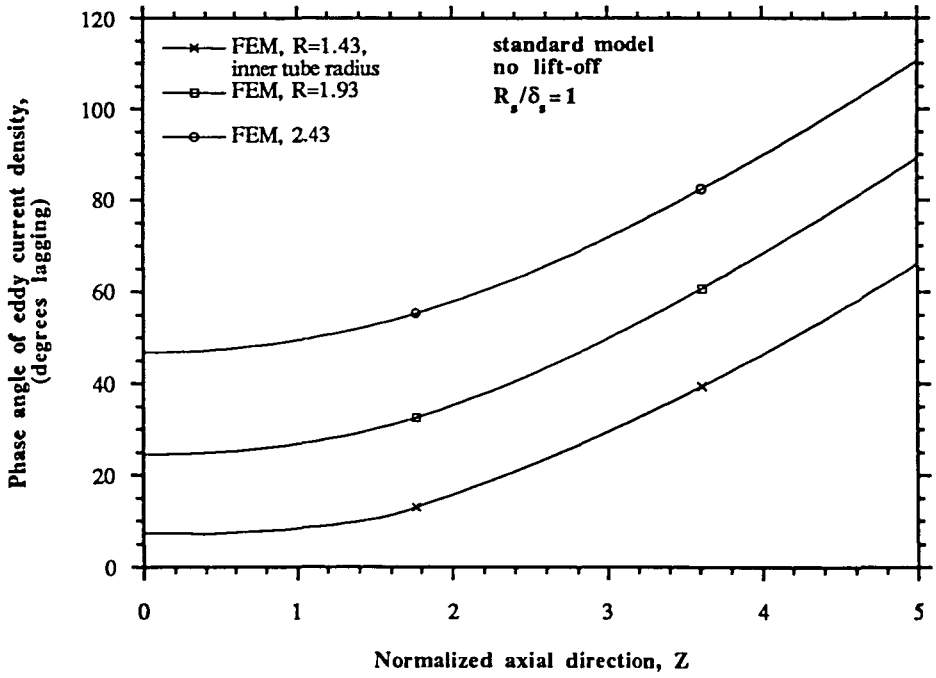

(b)

Figure 4.27: Induced eddy current density versus R, (a) magnitude, (b) phase

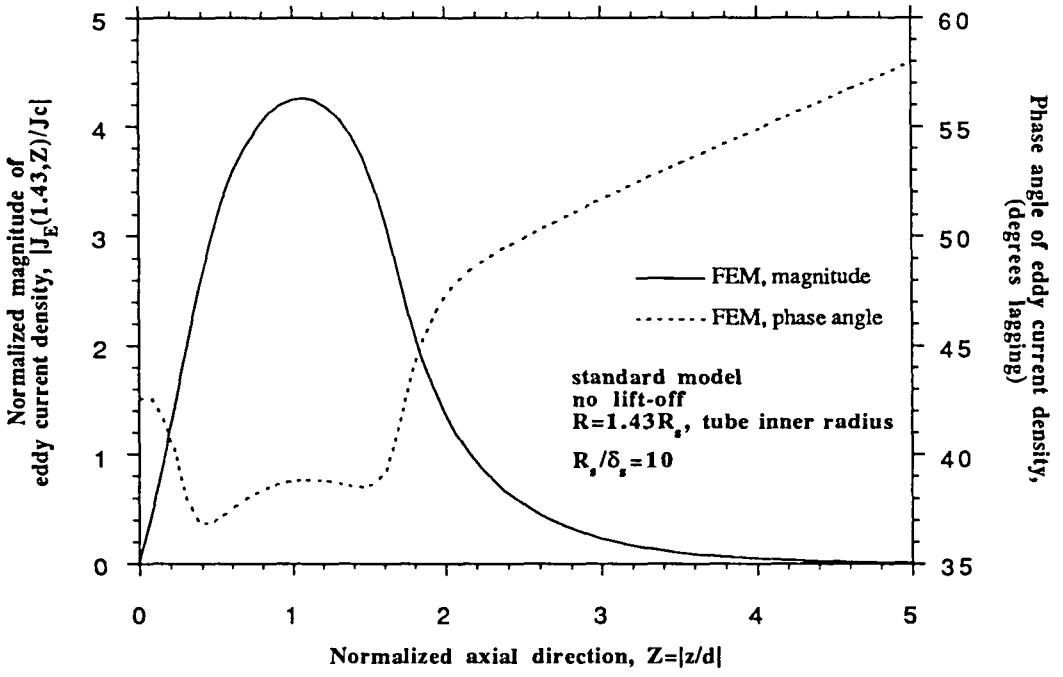

(a)

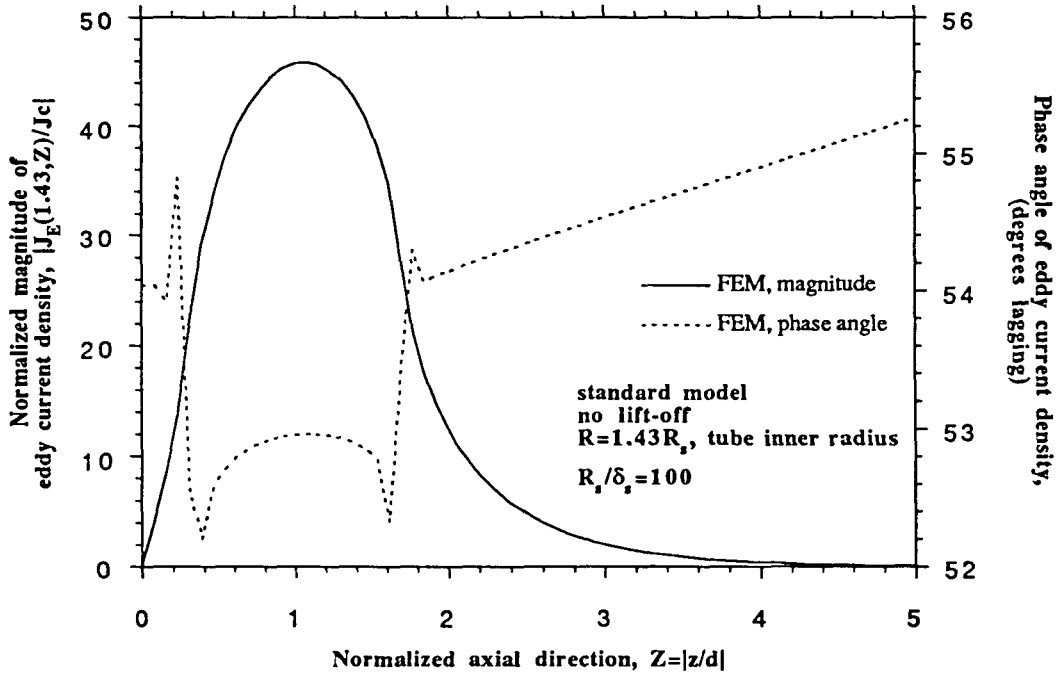

(b)

Figure 4.28: Induced eddy current density versus large R_S/δ_S, (a) $R_S/\delta_S = 10$, (b) $R_S/\delta_S = 100$

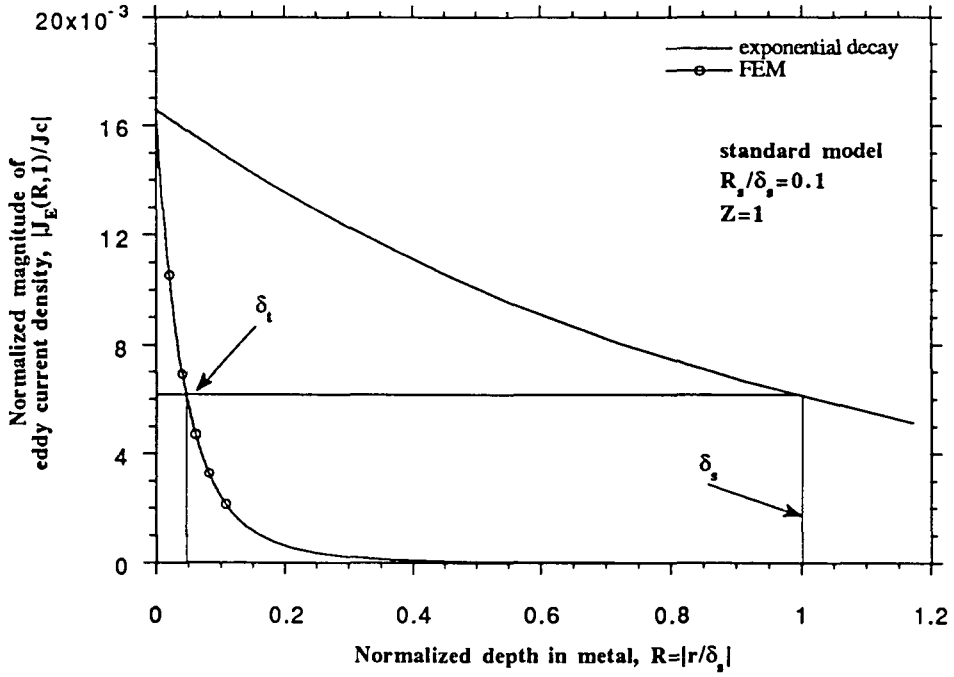

(a)

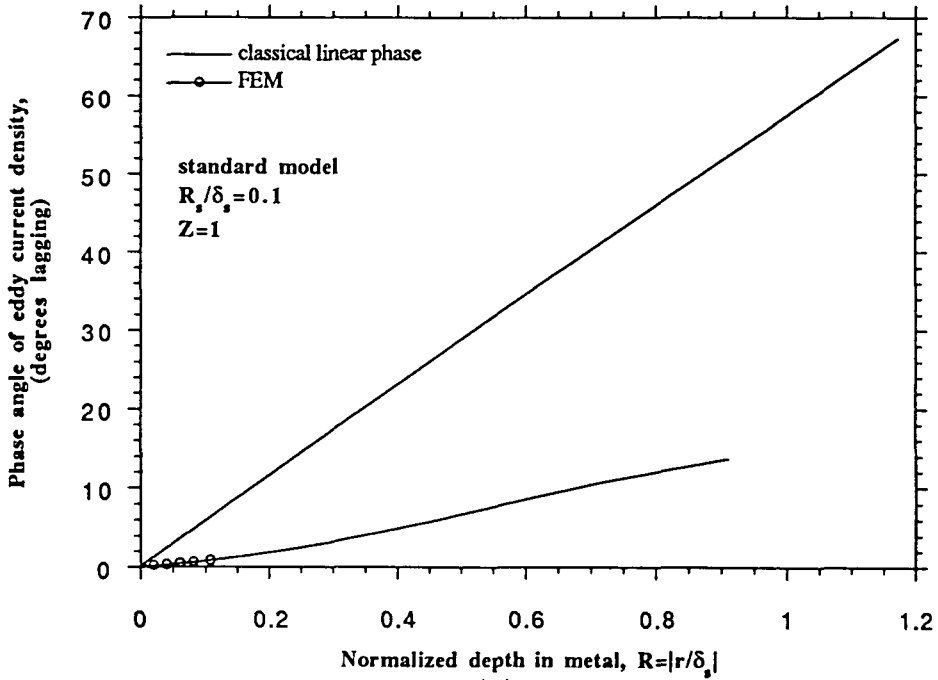

(b)

Figure 4.29: Induced eddy current density in the radial direction compared with the classical solution, $R_S/\delta_S = 0.1$, (a) magnitude, (b) phase

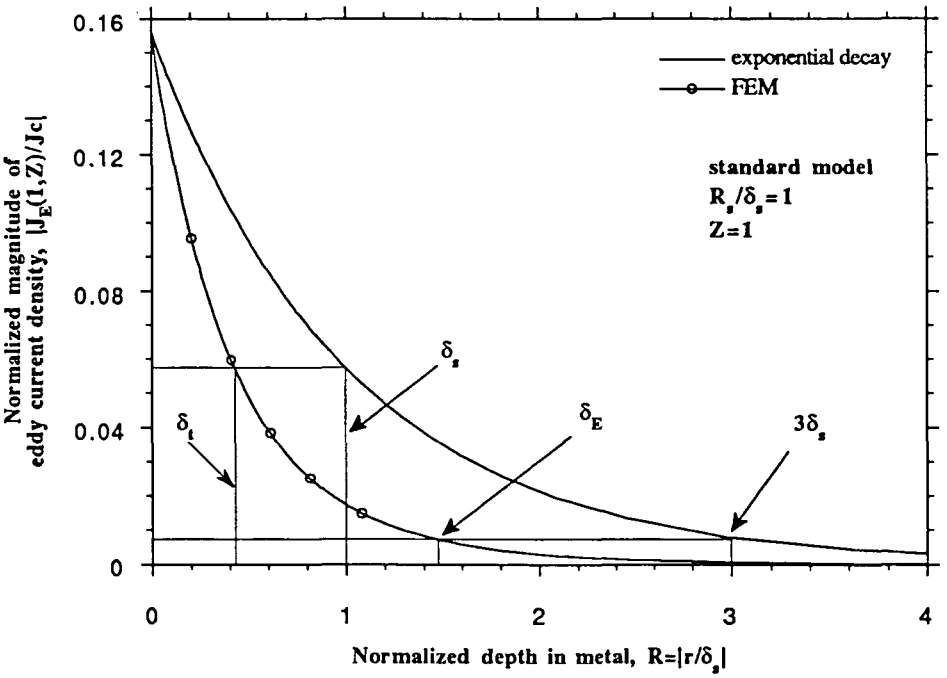

(a)

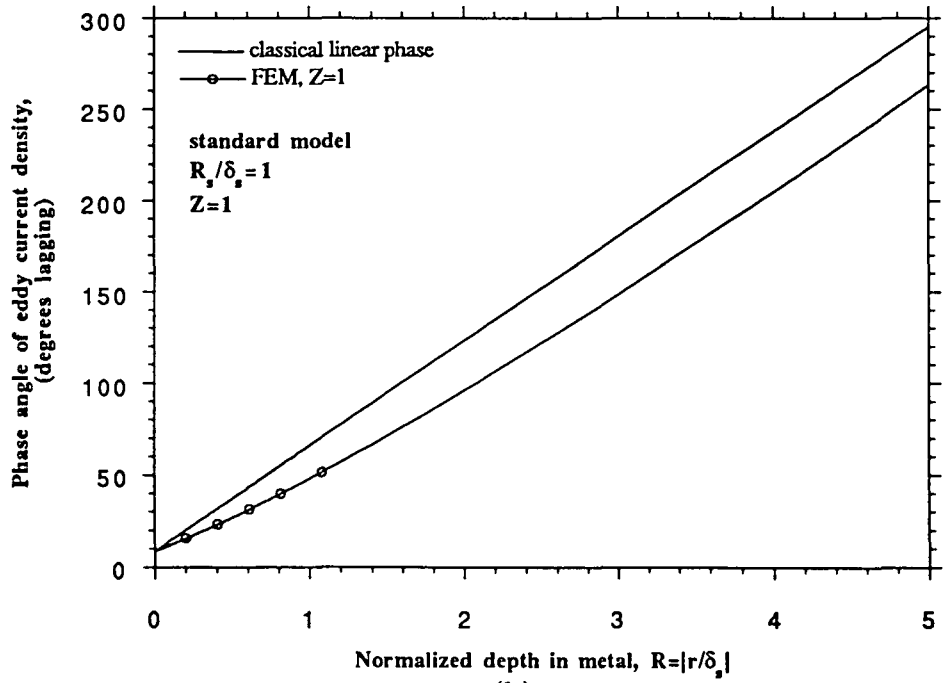

(b)

Figure 4.30: Induced eddy current density in the radial direction compared with the classical solution, $R_S/\delta_S = 1$, (a) magnitude, (b) phase

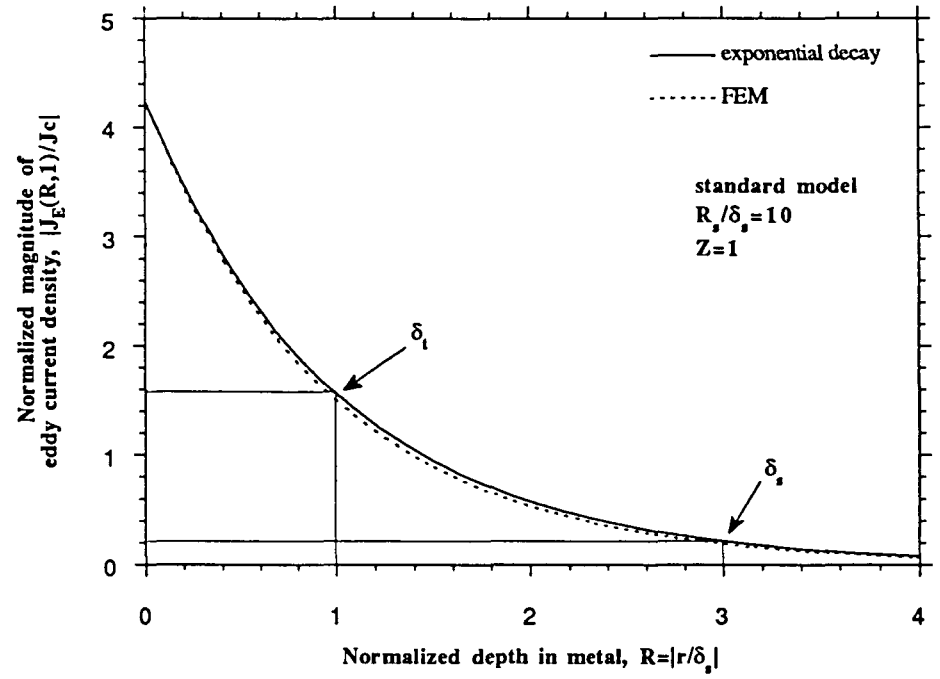

(a)

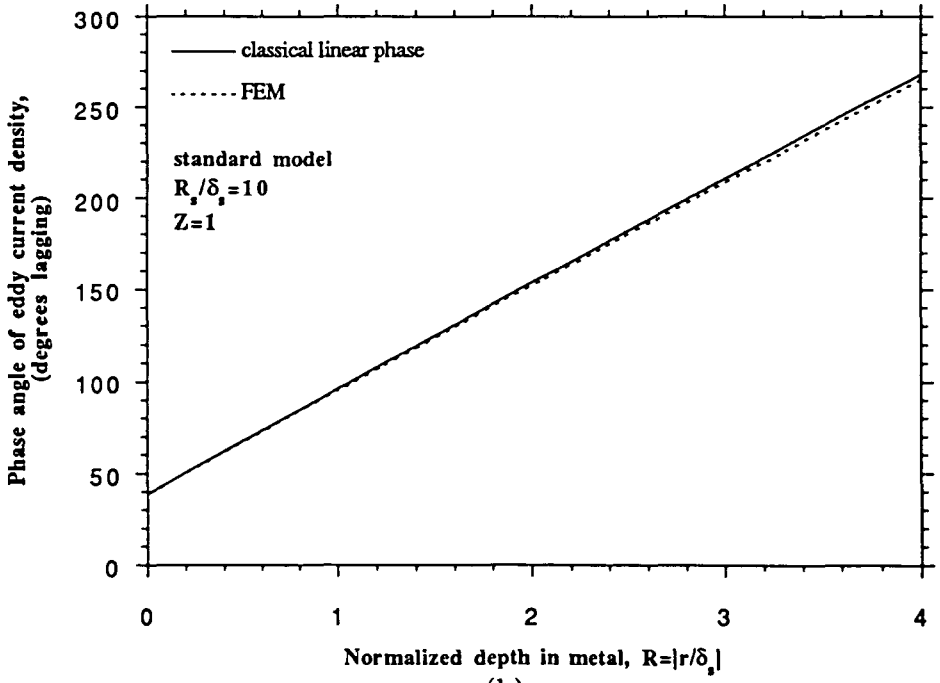

(b)

Figure 4.31: Induced eddy current density in the radial direction compared with the classical solution, $R_S/\delta_S = 10$, (a) magnitude, (b) phase

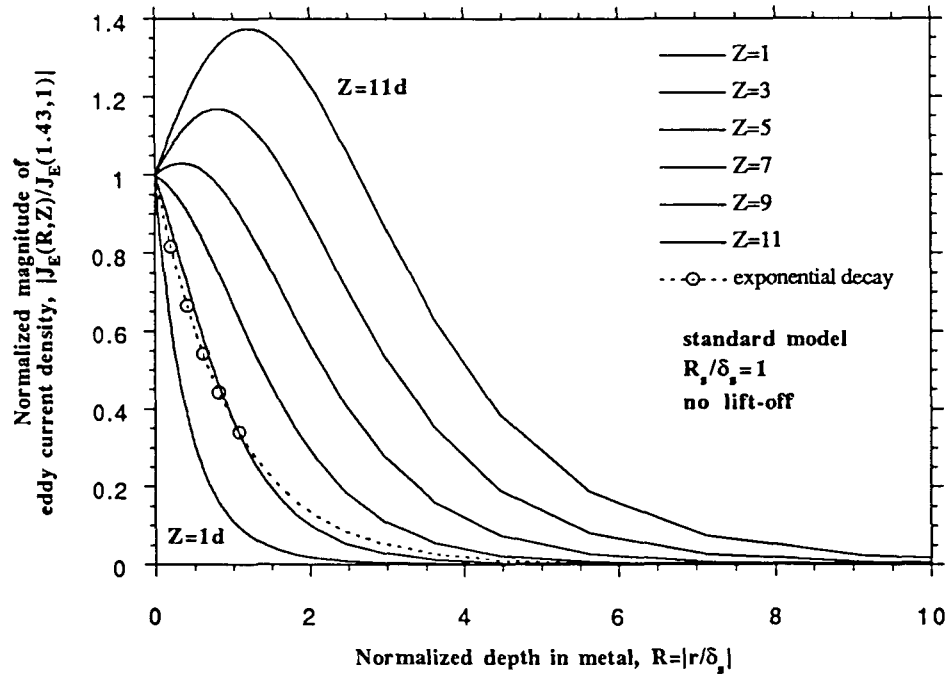

(a)

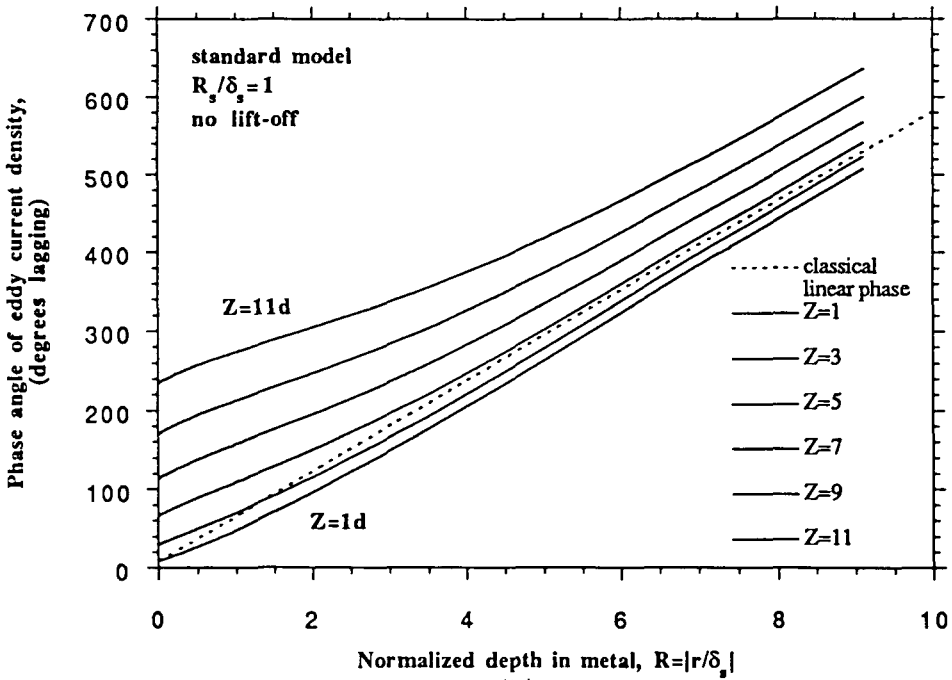

(b)

Figure 4.32: Normalized induced eddy current density in the radial direction versus Z compared with the classical solution, $R_S/\delta_S = 1$, (a) magnitude, (b) phase

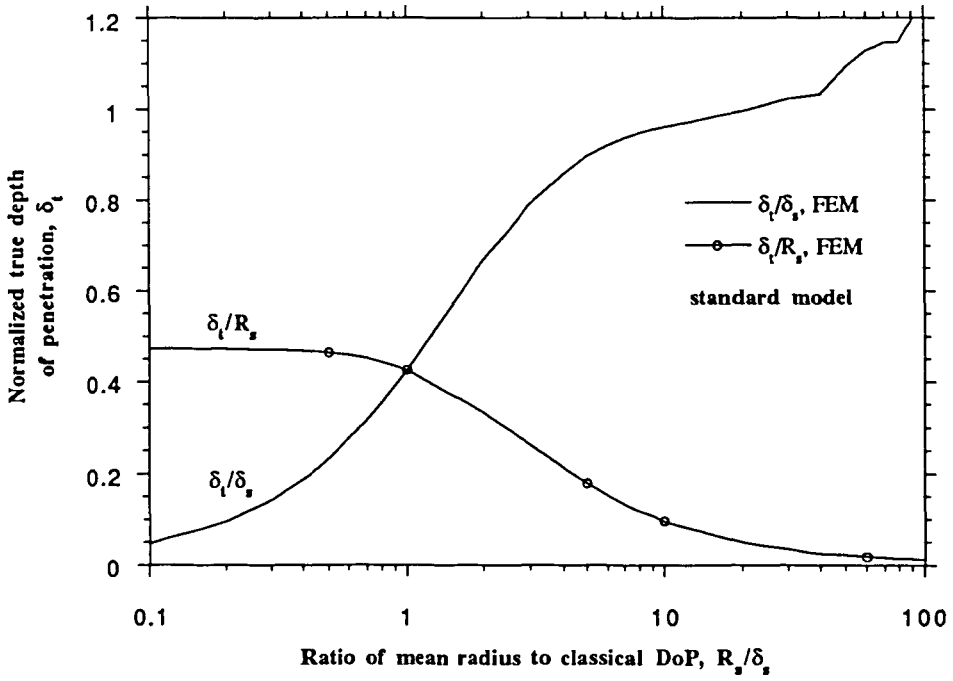

(a)

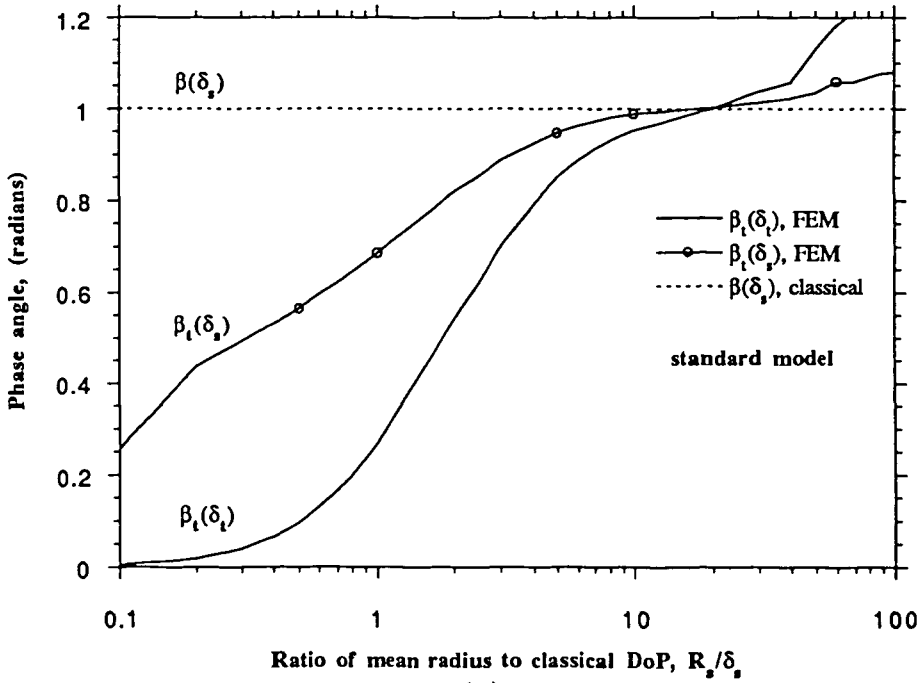

(b)

Figure 4.33: Normalized true depth of penetration versus R_S/δ_S for $Z = 1$, (a) DoP, (b) phase angle

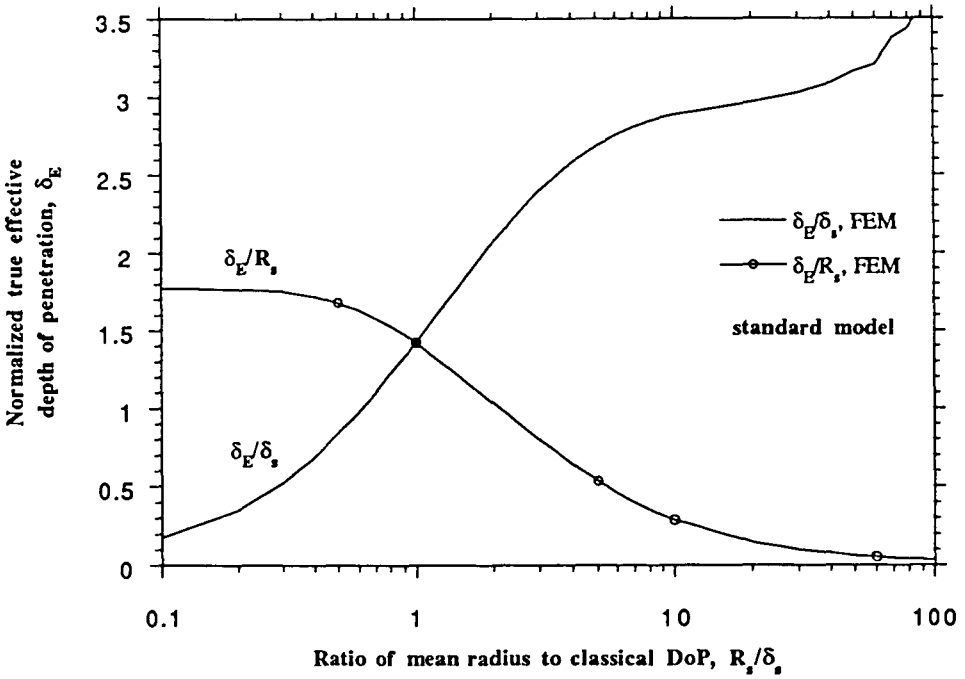

(a)

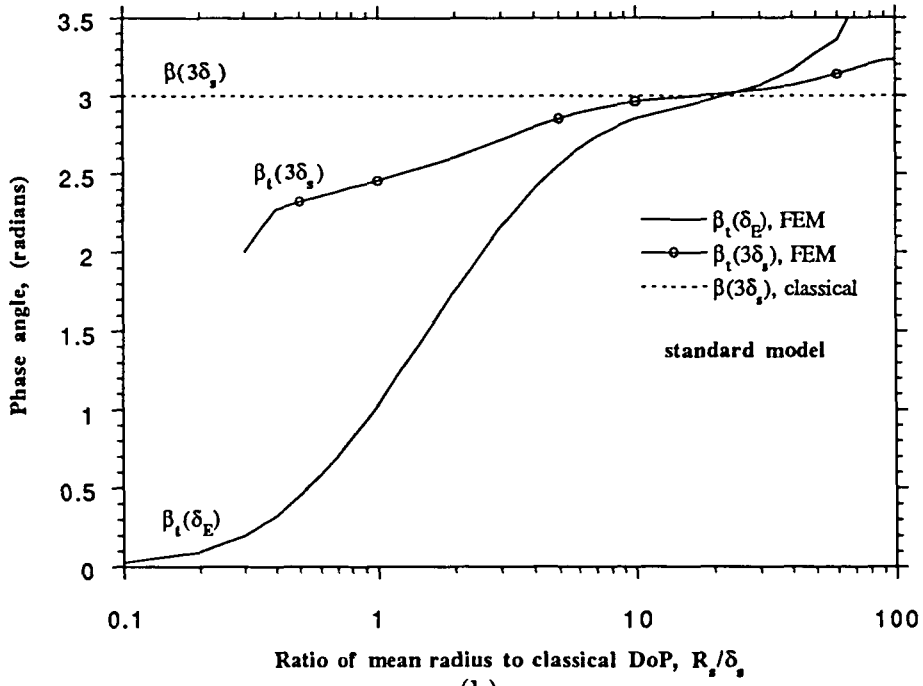

(b)

Figure 4.34: Normalized effective depth of penetration versus R_S/δ_S for $Z = 1$, (a) DoP, (b) phase angle

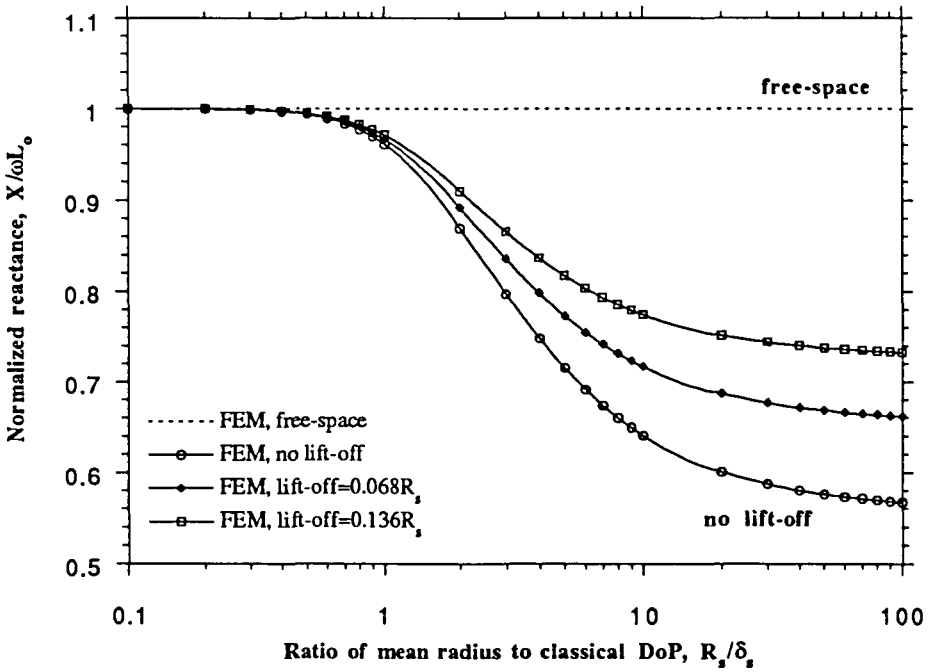

(a)

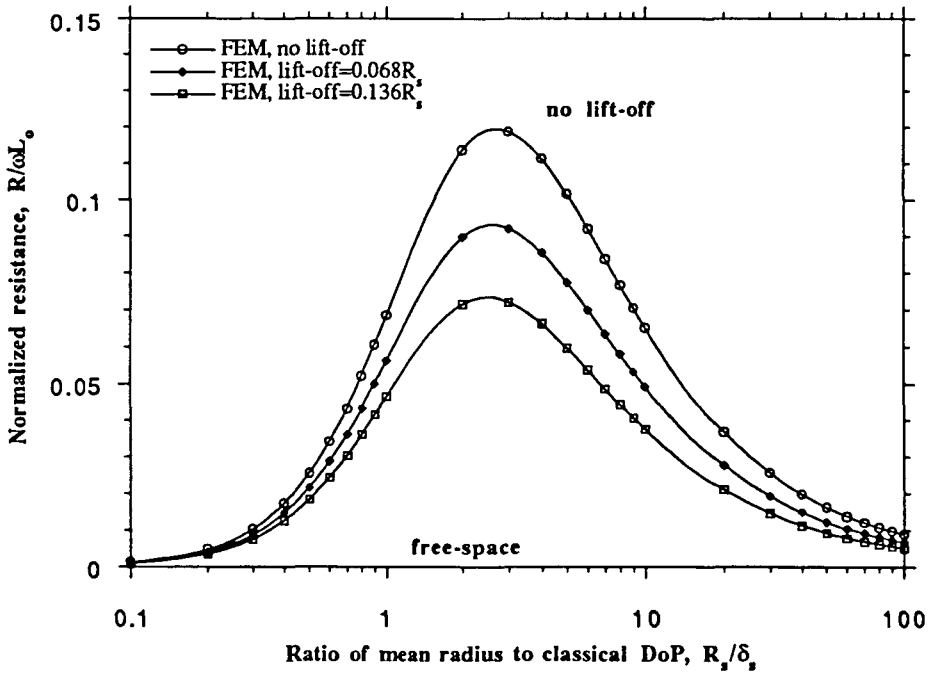

(b)

Figure 4.35: Normalized impedance, FEM, versus coil lift-off and R_S/δ_S, (a) reactance, (b) resistance

CHAPTER 5. CONCLUSION

The classical skin effect approximation cannot be applied in general to situations in which the source is finite and the induced field is localized and inhomogeneous. This study has shown that current density decays faster than exponential in the region near the coil where most defect detection occurs, that is, excluding remote field eddy current NDE. The exponential approximation can model the field distribution for certain values of the parameter R_s/δ_s, but for the coils used in this study the region of validity was beyond the useful inspection frequency range ($R_s/\delta_s \geq 10$). Since eddy current decay is faster than exponential for moderate and low values of R_s/δ_s, defects of a given size cannot be detected below a distance much less than three classical skin depths ($3\delta_s$). A more conservative but realistic estimate for defect detection would be one classical skin depth, but even this becomes poor at low measurement frequencies.

The measurements performed do, in general, confirm the validity and usefulness of the integral solutions and finite element method for frequencies below the self-resonant frequency of the coil, but only the FEM has the flexibility to investigate defect/field interactions in the presence of material inhomogeneities and nonlinearities.

Future Work

A direct extension of this work could include the construction and measurement of a differential coil pair to confirm the predictions. More care in coil construction should be taken to ensure as close a correspondence as possible with the model, at least physically.

In reality the coil is a continuous wire wrapped tightly into a coil shape with an ac potential applied across the two exposed ends; therefore, a three dimensional finite element solution is needed to accurately model the coil. More accuracy could be obtained with the axisymmetric code if the coil was modelled with a finite number of loops with dielectric material between them. In this way the interwinding capacitance can manifest itself and the self-resonant nature of the coil can be modelled. The dc resistance of the coil requires a finite conductivity in the coil, but the simple inclusion of a given conductivity did not alter the FEM solution appreciably. Also the wire comprising the coil has its own skin effect and the loops together will exhibit a proximity effect, that is, current in a loop affected by current in all other loops. These effects do not exist in the present finite element code.

A question suggested by this study is whether or not the remote field effect exists in the coil over a planar conductor. If it does then a logical question to ask is if it can be exploited for NDE purposes. The phenomena is interesting irrespective of its NDE uses. In fact, the subject of electromagnetic diffusion in general begs certain questions: Exactly what does it mean for EM fields to diffuse? How is the energy propagated? For a process which is diffusive how does one extract information about defects from measured data compared to a process which is mostly wavelike? Is there a way to quantify the available information from a diffusion process and compare that

amount to the amount available from a wave process? These are but a few questions which, if answerable, could affect the way in which eddy current NDE is conducted, that is, knowledge of the type and quantity of information available from a process suggests which process may be best suited to the detection of given defects.

Finally, the phenomena studied here is steady state ac which allows the parabolic diffusion equation to be written as an elliptic PDE ($\partial/\partial t \Rightarrow j\omega$). The fields while sinusoidally alternating in time are stationary in space or where their rate of decay and physical distribution is constant with time. Instead one could apply the FEM to pulsed or transient fields to determine what new defect detection possibilities may exist or simply investigate the physics of the phenomena.

BIBLIOGRAPHY

[1] Abramowitz, M., I. A. Stegun. *Handbook of Mathematical Functions.* New York: Dover Publications, Inc., 1972.

[2] Ashby, N. "Relaxation of Charge Imbalances in Conductors." *American Journal of Physics* 43:6 (June 1975): 553-55.

[3] Bochove, E. J., J. F. Walkup. "A Communication on Electrical Charge Relaxation in Metals." *American Journal of Physics* 58:2 (February 1990): 131-34.

[4] Brauer, J. R. "Finite Element Analysis of Electromagnetic Induction in Transformers." presented at *IEEE PES Winter Meeting, New York* Paper A77-122-5 (January 1977).

[5] Capobianco, T. E., J. D. Splett, H. K. Iyer. "Eddy Current Probe Sensitivity as a Function of Coil Construction Parameters." *Research in Nondestructive Evaluation* 2 (1990): 169-86.

[6] Casimir, H. B. G., J. Ubbink. "The Skin Effect." *Philips Technical Review* 28 (1967): 271-83, 300-15, 366-81.

[7] Chandrasekhar, S. "Stochastic Problems in Physics and Astronomy." *Reviews of Modern Physics* 15:1 (January 1943): 1-89.

[8] Chari, M. V. K. "Finite-Element Solution of the Eddy-Current Problem in Magnetic Structures." *IEEE Transactions on Power Apparatus and Systems,* PAS-93Z:1 (Jan./Feb. 1974): 62-72.

[9] Crank, J. *The Mathematics of Diffusion.* New York: Oxford University Press, 1975.

[10] Dodd, C. V., Deeds, W. E. "Analytical Solutions to Eddy-Current Probe Coil Problems." *Oak Ridge National Laboratory* ORNL-TM-1987 (November 1967).

[11] Dodd, C. V., W. E. Deeds, J. W. Luquire. "Integral Solutions to some Eddy Current Problems." *International Journal of Nondestructive Testing* 1 (1969): 29-90.

[12] Dodd, C. V., W. E. Deeds, J. W. Luquire, W. G. Spoeri. "Some Eddy-Current Problems and Their Integral Solutions." *Oak Ridge National Laboratory* ORNL-4384 (1969).

[13] Duchateau, P., D. W. Zachmann. *Schaum's Outline Series: Partial Differential Equations.* New York: McGraw-Hill Publishing Co., 1986.

[14] Dwight, H. B. *Electrical Coils and Conductors: Their Electrical Characteristics and Theory.* New York: McGraw-Hill Book Company, Inc., 1945.

[15] Feynman, R. *The Feynman Lectures on Physics.* New York: Addison-Wesley Publishing Company, Vol. II pg. 16-4, 1964.

[16] Hagemaier, D. J. "Eddy Current Standard Depth of Penetration." *Materials Evalution* 43 (October 1985): 1438-41.

[17] Heaviside, O. *Electromagnetic Theory.* London: "The Electrician" Printing and Publishing Co., Vol. I II III, 1893.

[18] Hildebrand, F. B. *Methods of Applied Mathematics.* 2nd ed. Englewood Cliffs: Prentice-Hall, Inc., 1965.

[19] Hummel, R. E. *Electronic Properties of Materials.* New York: Springer-Verlag, 1985.

[20] Jackson, J. A. *Classical Electrodynamics.* New York: John Wiley and Sons, 1975.

[21] Kennelly, A. E., F. A. Laws, P. H. Pierce. "Experimental Researches on Skin Effect in Conductors." *Trans. AIEE* 34 (1915): 1953-2018.

[22] Kennelly, A. E., H. A. Affel. "Skin-Effect Resistance Measurements of Conductors." *Proc. IRE* 4 (1916): 523-74.

[23] Konrad, A., P. Silvester. "Triangular Finite Elements for the Generalized Bessel Equation of Order *m*." *International Journal for Numerical Methods in Engineering* 7 (1973): 43-55.

[24] Libby, H. L. *Introduction to Electromagnetic Nondestructive Test Methods.* Huntington: Robert E. Krieger Publishing Co., 1979.

[25] Lord, W. "Development of a Finite Element Model for Eddy Current NDT Phenomena." Draft Interim Report prepared for Electric Power Research Institute, project no. RP1395-2 (NP-2026), (Sept. 1981).

[26] Maxwell, J. C. *A Treatise on Electricity and Magnetism.* New York: Dover Publications, Vol I II 1954, orig. 1891.

[27] Mottl, Z. "The Quantitative Relations Between True and Standard Depth of Penetration for Air-Cored Probe Coils in Eddy Current Testing." *NDT International* 23:1 (February 1990): 11-8.

[28] Ohanian, H. C. "On the Approach to Electro- and Magneto-static Equilibrium." *American Journal of Physics* 51:11 (November 1983): 1020-2.

[29] Palanisamy, R. "Finite Element Modelling of Eddy Current Nondestructive Testing Phenomena." Ph.D. diss., Colorado State University, 1980.

[30] Palanisamy, R. "Development of a Finite Element Model for Eddy Current NDT Phenomena." Draft Interim Report prepared for Electric Power Research Institute, project no. RP1395-2, (Oct. 1981).

[31] Palanisamy, R., W. Lord. "Finite Element Analysis of Eddy Current Phenomena." *Materials Evaluation* 38:10 (October 1980): 39-43.

[32] Palanisamy, R., W. Lord. "Finite Element Simulation of Support Plate and Tube Defect Eddy Current Signals in Steam Generator NDT." *Materials Evaluation* 39 (June 1981): 651-5.

[33] Prigogine, I. *From Being to Becoming.* San Francisco: W. H. Freeman and Co., 1980: 11-2.

[34] Sachdev, P. L. *Nonlinear Diffusive Waves.* Cambridge: Cambridge University Press, 1987.

[35] Saslow, W. M., G. Wilkinson. "Expulsion of Free Electronic Charge from the Interior of a Metal." *American Journal of Physics* 39:10 (October 1971): 1244-48.

[36] Scott, A. C. "The Electrophysics of a Nerve Fiber." *Reviews of Modern Physics* 47:2 (April 1975): 487-533.

[37] Silvester, P.P., R. L. Ferrari. *Finite Elements for Electrical Engineers.* 2nd ed. Cambridge: Cambridge University Press, 1990.

[38] Smith, G. S. "On the Skin Effect Approximation." *American Journal of Physics* 58:10 (October 1990): 996-1002.

[39] Vasiliev, V. A., Yu. M. Romanovskii, D. S. Chernavskii, V. G. Yakhno. *Autowave Processes in Kinetic Systems.* Dordrecht: D. Reidel Publishing Co., 1987.